THESIS

FLUID INCLUSION AND METAL RATIO ANALYSIS OF CORDILLERAN Pb-Zn-Cu-(Ag-Au) VEINS OF THE MONTEZUMA DISTRICT: SUMMIT COUNTY COLORADO, USA

Submitted by

Dominic Pyanoe

Department of Geosciences

In partial fulfillment of the requirements

For the Degree of Master of Science

Colorado State University

Fort Collins, Colorado

Fall 2015

Master's Committee:

Advisor: John Ridley

Sven Egenhoff
Bob Wilson

ABSTRACT

FLUID INCLUSION AND METAL RATIO ANALYSIS OF CORDILLERAN Pb-Zn-Cu-(Ag-Au) VEINS OF THE MONTEZUMA DISTRICT: SUMMIT COUNTY COLORADO, USA

Evidence from fluid inclusion microthermometry in Pb-Zn-Cu-(Ag-Au) veins and district scale metal ratio zonation analysis indicate that the Cordilleran veins of the Montezuma mining district Summit County, Colorado, USA are indicative of subepithermal setting about a central hydrothermal source. Cordilleran-type polymetallic mineralization is a class of ore deposits that are spatially and temporally related to felsic igneous centers and can also be genetically related to porphyry mineralization (Fontboté and Bendezú, 2009). At Montezuma, the Teritary-aged Montezuma Stock is cross cut by several Cordilleran-type veins and is spatially related to over 80 additional veins hosted in Precambrian country rock.

Five stages of mineralization in veins are identified: Stage 1. early quartz-pyrite, Stage 2. barite-incipient base metals Stage 3. base metals, Stage 4. carbonates and Stage 5. late quartz-lead-silver. There is a systematic decline in precipitation temperatures from 341 to 156°C along the progression of the paragenetic sequence, which suggests the waning of a source pluton. District scale metal ratio zonation maps from historical production data support the interpretation of a central magmatic source and that thermal decline is the primary control on ore deposition. Two district scale zones are identified: a copper rich zone (CRZ) in the center of the district, which is surrounded by a copper poor zone (CPZ). With distance from the inferred center of the district, there is a general decline in copper abundance relative to lead and silver. Thermal gradients accompanied by a decrease in metal solubilities are the mechanism for this zonation pattern, but developed late in the paragenesis. Other chemical and physical controls of

phase separation, ligand removal, dilution and pH increase are likely present during vein mineralization as well. Approximate salinities ranged from 11.69 to 3.70 wt.% equivalent NaCl and showed less systematic patterns, and may reflect these additional processes. Temperature decline and variable additional depositional processes are consistent with analogous Cordilleran-type vein fields, which have proven links to a magmatic source and possible underlying stockwork porphyry base metal mineralization. Therefore, data from this study indicates that there is most likely porphyry Mo mineralization under the copper rich zone, but this may be sub economic in nature.

TABLE OF CONTENTS

1. Introduction

The 125 km² Montezuma mining district is located in the Front Range of the Rocky Mountain Cordillera and within Colorado Mineral Belt (COMB) as defined by Tweto and Sims (1963). Over 80 veins bearing Pb-Zn-Cu-(Ag-Au) were historically exploited from the district, which is spatially related to a Tertiary aged quartz monzonite stock, the Montezuma Stock (Figure 1.1). Ore minerals occur as sulfides and sulfo-salts in veins, which have filled structural weakness. Host rocks are Proterozoic metasediments, metavolcanics and the Montezuma Stock.

One of the first formal studies in the district was that of Lovering (1935). He provided a detailed account of all geological aspects of the region with an emphasis on qualitative assessments of economic geology. This document is of particular importance because it holds valuable historic production data for abandoned mines. Later during the 1970s, several geologists (Neuerburg, 1974; Neuerburg, 1978; Botinelly, 1979) took an interest in the Mo potential of the district, which is of particular concern in this study as well. The construction of the Harold D. Roberts Tunnel also occurred in the 1970s in order to provide water to the population centers east of the Front Range. The tunnel transects the district along a southeast bearing roughly through the center of the district. Robins (1974) and Wahlstrom (1981) provide geologic descriptions of rocks encountered by the tunnel. The 1980s saw the closure of the last active mine in the area, the Burke Martin Mine. During the 2000s a renewed attention to Mo occurred along the SE margin of the district. Mineral Systems Inc. drilled 4 holes on Red Cone Peak and Webster Pass in search of Mo porphyry ore mineralization. The exploratory holes were unsuccessful. Recently, several authors (Bove et al., 2012; Caine et al. 2006; and others) have reported on the mineralogic and geologic controls that have induced acid metal rich waters in Handcart Gulch, which lies just outside the district to the SE.

This study focuses on the hydrothermal evolution of ore bearing veins of the Montezuma district. Multiple approaches were taken to analyse these veins in order to properly classify ore as Cordilleran-type veins and to investigate the causes of ore precipitation. First a general district wide paragenesis for vein mineralization was established by analysis of slabbed samples, doubly polished sections and a review of previous literature (primarily Lovering, 1935). Mineralization was divided into 5 stages in order to provide a temporal context for zonation and fluid inclusion (FI) data. Next a spatial data base was compiled from historical metal production values in order to address the district scale distribution of metals and the relationships among metals. The compilation of historic mine production values for each metal (Pb, Zn, Cu, Ag and Au) was sourced from Lovering (1935). Multiple relationships of each metal were plotted in order to find the best ratio for zonation patterns. The Pb:Cu and Ag:Cu ratios proved to be the best indicators of precipitation patterns in the district. The final products of this study were metal ratio interpolation maps, which defined zonation patterns in the district. This was then followed up by fluid inclusion microthermometry and petrography to link the paragenetic sequence of mineralized veins to associated temperatures and salinities of each stage. Additionally, microthermometry data was integrated with metal ratio zonation data. This integration allowed analysis of both spatial and temporal variations of salinities and temperatures. The results from the four above components then permitted a proper evaluation of vein classification and district scale fluid evolution patterns. The results from this study were then compared to analogous districts in order to better discuss the role of variables that were not directly addressed in this study like: fluid and metal source, meteoric water influences, additional ore mineral precipitation mechanisms and other variables. Additionally, implications for Mo porphyry exploration are discussed in this study.

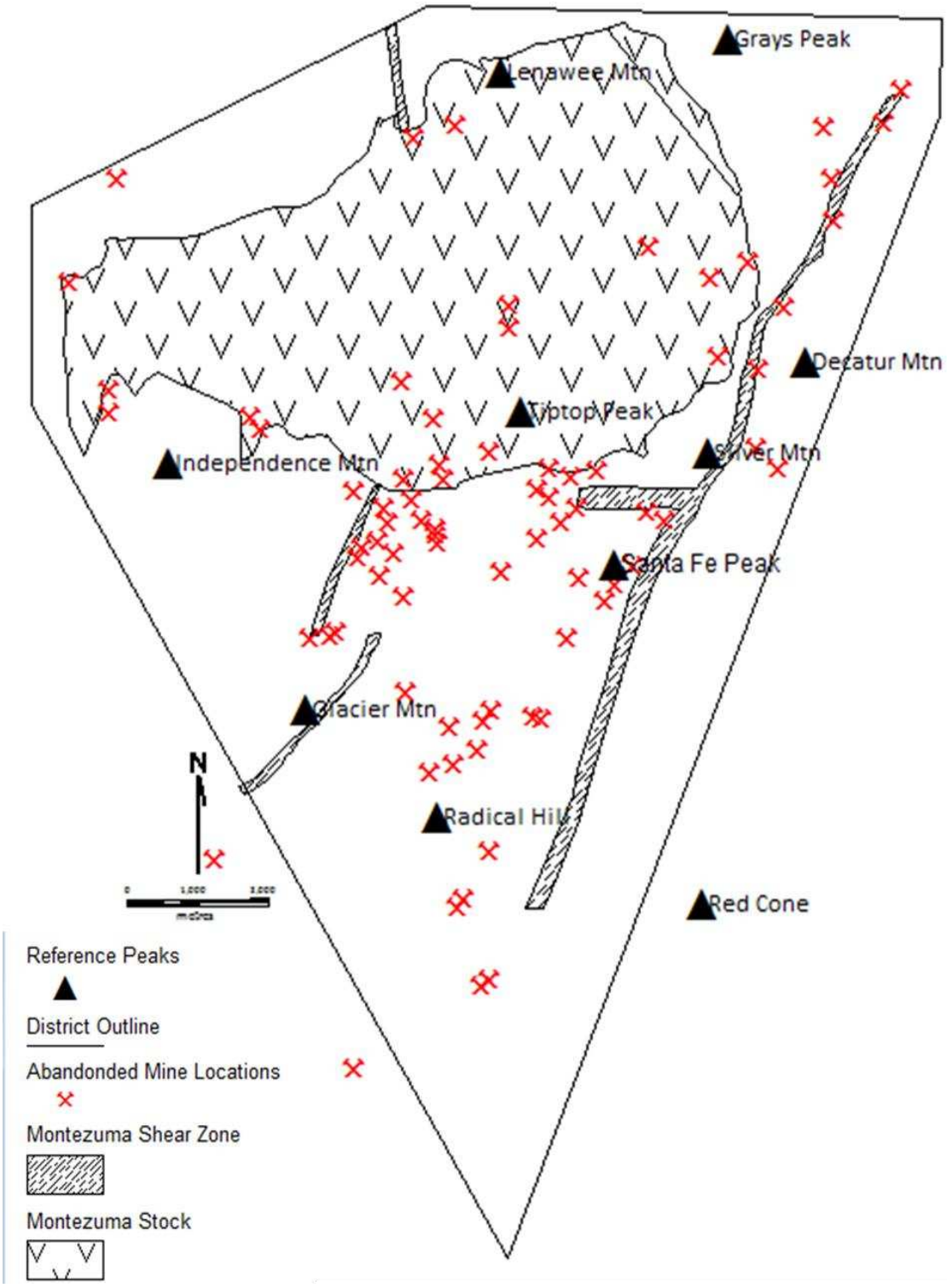

Figure 1.1 Map of the Montezuma mining district including surface exposures of the Montezuma Stock (quartz monzonite) and the Precambrian Montezuma shear zone. Textureless white regions are Precambrian gneiss and granite, which are host to the younger Tertiary aged Montezuma Stock and ore bearing veins. Vein location is correlated to abandoned mine locations. Gray's Peak is 426636 m E, 4387003 m N.

2. Geologic Background

2.1 Ore of the Colorado Rockies

Ore in the Colorado Rocky Mountain region is associated with hydrothermal fluids that have affiliations to Late Cretaceous to Late Tertiary magmatic centers. Mo porphyries (Climax, Henderson-Urad, Mt. Emmons and Silver Creek), Cordilleran Pb-Zn-Cu-(Ag-Au) vein fields (Montezuma, Breckenridge and Argentine), skarns (Leadville), carbonate replacement deposits (Italian Mountains and Leadville), and high sulfidation epithermal systems (Summitville) can be found in the mountains of Colorado. Historically the Colorado Rockies were exploited for veins or mantos bearing high grade gold, silver, zinc, lead and copper, but modern economics are now favouring molybdenum porphyries and the unique bulk tonnage gold deposits found in the Cripple Creek district.

Within the Colorado Rockies, there is a prominent northeast trend of ore deposits, which has been termed the Colorado Mineral Belt (COMB). The COMB was proposed by Tweto and Sims (1963) and has been an accepted concept until recently. The COMB runs from the La Plata District in the San Juan Mountains of the south western portion of the state and trends northeast to the Jamestown District of the Indian Peaks (Figure 2.1.1). The conspicuous regional north-east trend of the belt and post Laramide timing unify most of the deposits, although some deposits like the world class Cripple Creek alkaline gold district lie well outside the mentioned north-east trend and show little deposit or district scale orientation with a north-east trend. Authors have proposed that the northeast trend of the COMB is the result of reactivation of Precambrian structural weaknesses in the crust, which have been selectively intruded by Late Cretaceous-Tertiary magmatism (Allen, 2004; Lovering, 1929; Tweto and Sims, 1963; Wilson and Sims, 2002).

A key aspect in the COMB theory is that ore is localized by weaknesses in the crust that were once major sites of deformation during the Proterozoic. These proposed zones of weakness are commonly expressed as increased degrees of dynamic metamorphism within mining districts, for example the Idaho Springs Shear Zone and the Montezuma Shear Zone. Tweto and Sims (1963) interpreted these as fundamental breaks in the crust. Caine et al. (2010) and Wessel and Ridley (2010) discovered that this is not the primary control for localization and orientation of the mineral deposits. Wessel and Ridley (2010) were able to prove that the Idaho Springs-Ralston Shear zone is actually a steep limb of a Proterozoic syncline. This study suggests that a revaluation of shear zones within the state is needed to actually prove that these are true structural weaknesses.

An additional fundamental flaw in the COMB model is that a significant number of ore deposits lie well outside the COMB boundaries and some deposit clusters do not follow a northeast trend (Figure 2.1.2). These outliers and northwest trending deposit clusters were accounted for by simply terming them anomalies. In several studies the COMB has been reconfigured in order to account for some of these outliers (Tweto and Sims, 1963; Wilson and Sims, 2002). Matthews and Morgan (2012) followed up with an elegant GIS study and were able to prove that ore in Colorado is associated with general Precambrian metamorphic belts with higher concentrations along margins of Precambrian plutons rather than being along a single Proterozoic structure. The concentration of mineral districts along Precambrian pluton margins was first proposed by Lovering (1930). He suggested that these plutons acted as buttresses and their margins serves as weaknesses for magma to rise through the thick Laramide crust. This model better accounted for what would be called outliers in the COMB model. For example, the Tertiary Cripple Creek diatreme breccia was emplaced along the margin of the Precambrian Pikes Peak Granite and Precambrian metamorphics. Additionally, ore in the Montezuma district lies solely to the west of exposures of the Precambrian Silver Plume Granite and within the Precambrian Swandyke Gneiss and Idaho Springs Formation.

On the basis of their study, Morgan and Matthews (2012) suggested that the COMB is not a true geologic trend within the Colorado Rockies considering the abundance of deposits that lie outside the COMB boundaries. Yet, there is still a conspicuous concentration of ore deposits along what is termed the COMB. This concentration may be accounted for by means of regional scale tectonic models. The northeast trending deposit clusters have been attributed to rupture and roll back dynamics of the Farallon slab (Chapin, 2012), which may be a first order control whereas location of Precambrian metamorphic belts and plutons are second order controls. Precambrian shear zones may have localized Proterozoic plutons, but this relationship has not been conclusively proven.

The Montezuma District does conform to this north-eastern trend on regional, district and deposit scales. Regionally the district forms the link between the Breckenridge District 20 km to the south-west and the Argentine District 15 km to the north-east. On a district scale, the deposits form a north-east trend with a slight, but notable northwest widening from Independence Mountain through Glacier Peak to Sullivan Mountain. In fact, some of the more profitable deposits can be found along this widening. The vast majority of individual veins strike to the northeast, but some ore bearing veins do strike to the northwest. The mechanism of ore localization could follow the theories proposed by Tewto and Sims (1963) or Lovering (1930) or that of Matthews and Morgan (2012). In this study models proposed by Matthews and Morgan (2012) and Lovering (1930) will be the favoured interpretation of ore localization. Controls of Precambrian batholiths acting as buttresses are of particular interest for this study as the Silver Plume Granite outcrops in the Montezuma District. However, this study will consider the potential role reactivation of shear zones as described by Tweto and Sims (1963) in ore deposition at Montezuma as well.

Brief Summary of Exploration and Mining

Experienced prospectors from the Dahlonega District, Georgia (USA) passed through the eastern reaches of the COMB on their way to the California goldfields and believed that the rivers may contain

economic placers. Upon their return from California in 1858, the Georgians decided to work the South Platte, Cherry Creek and Clear Creek, which drain the northern portion of the COMB (Brchan et al., 2003). This prospecting rendered the first discovery of placer gold in Colorado. The following discoveries of lode gold and oxide gold near Blackhawk in 1859 attracted a wave of prospectors and miners to the mineral belt. This led to the comprehensive surface mineral exploration of the highlands in Colorado. As a result, the rich silver potential of the Colorado Mineral Belt was unveiled in 1864 with the first silver discovery in the state of Colorado, which would become known as the "Silver State." The first discovery was along the north slope of Glacier Peak above timberline by a man named Coley (Lovering, 1935). The peak rises from the Montezuma Mining District, and is host to a number of historically productive ore bearing veins including Sts. Johns Mine and the Tiger Mine. However, this discovery was during a gold centric Colorado mine industry, and it was not until the discovery of high grade carbonate replacement deposits in the Mosquito Range that silver became that target of many prospectors and miners. Discoveries across the state soon followed, spreading mining excitement to remote highlands like Creede, in the San Juan Mountains. Since the early discoveries of world class deposits like the carbonate replacement Pb-Zn-Ag at Leadville and the alkaline gold at Cripple Creek, the state of Colorado has been a source for economic ore bodies. Currently, the high grade bulk tonnage Climax-type porphyries of Climax and Henderson-Urad produce a significant portion of global molybdenum supply, which has upheld the legacy of the COMB. Additional active mining districts are Cripple Creek (Au) and Ouray (Ag).

2.2 Rock Types and Geologic History of the Montezuma District

Precambrian rocks and the Montezuma shear zone

Precambrian rock units occupy roughly 85 km² or 68% of the surface bedrock of the formally defined Montezuma District as mapped by Lovering (1935). Mappable units are the Idaho Springs Formation, the Swandyke hornblende gneiss, the Silver Plume Granite as well as subordinate pegmatite

dikes. All three major units are common in other portions of the Front Range, and are key basement units and host rocks for other mining districts in the Colorado Mineral Belt. A prominent structure, the Montezuma Shear Zone, can be found as a narrow north-east trending feature cross cutting all Precambrian units.

Lovering (1935) interpreted these Precambrian units through petrographic studies and years of experience with similar units in the Front Range of Colorado. The Idaho Springs formation is interpreted to be a metapelite package. The overlying Swandyke hornblende gneiss is interpreted to be a series of metamorphosed mafic lavas. These units were intruded by the Silver Plume granite, which represents a significantly smaller surface coverage than the older two units. Pegmatites are interpreted to be related to the Silver Plume Granite or to other nearby Precambrian intrusive bodies in neighbouring districts like the Pikes Peak Granite.

Reed et al. (1989) concluded that Early Proterozoic rocks in the central mineral belt, like those found at Montezuma, were formed during arc magmatism and associated sedimentation along a convergent margin. The Idaho Springs formation can be interpreted to be metamorphosed flysch and molasse type sedimentation while the Swandyke hornblende gneiss may represent a unit with increased volcanic input into the ancient basin. Two episodes of intrusive activity occurred in the region at 1.7 Ga and at 1.4 Ga (Wallace, 1988). The former is not represented in the study area, but is still of significance regarding the history of the region. Syn-metamorphic calk-alkaline magmatism reflecting convergent arc tectonic processes characterise this earlier episode (Wallace, 1988). Intrusives like the Silver Plume granite, are found to be 1.44 Ga (Hedge, 1969). The peraluminous nature of this suite of granites has favored an anorogenic environment for their emplacement (Wallace, 1988).

Precambrian shear zones are argued to be a control in the localization of later ore related magmatism in the Colorado Mineral Belt (Tweto and Sims, 1963). As the previous two paragraphs only detail host rocks for vein mineralization in the district, the discussion of Precambrian shears zones has

more significance with regard to exploration and structural trends found in the COMB. The reactivation of these shear zones is argued to be a variable in controlling the conspicuous district and regional scale northeast trend of the Colorado Mineral Belt. The Montezuma shear zone was first mapped by Wahlstrom and Kim (1959), and is believed to be analogous to other similar aged Precambrian weaknesses in the Colorado Mineral Belt like the Idaho Springs – Ralston shear zone and the Homestake shear zone. The Montezuma shear zone is roughly 270 m in width with a northeast strike length of 12,300 m from the top of Hall Valley north-east to Horseshoe Basin (Figure 1.1). Two sub-parallel subsidiary 2,500 m long shear zones have been mapped along the crest of Glacier Mountain and along Sts. Johns Creek with an anomalous small north-west shear zone on Lenawee Mountain. The Montezuma shear zone is "considered to be the boundary between the sillmanititc biotite gneiss and schist on the west and the biotite gneiss and schist to the east" (Robinson et al., 1974). Mylonites and other shear textures have been observed in the shear zone (Robinson et al., 1974). These structural weaknesses are proposed to be sites of future Tertiary magmatic ascent and associated mineralization. Accordingly, it is believed that the Montezuma shear zone facilitated the ascent of the Montezuma stock through the thick Laramide crust (Neuerburg et al., 1974).

Laramide Deformation

Deformation and uplift of the Front Range during the Laramide Orogeny have rendered many structures that have impacted subsequent magmatism and ore deposition in the Montezuma Mining District. A variety of structures and plutonism are preserved in the region from the Late Cretaceous to Paleocene (80 – 55 Ma) Laramide Orogeny that reflect the complex tectonics and crustal response of this event. Studies of the region are still attempting to fully understand the tectonic mechanisms that have rendered deformation 1500 km from the nearest paleo-subduction margin of the Farallon under the North American Plate. Laramide structures in the district are a function of pre-existing structures, tectonic stresses and crustal dynamics. These influences are mirrored in the topography and mineral trends of the Front Range and the Montezuma District.

The Front Range is a sub-range of the Rocky Mountain foreland. The range runs 290 km north-south and is 60 km wide from the east to the west. This mountain belt is an expression of significant Laramide deformation deep into the interior of the North American plate, an observation which has led to the development of new models to explain the mechanics of this orogeny. This form of mid-continent deformation has been termed "epeirogenic," a term which focuses on the relationship between vertical movements rather than horizontal compression (Tikoff and Maxson, 2001). This uplifted block of Proterozoic basement rock is bound by the vast Great Plains province to the east and additional block uplifts and basins to the west. Common Laramide-age structures in the Front Range are: first-order anastomosing arches that correlate with basement uplifts, second-order thrusts that margin the arches and basins, synclinal basins, north-east trending thrust belts and a thickened crust. Although the nature and geometry of these regional scale structures have been established, their mechanism of deformation and deep crustal profiles are a continued topic of discussion. These components have been affected by post Laramide events like Rio Grande rifting and Tertiary magmatism (eg. the Montezuma Stock), which have complicated interpretations and geometric understandings of this orogeny.

Discussion about theory for processes controlling the Laramide Orogeny began with a debate between horizontal compression and vertical tectonics. Vertical tectonic movements have been related to Pratt-type isostasy, in which vertical movements of crustal units of varying specific gravity cause topographic relief (Van Der Pluijm and Marshak, 2004). If this is the case, it would imply that the rocks of the Front Range and other foreland blocks are less dense than the rocks under adjacent basins. Additionally, the concept of thin-skinned versus thick-skinned tectonics was a center of debates on Rocky Mountain foreland tectonic development. Thin-skinned models invokes that folds and faults of foreland rocks in an orogenic belt involve only the upper crust, and lie on a décollement such that deformation did not affect the basement rocks (Bates, 1985), while a thick-skinned fault penetrates deeper than 10-15 km. Modern models of the Laramide orogeny are adapted thick-skinned interpretations, which integrate concepts of thin-skinned mechanisms. This combination reflects the idea that many mountain belts show a transition between these two systems (Van Der Pluijm and Marshak, 2004). Higher proportions of

thick-skinned deformation characterize the Rocky Mountain foreland, while higher proportions of thin-skinned structures are found in regions closer to the plate margins further to the west. The transition from thin to thick-skinned distinguishes the Laramide orogeny from other western North American orogenies. Structures that extend into the deeper crust would certainly aid in later magma ascent and undoubtedly play a role in ore deposit distribution within Colorado.

English (2004), Erlsev (2005), and Tikoff and Maxson (2001) have outlined an array of stress transfer models to explain geometric, kinematic and crustal relationships of Rocky Mountain structures that are Laramide in age. The models present work from a variety of data sources and geographic regions of the Rockies in order to explain the basement cored topographic highs of this province. Two possible mechanisms that explain the transmission of stresses to the foreland are: basal traction and endload models (English, 2004). Basal traction models assume that North American crust was not decoupled from the subducting plate, and that the interface of the shallow subducting slab of Farallon plate with this crust transmitted shear stresses. Endload models focus on the horizontal transmission of stresses along a decoupled mantle and crust. Both mechanisms have their merits and flaws. While both models account for deformation deep in the interior of continents, the endload model does not directly account for later magmatism, which is a key component of ore genesis in the Colorado. Therefore basal traction of a shallow subducted Farallon plate will be favoured in this study. Subduction of buoyant oceanic lithosphere is the proposed mechanism for low angle vergence of the subducted Farallon slab during the Cretaceous, (McGeary et al., 1985; Gutscher et al., 2000). Magmatism will be summarized in the next section.

The Montezuma Stock and Tertiary Magmatism

The middle Tertiary aged Montezuma stock covers 40km² or 32% of the surface of the district as mapped by Lovering (1935). Intrusions of similar age are common in the Colorado Mineral Belt, and magmatism of this time is found to be linked to ore mineralization. Based on zircon fission-track data, Cunningham et al. (1994) have determined that the Montezuma stock is 35.0±3.2 Ma which is within the

40.0 to 35.0 Ma range found by previous investigators (Simmons and Hedge, 1978; Bookstrom et. al, 1987; McDowell, 1971). The stock is a sub-alkaline quartz monzonite composed of coarse grained 1 – 3 cm white-pink orthoclase within a finer equigranular 0.2 – 0.5 cm plagioclase, quartz and biotite.

Tertiary magmatism in the Front Range has been divided into three groups based on chemical composition: 1. a silica-saturated, high-alkali, monzonite suite; 2. a silica-oversaturated, granodiorite-quartz monzonite suite; and 3. an evolved alkali feldspar granite suite. The Montezuma stock falls in the second group, and similarly the stocks related to Mo porphyries at Climax and Urad-Henderson fall into this group. Isotope and REE data have concluded that granitoids of the COMB are dominantly from a crustal source (Stein and Crock, 1990). Magma generation in Climax-type systems are a function partial melting of lower crustal rocks followed by differentiation (Stein and Crock, 1990), possible mantle input (Stein et al., 1993) and upper crustal rock assimilation (Wallace, 1995). Partial melting of lower crustal rock is favoured by tensional stress regimes. The development of the Rio Grande Rift system provides the necessary stress conditions for this magma generation.

Cretaceous and Tertiary magmatism in the COMB has also been divided into three groups based on age: 1. 75 - 43 Ma 2. 43 - 18 Ma and 3. 18 - 0. Peak felsic magmatism occurred from 43-18 Ma (Chapin, 2012), which is when the Montezuma Stock was emplaced. This second group is termed Middle Cenozoic Magmatism. Chapin (2012) attributes this group to the rupture of the Farallon flat slab, which resulted in sinking of slab material. Earlier horizontal movement of the Farallon plate under Colorado inhibited melt production. The rupture of the slab allowed the sinking of slab material. The descending slab would then reach depths of the asthenosphere that permit melting of crustal material. This rupture is also proposed to explain the northeast to southwest propagation of magmatism in the southern Rocky Mountains and the COMB. The rupture induced a rollback of the slab to the south west as indicated by the temporal formation of caldera clusters in Colorado and New Mexico. This rupture-rollback process began during the transition from Laramide compression to subsequent Rio Grande extension, which may

explain how magma rose to shallow levels in a thickened Laramide crust. This may also provide clues to the unique nature of Mo concentration in intrusives of this time.

An understanding of the exact nature of magmatism in the COMB is still being developed. For example the interaction of slab rollback and magma generated during rifting could be better understood. Did rollback induce rifting or did Rio Grande Rifting induce slab rollback? What are the exact mechanics behind magma generation that predate slab rollback and rifting? Considering that the final product of this enigmatic magmatism can render world class mineralization of Au and Mo justifies the study of these petrogenetic processes.

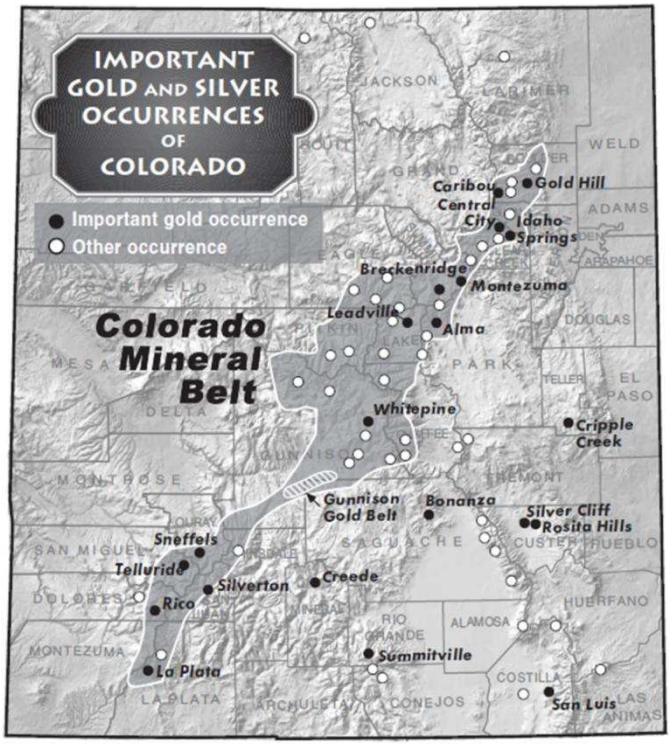

Figure 2.1.1 Mining districts within the Colorado Mineral Belt of Tweto and Sims (1963) including outliers. Image from Brchan et al. (2003). Note significant outliers include the world class gold deposit at Cripple Creek.

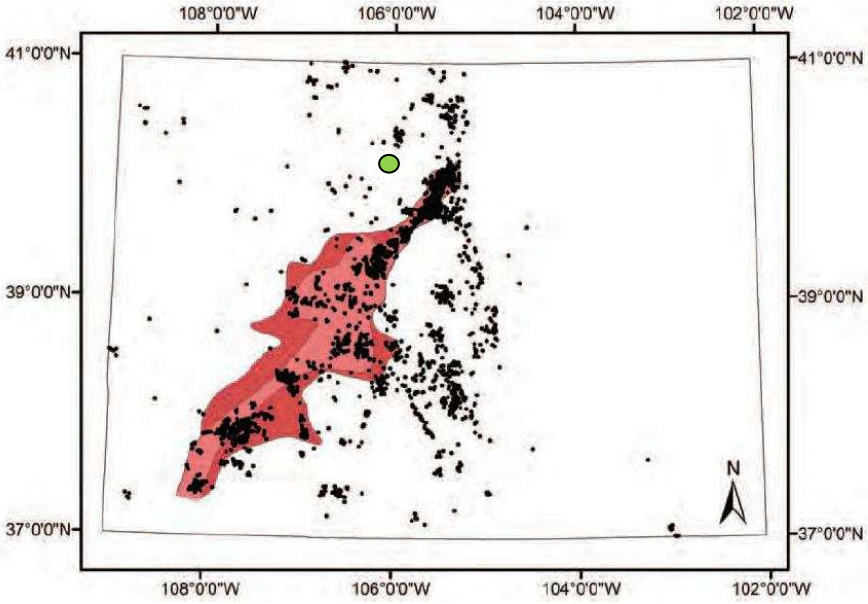

Figure 2.1.2 Map comparing total mineral deposits (black points) according to the the USGS Mineral Resource Data Base and the proposed Colorado Mineral Belt (red region). Note that many deposits do not lie within the COMB. The green point is the approximate location of Montezuma. Modified from Matthews and Morgan (2012).

3. Cordilleran Polymetallic Veins

Veins bearing variable amounts of Pb-Zn-Cu-(Ag-Au) that are spatially related to felsic to intermediate magmatism are a distinct ore deposit class within the porphyry family of ore deposits. These deposits were of historic significance where selective mining of low tonnage – high grade material were extracted from fields where these ore bodies may occur in high numbers (Ridley, 2013), although there are several localities like Morococha (Peru) and Ouray (Colorado, USA) that continue to be economic. Well studied type localities for these deposits are Butte, Montana USA (Reed et al. 2013; Meyer et al., 1968), Casapalaca, Peru (Rye and Sawkins, 1974), Morococha, Peru (Catchpole et al. 2015; Catchpole et al. 2012; Catchpole et al. 2011;), Colquijirca, Peru (Bendezú and Fontboté, 2009), Central City, Colorado USA (Spry, 1987; Rice et al. 1985; Sims and Barton, 1962) with lesser studied occurrences in Bor, Serbia (Drew, 2005), Magma, Arizona USA (Hammer and Peterson, 1968; Gustafson, 1961), Bisbee, Arizona, USA (Bryant and Metz, 1966) and others. These deposits have been observed by researchers, miners and prospectors for many generations, but a formal title for these lodes has only recently been established. Sawkins (1972) first proposed the term Cordilleran deposits for active margin related magmatic-hydrothermal ores. He implied that this be a broad term including a wide array of affiliated deposit types, which are now placed into specific classifications. Fontboté and Bendezú (2009) specified by suggesting that these veins and carbonate replacement ore be placed as a distinct deposit class within the porphyry system. The authors proposed the terms Cordilleran or Butte-type veins and replacements. Other authors have termed these deposits polymetallic vein fields (Ridley, 2013; Drew, 2005), base metal lodes (Bartos, 1989; Einaudi, 1977), zoned Cu-Zn-Pb-Ag deposits (Petersen, 1970) and subepithermal vein Zn-Cu-Pb-Ag±Au (Sillitoe, 2010). The term Cordilleran-type veins will be applied in this study because this seems to be the most commonly used term in literature and to reflect the charm of the alpine environment in which the Montezuma mining district and many analogue districts are found.

The formal study of this class may be attributed to Sawkins (1972) and Einaudi (1977), in their efforts to establish their identity and their geologic framework as a distinct ore deposit class. The following characteristics are commonly used to define this deposit class. Districts are found in close association with calk-alkaline felsic intrusives (Sawkins,1972). Ores are polymetallic Cu-Zn-Pb-(W-Sn)-(Ag-Au-Bi) and are deposited by late stage fluids relative to associated magmatic bodies and associated hydrothermal activity. Veins are deposited in the upper crust from 200-3000 m below the paleosurface (Bartos, 1989). Ag/Au ratios are notably higher than high-sulfidation epithermal Au-Ag mineralization (Fontboté and Bendezú, 2009). Ore bodies occur as open space fissure fillings termed lodes or veins and as mantos and chimneys replacing carbonate rich strata termed replacement bodies. The Montezuma mining district is dominated by fissure fill lodes, and therefore this review will place an emphasis on geologic controls of Cordilleran-type veins rather than their akin carbonate replacement ores. The above characteristics are consistent among Cordilleran veins while the following characteristics are less-consistent yet very common among deposits globally: well-developed metallic zonation and a link to mineralized porphyries are both common among many known Cordilleran-type deposits, but are not ubiquitous. For example, at Butte, Cordilleran-type veins (termed the Main Stage veins) overprint parts of an earlier Cu-porphyry stockwork (Meyer et al., 1968). The overprinting nature also reflects the late-stage nature of these veins relative to porphyry type mineralization. Contrary to Butte, at Central City there is no proven link to underlying mineralized porphyries, but is suggested by Rice et al. (1985).

Skarns and epithermal veins are both spatially and genetically related to Cordilleran-type veins. Skarns are distinguished from Cordilleran-type veins by their proximal location to porphyries, ore body geometries and unique textures. Also the timing of ore deposition in skarns tends to be closer to that of the of associated porphyries rather than the late timing of the Cordilleran polymetallic veins (Catchpole et al., 2012). Therefore these deposits will be considered, but will not be the focus of this review. The distinction of epithermal veins and Cordilleran-type veins is less obvious. The Main Stage veins at Butte are a deeper hotter variant of epithermal veins that apparently formed from the same primitive fluid, but at

a greater depth (Sillitoe, 2010; Reed et al. 2013). Thus epithermal and Cordilleran-type veins are both from an evolved fluid, yet the degree of chemical evolution of from a magmatic fluid may be the distinction. This relationship will be the favoured interpretation for Cordilleran-type veins in this review. Geochemically, the high base metal content and higher Ag:Au ratios of Cordilleran veins serve as distinguishing features from epithermal Ag-Au veins. Figure 3.0.1, from Sillitoe (2010), will be the favoured model for distribution of ore and relation to magmatism. This image depicts the array of ore deposit types found in the porphyry family of ore deposits where subepithermal veins are Cordilleran-type veins.

3.1 Ore Body Geometries

Ore bodies are commonly steeply dipping and planar reflecting mineral fill of structural weaknesses found in orogenic belts. These structural weaknesses are ubiquitously reactivated during mineralization, concentrating fluid flow along established channelways. Ore veins can range from a few centimetres to several meters in width (Ridley, 2013) and strike lengths for historically economic veins range from 200 m to 3,000 m. The vertical extent of veins is commonly no more than 800 m (Lovering, 1935), but are greater at Butte (Meyer et al., 1968). Their shallow depth of emplacement (Sawkins, 1972) renders them susceptible to erosion. This implies that these deposits are unlikely to be preserved in the geologic record. Evidence for this can be found at Montezuma and Breckenridge (and certainly other districts) where near-surface shallow enrichment zones exist of secondary silver minerals and gold (Lovering, 1934). Although, it should be noted that significant supergene enrichment may be limited by glaciation and steep topography (Lovering, 1934), which may be a theme in districts located in high altitude environments with ample precipitation.

Ore body geometries observed in Cordilleran-type veins imply that mineralization is highly structurally controlled. At the Magma mine in Arizona (USA), a correlation was made between width of a vein and bonanza grades found in wider segments (Guilbert and Park, 1986). This correlation is most

likely a result of precipitation mechanisms related to fluid depressurization in a fracture that abruptly increases in volume. Regions of greater volume in veins are commonly found at intersections of major brittle structural features or along zones of increased dilation along a single brittle feature. At Butte, Reed (1999) observed horsetail ore as a master vein splays into numerous subsidiary veins at depth. This is attributed to the deformation mechanics found at a transition from a brittle unaltered quartz monzonite and a more ductile quartz-sericite-pyrite altered equivalent. These geometries present a fundamental distinction between their akin carbonate replacement deposits. Wall rock chemistry has less of an influence on the precipitation of ore in Cordilleran-type veins than replacement deposits and skarns, which are dependent on carbonate wall rock chemistries. Although, it will be revealed later that wall rock alteration can influence buffering capacities, which are linked to abnormalities in zonation patterns on a district scale.

3.2 Hypogene Mineralogy and Alteration

Mineralogy and Paragenesis

Veins of the Cordilleran-type host Cu-Zn-Pb-(W-Sn)-(Ag-Au-Bi-As) as sulfide and sulfo-salt mineral assemblages. Gangue minerals are quartz, a variety of carbonates, pyrite, sulfates, clays and sericite. Veins in many ore fields record a systematic succession of ore fluids. Multiple episodes of refracturing with subsequent mineral fill is a constant in these veins. Depending on the location of a vein in a district, it is possible to reconstruct the paragenesis of the entire ore field (Catchpole et al., 2011). There is a common, but not ubiquitous, succession of mineral fill and associated wall rock alteration in the veins of this type: early pyrite-quartz fill with sericite alteration and later base metal-silver mineralization with advanced argillic alteration. In addition to the two general stages, carbonate stages are observed at any time after the early quartz pyrite stage. Copper mineralization is typically slightly earlier than other metals (Catchpole et al., 2012). Silver mineralization is commonly observed as a contemporaneous stage with base metals or as a later stage.

An early quartz-pyrite stage is very common in Cordilleran-type vein fields. Vughs are commonly preserved in which subsequent mineral infill can occur. At Cerro de Pasco (Einaudi, 1977), pyrrhotite occurs in this stage within parts of the district that are subjected to lower sulfidation states. This quartz-pyrite (or pyrrhotite) stage marks the beginning of Cordilleran mineralization and the end of porphyry-type mineralization. Following this stage, a composite base and precious-metals stage occurs. The Main Stage veins at Butte Montana are the type locality for this composite base and precious-metal stage, and many analogue districts in North America have adapted the Main Stage title for this period of mineralization in the paragenetic sequence (Meyer et al., 1968; Musgrave and Thompson, 1991; and others). The order of metal mineralization is variable, but copper tends to predate all other base metals. Copper can occur as enargite, tennantite-tetrahedrite, chalcopyrite or bornite depending on sulfidation state of the hydrothermal fluid at the point of copper mineralization. Sphalerite may occur slightly before galena, but the lead and zinc mineralization is more or less contemporaneous. Sphalerite is commonly found with chalcopyrite guest, while galena is more likely to be a host to silver (eg. argentite) or bismuth (eg. bismuthinite) minerals. A large array of silver sulfo-salts and sulphides occur in theses veins in addition to native silver.

In addition to the early quartz, other gangue minerals include carbonates and sulfates. At many deposits, rhodochrosite is an abundant carbonate, but calcite, ankerite and siderite are also found. Barite, anhydrite and other sulfates exist when sulfidation states or pH conditions are appropriate to facilitate their mineralization. In deposits associated with magmas of higher alkalinities (eg. Sweet Home and the veins near Urad-Henderson), fluorite is a common gangue mineral.

Alteration

Phyllic, argillic, advanced argillic and propylitic alteration assemblages are observed along margins of Cordilleran veins. Solution acidity plays an important role in wall rock alteration. Phyllic wall rock alteration in association with an early quartz-pyrite fissure fill assemblage is documented at

most Cordilleran-type vein districts including Montezuma. Locally pervasive phyllic alteration results when an acid hypogene hydrothermal fluid and a host rock are brought closer to equilibrium. This may be achieved by a hydrolysis reaction involving potassium feldspar and H^+ yielding sericite + quartz + potassium (Guilbert and Park 1986):

$$3KAlSi_3O_8 + 2H^+ (aq) \rightarrow KAl_3O_{10}(OH)_2 + 6SiO_2 + 2K^+ (aq) \qquad \text{(Eq. 3.1)}$$

It follows that as a wall rock is subjected to this reaction or other fluid neutralizing reactions, the altered wall rock becomes less effective in buffering later hypogene hydrothermal fluids. Therefore, future ore bearing solution may to travel with a low pH further away from its source. It also follows that phyllic alteration should be more intense in proximal regions of the fluid source than in more distal regions. These two implications can have significance in the interpretation of the evolution of the hydrothermal solutions in a mining district.

The Main Stage veins at Butte, exhibit a consistent zonation of alteration away from the mineralized vein from phyllic to argillic to propylitic to fresh country rock (Meyer et al., 1948). Figure 3.2.1 summarizes the chemical changes in wall rock alteration along a perpendicular transect from a Main Stage vein margin to fresh wall rock. Notable leaching of CaO, MgO and Na_2O occurs in this example while K_2O and Al_2O_3 are relatively unaffected. Bartos (1989) also notes an overprinting sequence at Quiruvilca, but from propylitic to argillic to sericitic and finally to advanced argillic. Therefore, the alteration succession is not entirely uniform in these veins in all districts. Two explanations exist for these different zonations and overprinting patterns: 1. progressive equilibration with a wall rock or 2. differing equilibrations between wall rock and a hydrothermal fluid whose composition evolved with time. The latter is favoured by Bartos (1989) based on observations of cross cutting relationships of veinlets at Quiruvilca and Cerro de Pasco. The interpretation is that the alteration fluid progressed from sericite-quartz stable to clay-quartz-carbonate stable with an accompanied decrease in temperature, increase in hydrogen ion activity and change in sulfidation state (Bartos, 1987). Bartos (1989) notes that at Central City (Sims, 1983) and Quiruvilca (Bartos, 1987) early quartz-pyrite veins are associated with

zoned sericitic-argillic-propylitic alteration halos, while later copper mineralization is associated with advanced argillic alteration. This presents a two phase alteration history. Initial early stage quartz pyrite veins are associated with a sericite alteration that is flanked by argillic and propylitic alteration as the hydrothermal fluid diffuses cools and equilibrates with the wall rock during their first phase. The second phase of alteration is introduced during base metal mineralization, which can overprint the quartz-pyrite mineralization. The advanced argillic alteration is the product of a more acid fluid associated with this second base metal phase. Therefore a more neutral fluid (relative to the latter fluid) is overprinted by a more acid fluid in this general model.

Although, the development of wall rock alteration in these systems is complex, there are known systematics regarding temperature decline and pH. This succession of vein minerals and alterations reflect the evolution of hydrothermal fluids related to waning stages of pluton emplacement. Reed et al. (2013) have found that a magmatic fluid is neutral at temperatures above 550°C, but will become acid at lower temperatures due to disproportionation of SO_2:

$$SO_2\,(aq) + H_2O\,(aq) \rightarrow \qquad \text{(Eq. 3.2)}$$

$$1\tfrac{1}{2}\,H^+(aq) + \tfrac{3}{4}SO_4^{2-}\,(aq) + \tfrac{1}{4}\,H_2S\,(aq)$$

Figure 3.2.3 depicts the computed pH gradients in relation to temperature and pressure, which are the results from varying progress of the above reaction with temperature decline. This process can explain the observed succession of porphyry alteration facies as pH decreases in later stages of porphyry evolution. The acid fluid depicted in the sericitic box of Figure 3.2.3 is the proposed parent fluid for subsequent Cordilleran-type veins. Cooling linked to pH decrease explains the systematic cross cutting relationships of veinlet and alteration overprints in porphyry systems (eg: phyllic and D-veins overprinting potassic and A-type veins) and can be applied to wall rock alteration in Cordilleran-type veins. The understanding of fluid evolution of the parent magmatic fluid helps to better develop knowledge of the later Cordilleran-type vein and epithermal vein systems. The decrease in pH due to processes detailed above will be the used in the model discussed in Chapter 7.

Based on this model, there should be a district scale zonation of alteration assemblages. At Butte, cooling of the parent fluid to less than 380°C yields an acidic fluid with a pH less than 2 (Rusk et al., 2008). As water/rock ratios increase, alteration envelopes evolve from advanced argillic to sericitic (Figure 3.2.4) (Reed et al., 2013; Meyer et al. 1968). In this figure "ω" represents the path of Main Stage fluids with regard to alteration as a function of temperature and water/rock ratios. With decreasing temperature and decreasing water/rock ratios, a Cordilleran-type fluid should in theory produce a succession from advanced argillic to argillic to sericitic alteration as the fluid is buffered. If water/rock ratios increase (with assumed temperature decline), the succession will be from sericite to argillic assemblages. Presumably this concept would apply to district scale and deposits scale zonations. Overprinting fluids can complicate mapping efforts, but a measurement of a bulk ratio of sericite to clays along alteration halos of veins could possibly reveal an increase in relative abundance of sericite in distal veins, while veins in closer the center of the district would have higher amounts of clay minerals. Also, as seen from Figure 3.2.4 the precipitation of gangue carbonate may be explained as a result of the system becoming rock buffered. Key conclusions from Reed et al. (2013) are that as a pluton wanes, pH of generated fluids decreases, but as the acid fluid migrates pH will increase as it will be buffered by wall rock interaction.

3.3 Zonation

District scale zonation of metals in Cordilleran veins is observed at Morococha (Catchpole et al. 2011, Catchpole et al., 2012), Butte (Rusk et al., 2008), Casapalca (Rye and Sawkins, 1974), Julcani (Goodell and Ulrich, 1974), Colquijirca (Bendezú and Fontboté, 2009), Central City (Sims and Barton, 1962) and at Montezuma as well as other districts of this type. Much emphasis is placed on zonation and spatial distribution of minerals because this characteristic can reveal much about fluid evolutionary paths and can potentially reveal mineralized porphyry prospects. Cordilleran-type vein fields are known to be less systematically zoned than their akin carbonate replacement ores (Fontboté and Bendezú, 2009)

which, could be due to a higher rate of structural control rendering spatially variable travel distances of ore bearing solutions.

Zonation is typically defined with regard to metals, but districts also show systematic variation in gangue and alteration minerals, which are equally important clues in establishing zones. Researchers have developed a multitude of methods to identify boundaries of each zone, which will be detailed below. Varying zonation configurations exist among deposits globally, but there are patterns that are consistent among most vein fields. Three general zones based solely on metal contents are found at most Cordilleran vein fields: a Cu-rich core, an intermediate zone with higher Zn and an outer zone where Pb-Zn-Ag are the major ore metals. In some deposits a distal Au-Ag zone also exists, which may reflect a transition from Cordilleran-type veins to epithermal mineralization. Figure 3.3.1 from Fontboté and Bendezú (2009) has been produced to depict metals and temperature gradients as a fluid cools away from a source cupola. Each progressive range of temperature decrease renders solubility declines of particular metals. It should be noted that simple cooling by wall rock conduction is not the only mechanism of ore mineral precipitation, and hence Figure 3.3.1 is only a generic model. Many sub-divisions can be made within this framework based on the resolution of data within a district, or conversely lumping can occur when a district displays a weak zonation. Fontboté and Bendezú (2009) have defined a spectrum from weakly zoned deposits to strongly zoned fields. "Strongly zoned deposits have cores of enargite, pyrite, quartz ± (tennantite, wolframite, chalcopyrite, covellite, alunite, dickite, kalonite) and an external part with Fe-poor sphalerite, galena ± (sericite, kaolinite, dickite, hematite, siderite). Weakly zoned deposits consisting of internal parts bearing pyrrhotite, pyrite, quartz ± (chalcopyrite, arsenopyrite, tetrahedrite, carbonates, sericite, chlorite, quartz) and external parts of Fe-rich sphalerite, galena, pyrrhotite ± (rhodochrosite, siderite and other carbonates, sericite, chlorite, quartz)."

Several variables additional to temperature potentially influence the Cordilleran vein environment including sulfidation state, pH and meteoric water dilution. These additional variables are likely responsible for particular mineral assemblages, while temperature is considered to be the main control on

metal ratios. Note that overprinting of earlier assemblages by later assemblages is a common occurrence thus depth, timing, cooling and possible magmatic resurgence are key variables in fluid evolution, which in turn will alter zonation patterns.

Cu Core

Copper ore minerals in Cordilleran-type veins are chalcopyrite, bornite, enargite, tennantite-tetrahedrite and chalcocite. These minerals tend to be in higher relative abundances within central regions of many districts. In districts with known links to mineralized porphyries, the Cu core either overprints the porphyry mineralization (eg. Butte, Reed et al., 2013) or is directly marginal to porphyry mineralization (eg. Bingham Canyon in Utah, Babcock et al., 1995; Park in Arizona, Lang and Eastoe, 1988). The position of a Cu core can be used as an exploration guide for potential associated mineralized porphyries. Pyrite or pyrrhotite is commonly in higher abundances in the core relative to other zones, which is observed in the Montezuma district. Some authors have used the succession of copper minerals within the Cu core to determine the sulfidation state of ore forming fluid as it passed through the district (Bendezú and Fontboté, 2009; Bartos 1989; Catchpole et al., 2012). At Morococha for example, the center of the core is dominated by enargite, while marginal regions of the core are dominated by tennantite and chalcopyrite (Catchpole et al., 2012). This reflects a decreasing sulfidation state of the hydrothermal fluid. This is not a ubiquitous trend in Cordilleran-type deposits, but it does show how systematic mineral studies can reveal much about fluid evolution and subsequent zonation. Alteration associated with vein mineralization in the core is found to be pervasive and intense phyllic and/or advanced argillic (Einaudi, 1977). Ore stage fluids responsible for this zone are found to be at temperatures greater than 350°C (Bendezú and Fontboté, 2009).

Zn-Cu Intermediate Zone

This zone reflects a transition from copper dominated mineralization to lead-silver mineralization. The appearance of sphalerite is used an index mineral for this zone. Cu+Zn weight percentages are

typically greater than Pb+Ag weight percentages for this zone. Sphalerite is the dominant zinc mineral in most ore fields. Attention to red, green and marmatite varieties of sphalerite and their distribution across an ore field can be used to determine the sulfidation state of an ore fluid. Fluids responsible for mineralization are from 250°C to 350°C (Bendezú and Fontboté, 2009). As the fluid reaches the outer margins of this zone, much of the copper has been remove from the hydrothermal solution.

Pb-Zn-Ag Outer Zone

This zone is found in the outer reaches of a district (assuming a lack of distal epithermal veins). At this point temperatures are cool enough to precipitate Pb-Ag minerals and the remaining Zn. Dominant mineralization temperatures are from 150°C to 250°C (Bendezú and Fontboté, 2009). Lead is removed from solution by the precipitation of galena. Silver can be precipitated as a guest in galena or as Ag bearing sulphides or sulfo-salts.

Temperature Decrease and Metal Solubilities in Hydrothermal Fluids

There is an overall decrease in metal content of the hydrothermal fluid with decrease in temperature, which reflects the corresponding precipitation sequence of metals in veins (Catchpole et al., 2011; Beuchat et al., 2004). This has been proven by district scale metallic zonation and the application of microthermometry and LA-ICP-MS to fluid inclusions from porphyry related polymetallic vein fields (eg. San Cristobal, Beuchat et al., 2004). Woitsekhowskaya and Hemley (1995) have produced a comprehensive integrated model detailing metal transport and deposition of Butte-type hydrothermal systems. The application of the model is perhaps affected by unknown or poorly understood variables, but it still serves to explain metal patterns found in these systems. Figure 3.3.2.A displays the solubility of metals considering variable temperature and metal molality. 1 *m* total chloride and 0.05 *m* H_2S are the assumed ligands, and were chosen to reflect those found in these systems. Additional ligands and transport mechanisms may exist, but the results in 3.3.2.A exemplify how decreasing temperature renders the progressive precipitation of metals and disasociation of ligands. Surely the interplay of other

variables such as varying molality of metal ratios with precipitation and pH decrease are at play in this Cordilleran environment, but the fact remains that with decreasing temperatures there is a decrease in solubility of metals. The horizontal segments of curves reflect metals in transport and the inflection points where the curves sharply decline in slope indicate the progressive depletion of the metal from solution by means of precipitation. The succession is as follows: Fe, Cu, Zn and finally Pb. Figure 3.3.2.B graphs the temperatures of precipitation of sulphides in this system. For galena, sphalerite and chalcopyrite there is an initial spike in precipitation followed by long decline in precipitation rates. These curves explain why sphalerite is intermediate in zonation between chalcopyrite and galena in most paragenetic sequences and in district scale zonations. The concurrence of sphalerite and galena curves explains the near equal proportions of sphalerite and galena in ores where conditions are appropriate. It should be noted that this model predicts precipitation at higher temperatures than observed in fluid inclusion data. Woitsekhowskaya and Hemley (1995) have explained this by indicating that the low pH of the model fluid will inhibit precipitation to lower temperatures.

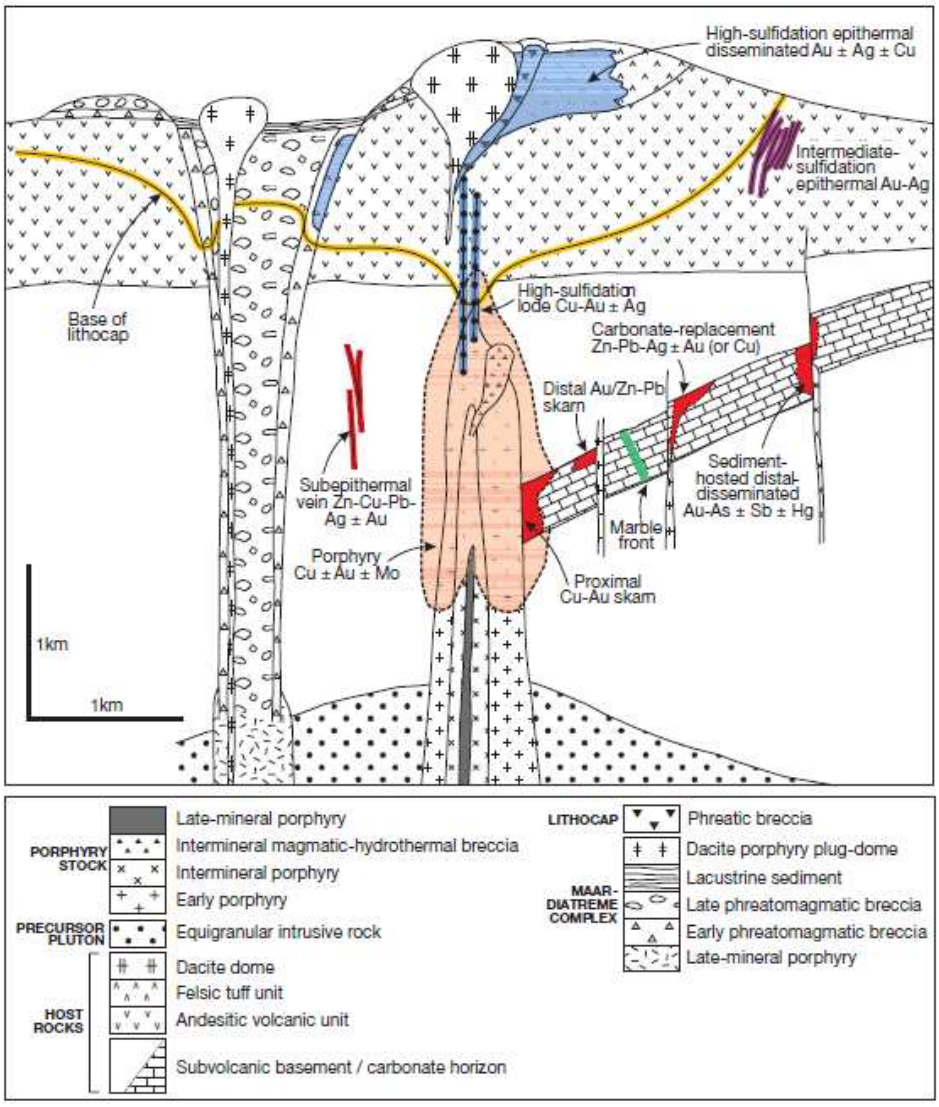

Figure 3.0.1 from Sillitoe (2010). Cartoon model depicting the array of ore deposits found in the magmatic-hydrothermal environment. Subepithermal vein Zn-Cu-Pb-Ag±Au are equivalent to Cordilleran-type.

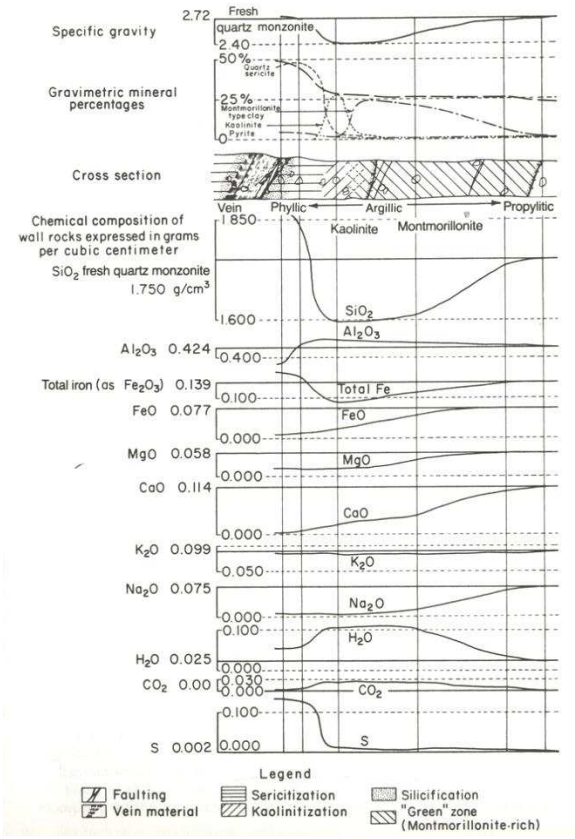

Figure 3.2.1 from Sales and Meyer (1948). Succession of alteration facies and associated chemical attribution with distance from mineralized Main-Stage vein from Butte Montana. CaO, MgO and Na_2O become progressively leached with increasing intensity of alteration to the left on the figure. K_2O and Al_2O_3 are relatively unaffected. The scale of this alteration can range from centimeters to tens of meters.

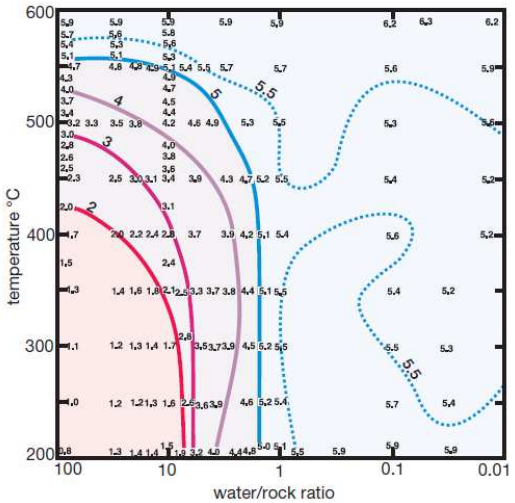

Figure 3.2.2 from Reed et al. (2013). Computed pH as a function of temperature and water/rock ratio. Colored lines are iso-pH curves plotted with respect to the numerical pH value. pH values are highly acidic at lower temperatures and high water/rock ratios (red shading) and neutral at all high temperatures and at low water/rock ratios (blue shading).

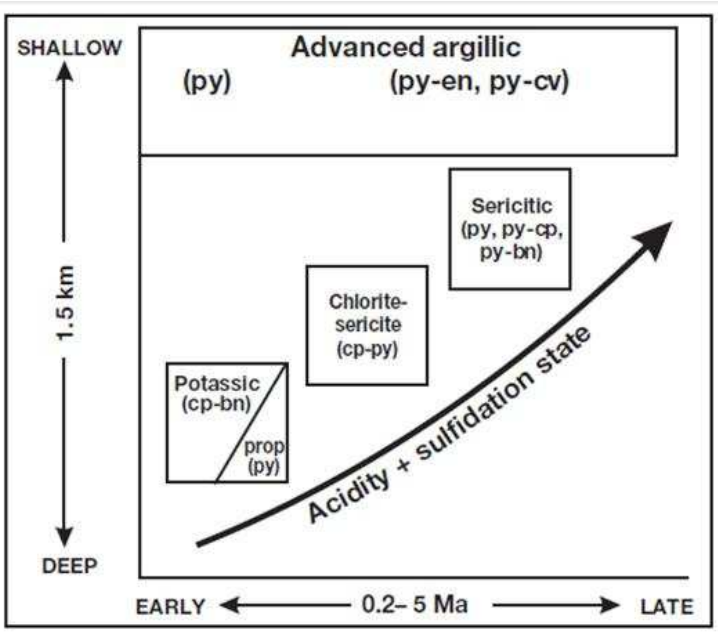

Figure 3.2.3 from Sillitoe (2010). Generalized alteration mineralization sequence in porphyry Cu deposits with regard to timing and depth.

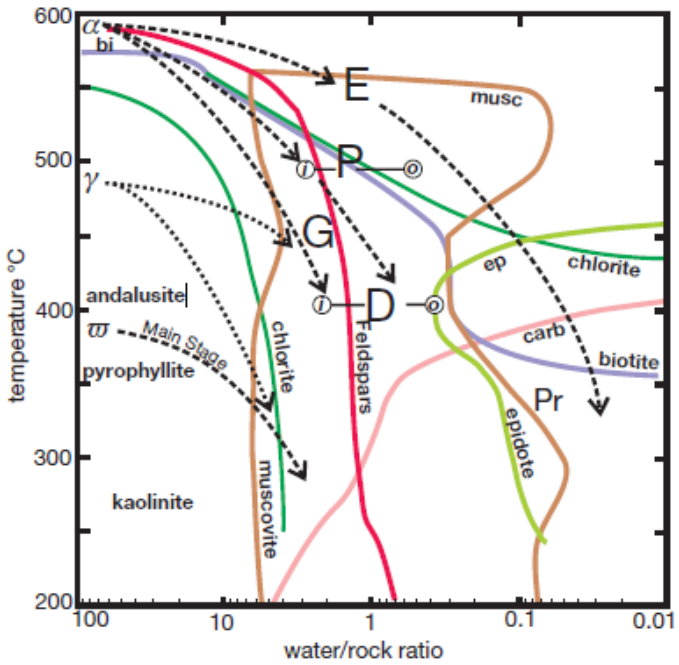

Figure 3.2.4 from Reed et al. (2013). Mineral stability relative to temperature and water/rock reaction ratios. Dashed lines are fluid reaction trajectories and alteration mineral assemblages found at Butte and other porphyry copper deposits. ω refers to a fluid that has been strongly cooled and depressurized (relative to fluids α and γ). This trajectory many may explain alteration envelops around Cordilleran veins. High water rock ratios are render argillic alteration while decreasing water rock ratios favor sericite and chlorite.

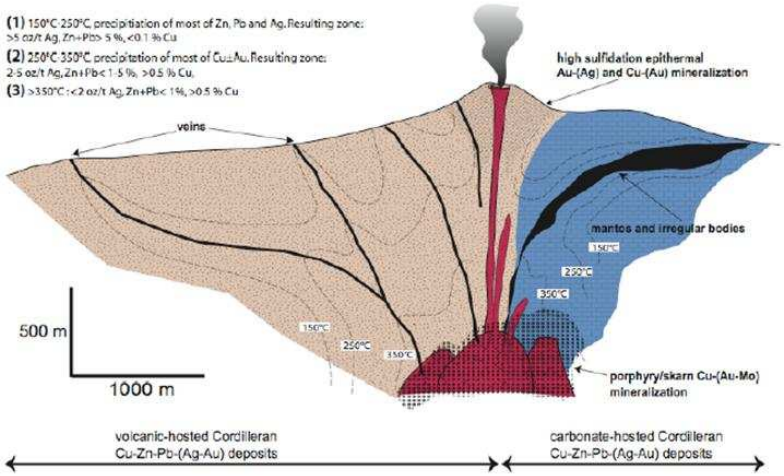

Figure 3.3.1 from Fontboté and Bendezú (2009). Schematic position of Cordilleran polymetallic deposits and other porphyry-related ore deposit types with reference to thermal gradients and metals precipitated.

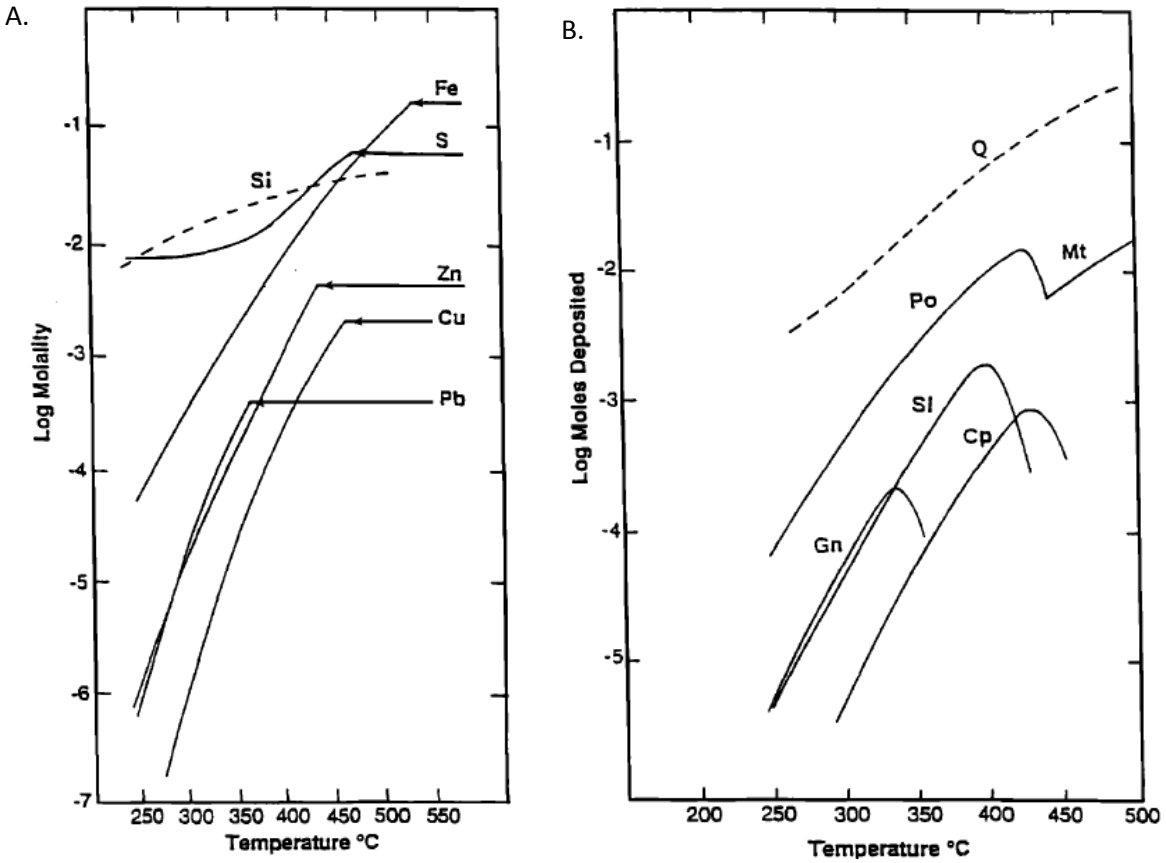

Figure 3.3.2 from Woitsekhowskaya and Hemley (1995). (A) Calculated metal solubility or precipitation curves in a system with the same initial metal concentrations and buffered in pH by K feldspar-muscovite-quartz at 1 kbar an 1 *m* total chloride. (B) Quantitative depositional curves for the minerals corresponding to (A), log moles/kg H_2O for each 25°C temperature decrease. Abbreviations: Q = quartz, Mt = magnetite, Po = pyrrhotite, Cp = chalcopyrite, Sl = sphalerite.

4. Ore Bearing Veins and Alteration of the Montezuma District

In this study, 93 Samples were taken from mine dumps, walls of abandoned adits and outcrops. All 93 samples were slabbed for better interpretation of ore textures and paragenetic studies. Of these 93 samples, 26 were cut and mounted as doubly polished sections with a thickness of 100μm. Polished section samples were selected based on perceived fluid inclusion potential and location within the district. Each section was photographed and observed for textures of interest before preparing the samples for fluid inclusion heating and cooling. Ore petrographic data from this study was then compared to Lovering (1935) in order to produce the following summary of ore mineralization in the Montezuma District.

Polymetallic veins in the Montezuma district were mined for Pb-Zn-Ag-Cu-Au from the 1860s until the 1980s with the closure of the Burke Martin mine. Over eighty mines existed in the district. Each mine may have exploited one to several veins. Average grades from veins mined between 1870 and 1935 were: 1744 g/t Ag, 22% Pb, 7.9% Zn. Depending on mining method and spatial frequency of bonanza shoots in veins, some mines like the Revenue mine of Cinnamon Gulch averaged over 7,000 g/t Ag. Veins that produced significant copper and gold contained average grades of 6 g/t Au and 2.82% Cu. At the time a grade of 6g/t Au would render this metal a by-product rather than a co-product. Sphalerite and galena are the primary Pb and Zn minerals; tennantite-tetrahedrite and chalcopyrite are found to be the dominant copper minerals; while proustite-pyrargyrite are the most common silver sulfo-salts. Gangue minerals include quartz, pyrite, ankerite and barite. Mineralization occurs as fissure fill of structural weaknesses in host rocks.

Veins of the district are commonly planar features ranging from 300 m to 2,600 m along strike. Most veins strike northeast with steep dips to the west, but some veins strike east and northwest veins can also be found in the district (Lovering, 1935). Mined veins varied in width from 5 cm to 38 cm. These

are fissure fill features occupying Laramide and post-Laramide deformation structures. The veins exhibit a succession of 5 identifiable stages of mineralization from early quartz-pyrite, barite and incipient base metals, base metals, carbonate infill and overprint to a final silver-lead mineralization with quartz infill.

4.1 District Scale Alteration

The veins are superimposed on district wide alterations mapped by Neuerburg et al. (1974) (Figure 4.2.2). Propylitic and vuggy quartz-sericite are two alteration facies that are widespread in the district, and are not limited to the margins of mineralized vein. The presence of these facies opens the discussion of extensive diffuse or microfracture controlled fluid flow or circulation throughout the district in addition to the narrow structurally controlled fluid flow associated with vein mineralization. The presence of this widespread alteration suggests that more fluids than those that migrated in Cordilleran-type veins migrated in the district.

Propylitic

Propylitic assemblages are the most widespread alteration in the district. Neuerburg et al. (1974) found that surficial rusty to bleached colored rock is a supergene weathering product of a hypogene assemblage of chloritized biotite and moderately sericitized plagioclase with an addition of carbonate, pyrite and geochemically variable addition of zinc. This rusty to bleached color is visible from satellite imagery (Figure 4.2.1) and is distinct in regions above treeline (Figure 4.2.3.A and 4.2.3.B). Figure 4.2.3.C is an example of how this alteration appears at outcrop scale. The alteration zone runs in close association, yet irregularly, with the Montezuma shear zone running from the head of Hall Valley and striking 12,180 m to the northeast were the alteration terminates along the southern flank of Grays Peak. The width of the alteration zone is highly variable from 466 m to 2,800 m with an east-west to northwest spurs in the area of Silver Mountain, which roughly correlate with a east-west spur of the Montezuma shear zone.

Vuggy Quartz-Sericite

In plan view, this alteration is found as circular regions that are 250 m – 900 m in diameter, which overprint areas of propylitic alteration (Figure 4.2.2). Neuerburg et al. (1974) distinguishes this zone of alteration by the conspicuous vugs lined with muscovite, quartz and pyrite. The paper further details that this is comparable to what is locally called bug-hole porphyry at the Urad-Henderson molybdenum mine, and it is interpreted to identify major conduits of hydrothermal plumbing. This alteration only occurs in the Cu-rich zone of the district (Figure 5.2.8), and is confined to within fields of propylitic alteration.

4.2 Vein Paragenesis

The mineralized polymetallic veins of the Montezuma mining district show a relatively consistent paragenetic sequence, which can be organized into stages. The stages are based on timing of particular mineral assemblages as indicated from petrographic and hand sample analysis. After a review of 24 doubly polished samples, 93 slabbed samples and of previous literature (Lovering, 1935) the following 5 stages have been identified with a questionable 6^{th} stage of mineralization (Figure 4.3.1). The paragenetic sequence is as follows: Stage 1 early quartz-pyrite, Stage 2 barite and incipient base metals, Stage 3 base metals, Stage 4 carbonates, Stage 5 Pb-Ag and quartz and finally the questionable Stage 6 late copper. Two general vein types have been identified in the district based on presence or lack of Stage 2 barite and Stage 4 carbonate (Figure 4.3.2). Type one veins tend to be richer in pyrite and lack significant Stage 2 barite and Stage 4 carbonate mineralization. Type two veins have abundant barite and carbonate and are located in a zonal arrangement marginal to Type one veins. The distinction reflects a spectrum from pyrite dominant to barite-carbonate dominant veins.

Stage 1: Early quartz-pyrite

Quartz-pyrite is the first mineral assemblage to fill fissures, and this early event is commonly accompanied by phyllic alteration of adjacent wall rock. In some veins, it has been observed that quartz

is slightly earlier than pyrite as pyrite can be found as triangular acute angle infill in quartz interstitial sites (Figure 4.3.2.A), but in many veins the minerals are contemporaneous. Infill quartz is milky to clear in color, and from microcrystalline to coarse crystalline of several millimetres in grain size. Clear coarse grained euhedral comb quartz is very common along vein margins with wall rocks (Figure 4.3.2.B). After comb quartz has established itself, subhedral to granular sub-millimeter scale quartz infills the space between the comb quartz. Pyrite is more likely to be euhedral when contemporaneous with quartz, and is subhedral to granular when later than quartz. Pyrite can be found as 0.1 cm to 1.0 cm striated euhedral cubic crystals or as centimetre scale aggregates of massive pyrite. In many instances these infill textures are overprinted by subsequent mineralization events. Pyrite is commonly partially replaced by later sulphides and early quartz is partially overprinted by later carbonate alteration. Vugs or incomplete infill are ubiquitous in this stage and serve as potential sites for later mineralization.

A pervasive fine grained quartz-sericite-pyrite alteration of proximal wall rock is associated with this vein stage. This assemblage fits in the phyllic classification, and is consistent among Cordilleran-type vein deposits. Sericite occurs in irregular white to pale green masses with very fine less than 50 μm isolated anhedral pyrite grains along with equally fine grained quartz. Lovering (1935) summarizes that iron, potassium, silica, and sulfur were added to the wall rock during this alteration event. However, clay is also observed directly along margins of veins (Figure 4.3.3.A), which could be associated with this stage or could be an overprint.

Lovering (1935) notes that near the end of this stage of mineralization there was a widespread brecciation event. During this event local manganosiderite precipitation occurred on Glacier Mountain in the deeper portions of veins. This carbonate precipitation was not observed in this study.

Stage 2: Barite and incipient base metals

Barite growth occurs directly before widespread base metal mineralization and continues into the phase of base metal mineralization. Barite occurs as white very coarse 1 – 2 cm blades (Figure 4.3.4),

which are commonly twinned. In many instances, large barite crystals are fractured due to later brecciation. Barite mineralization is abundant yet local in nature. There is a rough zonal arrangement of veins bearing barite in abundance about what is inferred to be the center of the copper-rich zone and along the Montezuma shear zone.

In many instances base metal mineralization is after barite, but at a few mines it is contemporaneous. This is why this stage has been termed "incipient base metals," with reference to low amounts of sphalerite and chalcopyrite precipitation during this stage. Gold mineralization also accompanies this stage and occurs as small grains in chalcopyrite (Lovering, 1935)

Stage 3 Base metal mineralization

Sphalerite infill with chalcopyrite exsolution occurs directly after coarse bladed barite (4.3.4.A) if barite mineralization is present. In barite ore, sphalerite grows within interstitial vugs created by the irregular network of coarse barite blades. Sphalerite can be centimetres in scale depending on the availability of open space, but is more commonly found on the scale of several millimetres in smaller vugs. Chalcopyrite occurs as small blebs in sphalerite in a texture called chalcopyrite disease (4.3.5.B), along the rims of sphalerite grains (4.3.5.E), or as replacements of pyrite (4.3.5.F). Oriented chalcopyrite blebs along zonal growth boundaries are evidence that in some instances, chalcopyrite has grown contemporaneously with sphalerite (4.3.5.A). Chalcopyrite is commonly only several microns in scale, but can be several millimetres in scale when replacing pyrite grains or pyrite aggregates. Galena is noted to form contemporaneously to slightly later than the sphalerite-chalcopyrite mineralization (Lovering, 1935). Galena is found as large anhedral aggregates of finer grained crystals with well-developed cleavage planes. These aggregates are almost always infill, and replacement of any minerals by galena has not been observed.

In hand specimens, sphalerite is green, red or Fe-rich black marmatite in color. In the collected samples, a combination of green and red are the dominant colors. The combination is due to the varying

degrees of iron abundance in sphalerite crystals during growth: lighter green-white bands indicating less iron content and darker brown-red bands indicating higher iron content. The zonation is very clear in doubly-polished section. In some samples (4.3.5.D) the growth zones are regular and systematic, while in others the zones are less regular (4.3.6.B). A general trend from high-Fe sphalerite at nucleation sites to low-Fe sphalerite in outer portions of crystals has been noted. This could be a result of several controls: a decrease in Fe content of the initial hydrothermal fluid, a consequence of pyrite replacement rendering a local initial iron increase due to assimilation, or an increase in sulfidation state. Sphalerite appears to selectively replaces early pyrite (4.3.5.C) and utilizes early pyrite grains as sites for nucleation (4.3.5.D) in addition to filling fractures within pyrite grains (4.3.5.B). Based on these observations, it is hypothesized that early high-Fe zones in sphalerite are a function of excess iron from replaced pyrite. Therefore, the initial hydrothermal fluid responsible for sphalerite does not vary in iron content or changes in sulfidation state; rather assimilation of iron from Stage 1 pyrite has rendered these zonal bands. The following equations attempt to represent this replacement:

$$4FeS_2 + 3Zn^{2+} + 4H_2 \rightarrow 4Zn_{.75}Fe_{.25}S + 3Fe^{2+} + 4H_2S \qquad \text{(Eq. 4.1)}$$

and/or

$$2FeS_2 + 3Zn^{2+} + 2H_2 \rightarrow (Zn_3Fe)S_4 + Fe^{2+} + 4H^{+} \qquad \text{(Eq. 4.2)}$$

The two equations detail how early growth zones near the nucleus can be enriched in iron relative to distal later growth zones. Equation 4.1 represents a reaction with attention to constant volume, which is relevant for replacements. The release of H_2S in this reaction would favour subsequent sulfide mineralization near this site. Equation 4.2 accounts for constant sulfur from the replacement of pyrite to marmatite. This latter equation shows how Fe-rich sphalerite can be produced with a constant redox state. However, this equation releases significant acid, which would not favour sphalerite/marmatite stability. Therefore, Equation 4.1 is the hypothesized reaction for the replacement of pyrite by marmatite, which actually does increase the sulfidation state of the fluid by release of H_2S. A similar equation could explain sphalerite with chalcopyrite guests:

$$6FeS_2 + 3Zn^{2+} + 2Cu^{+} + 5H_2 \rightarrow \quad \text{(Eq. 4.3)}$$

$$3ZnS + 2CuFeS_2 + 4Fe^{2+} + 5H_2S$$

This equation is for 1:4 ratio of chalcopyrite to sphalerite, which is on the higher end of what is observed at Montezuma.

In this stage there is a conspicuous tennantite-tetrahedrite±chalcopyrite association that occurs in many instances along the faces of galena (Figure 4.3.6.A) and sphalerite (Figure 4.3.6.B). This association is also observed replacing early pyrite grains (Figure 4.3.6.C). The association itself crystallizes in complex exsolution or intergrowth textures (Figure 4.3.6.D), which are not entirely understood.

Stage 4: ankerite-dolomite

Ankerite is the dominant carbonate during this phase of mineralization (Lovering, 1935). Infill is commonly beige-red to black in color with a massive habit, which renders a "cloudy" appearance (Figure 4.3.2.B Stage 4). In doubly polished section under plane reflected light this assemblage appears black with dark olive to gray patches, while under crossed polarizers the carbonate is white and red in color (Figure 4.3.7.A and 4.3.7.B). It is hypothesized that carbonate has replaced pyrite (Figure 4.3.7.C) in minor instances.

Stage 5: Lead-silver and late quartz mineralization

Stage 5 mineralization includes quartz, galena, silver sulfo-salts and silver sulphides. Silver minerals identified in the district are: native silver, argentite, miargyrite, stromeyerite, pyrargyrite, freibergite, polybasite, proustite, stephanite and pearceite with miargyrite, pyrargyrite and proustite as the dominant silver minerals (Lovering, 1935). Quartz of this stage is ubiquitous in veins, while galena and silver sulfosalts are more variable. Directly after this stage, Lovering (1935) includes a questionable

stage of bismuth mineralization as bismuthinite, emplectite, beegerite and other Bi bearing minerals. Quartz also accompanies this assemblage. This stage was not observed in this study, and has been combined into Stage 5.

Late quartz is distinguished from early quartz by lacking associated pyrite, grains are typically unfractured and mineralization is found as late overgrowths on earlier minerals or as infill. Late quartz is transparent subhedral to euhedral and commonly lines vugs. In ores with barite (Figure 4.3.10) this stage is found occupying interstitial sites that were not already filled by previous base metals or carbonates. This stage can also be found as fracture fill (Figure 4.3.9 Stage 5).

Miargyrite, proustite and pyrargyrite are black and opaque to scarlet red and translucent in thick section (Figure 4.3.8.A). Miargyrite and proustite are commonly intergrown (Lovering, 1935). These minerals are found as infill and are also observed healing microfractures in earlier minerals (Figure 4.3.10.B Stage 5), intergrown with quartz and are proposed here also to have replaced earlier carbonate in veins bearing Stage 4 carbonates (Figure 4.3.8.B). Lovering (1935) notes that "manganiferous ankerite is generally associated with ruby silver minerals." This is observed in Figure 4.3.8.B as regions of ruby silver also contain carbonate. Carbonates are generally very fine grained to massive in these veins and this possibly accounts for the lack of relict textures. In Figure 4.3.8.B a progressive degree of replacement can be observed from dense nearly pure ruby silver intergrown with an unknown magnetic phase to the lower right to unaltered carbonate to the upper left. The cloudy region in the central upper left of Figure 4.3.8.B indicates higher ratio of carbonate to ruby silver. The magnetic phase, which is only associated with regions of carbonate and ruby silver, is possible evidence of carbonate replacement type reactions.

Stage 6: Late copper?

A late copper stage of chalcopyrite, covellite and chalcocite is noted by Lovering (1935) and has been identified in this study (Figure 4.3.11). Lovering (1935) presents the possibility that this stage only

reflects supergene processes, which is a favoured interpretation for this study. However, it should be noted that this mineralization could be a function of other processes such as magma resurgence or with associated fluctuations in oxidation state.

Figure 4.2.1 satellite image of Montezuma Mining District showing weathered district scale propylitic alteration that is distinguishable in regions above treeline. Alteration appears as rusty to bleach in color. Town of Montezuma is to the lower left of the image. Red outline is rusty altered rock field area as mapped by Neuerburg et al. (1974). Image covers central portion of the district, reference red alteration fields to "rusty altered rock field" in Figure 4.2.2 below. Image from Garmin Bird's Eye 2014.

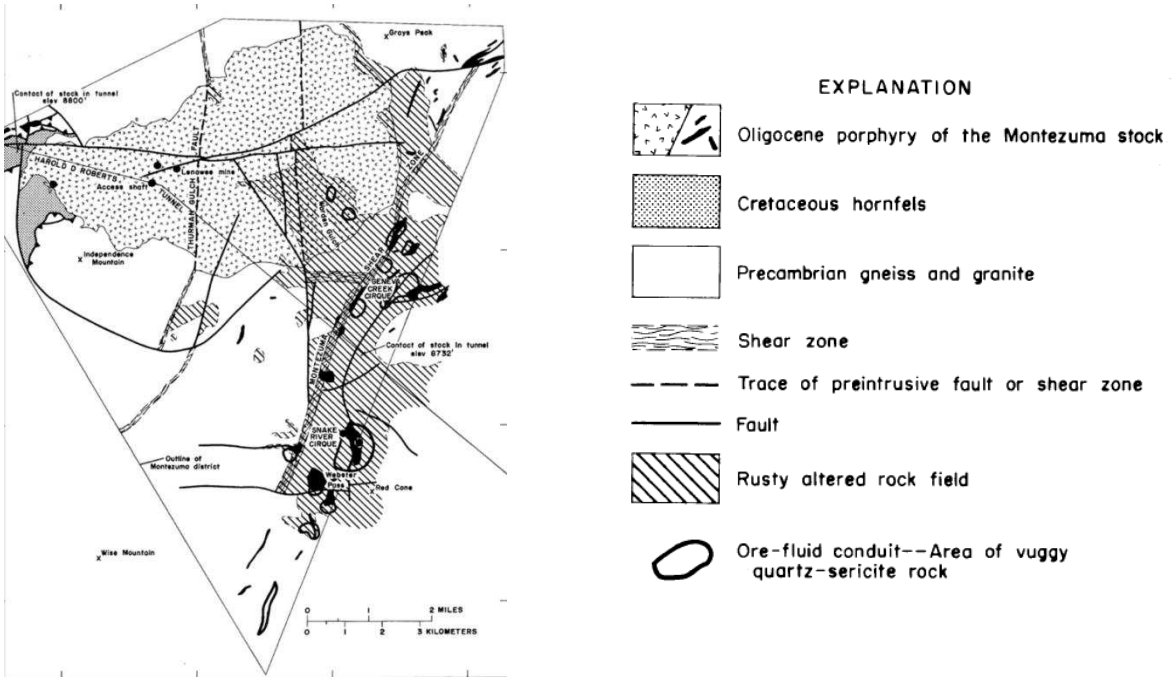

Figure 4.2.2 Map showing distribution of alteration across the district including key structural features. From Neuerburg et al. 1974.

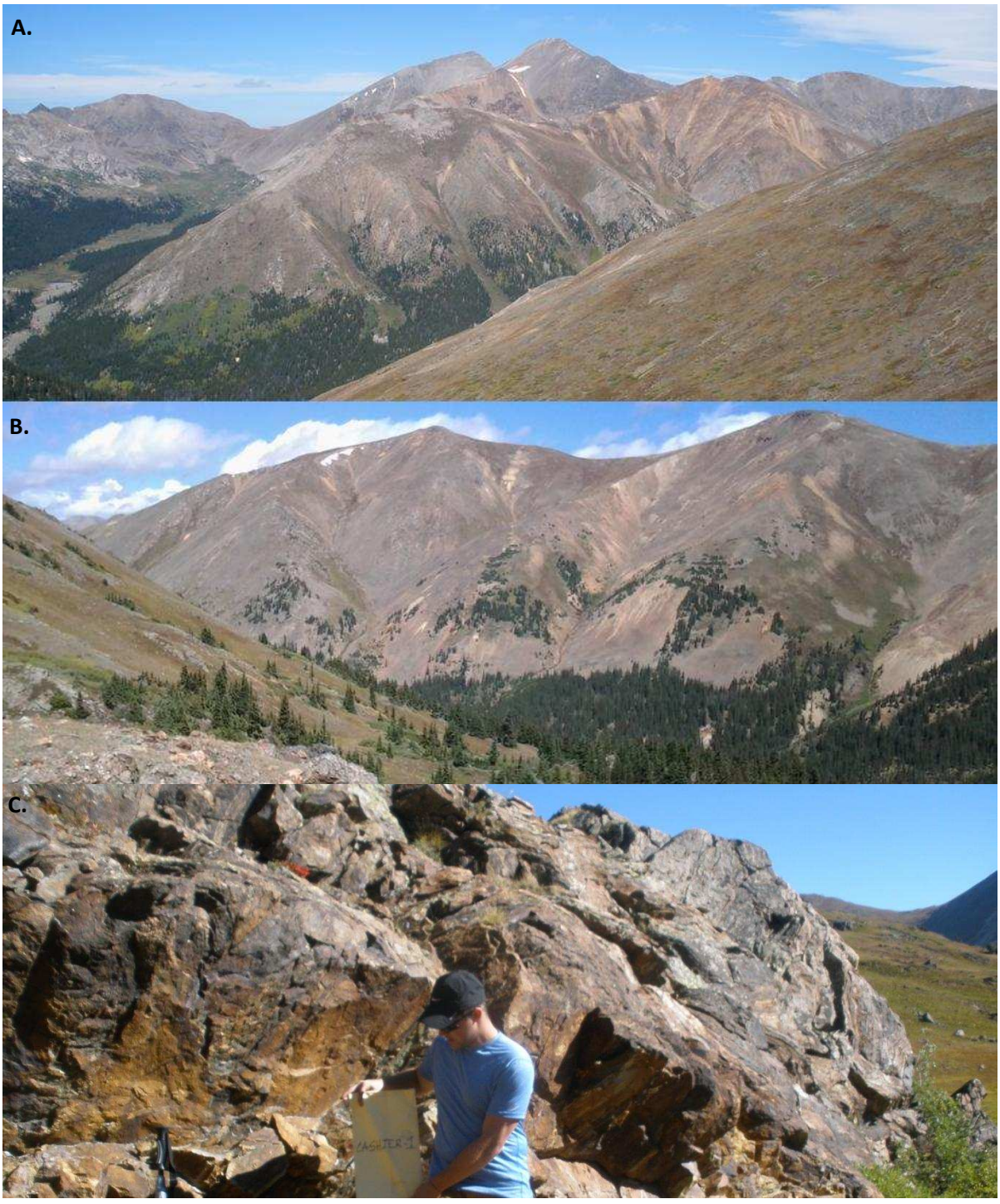

Figure 4.2.3 surface exposures of weathered propylitic alteration. (A) view looking north from Collier Mtn. of alteration along the slopes of Ruby Mtn. and Copper Mtn. Chihuahua Gulch to the far left (west) and the tall peak in the background is Grays Peak (north). (B) view looking east from the west flank of Teller Mtn. at alteration along the west flank of Landslide Peak. (C) Outcrop of propylitic alteration near the head of Snake River.

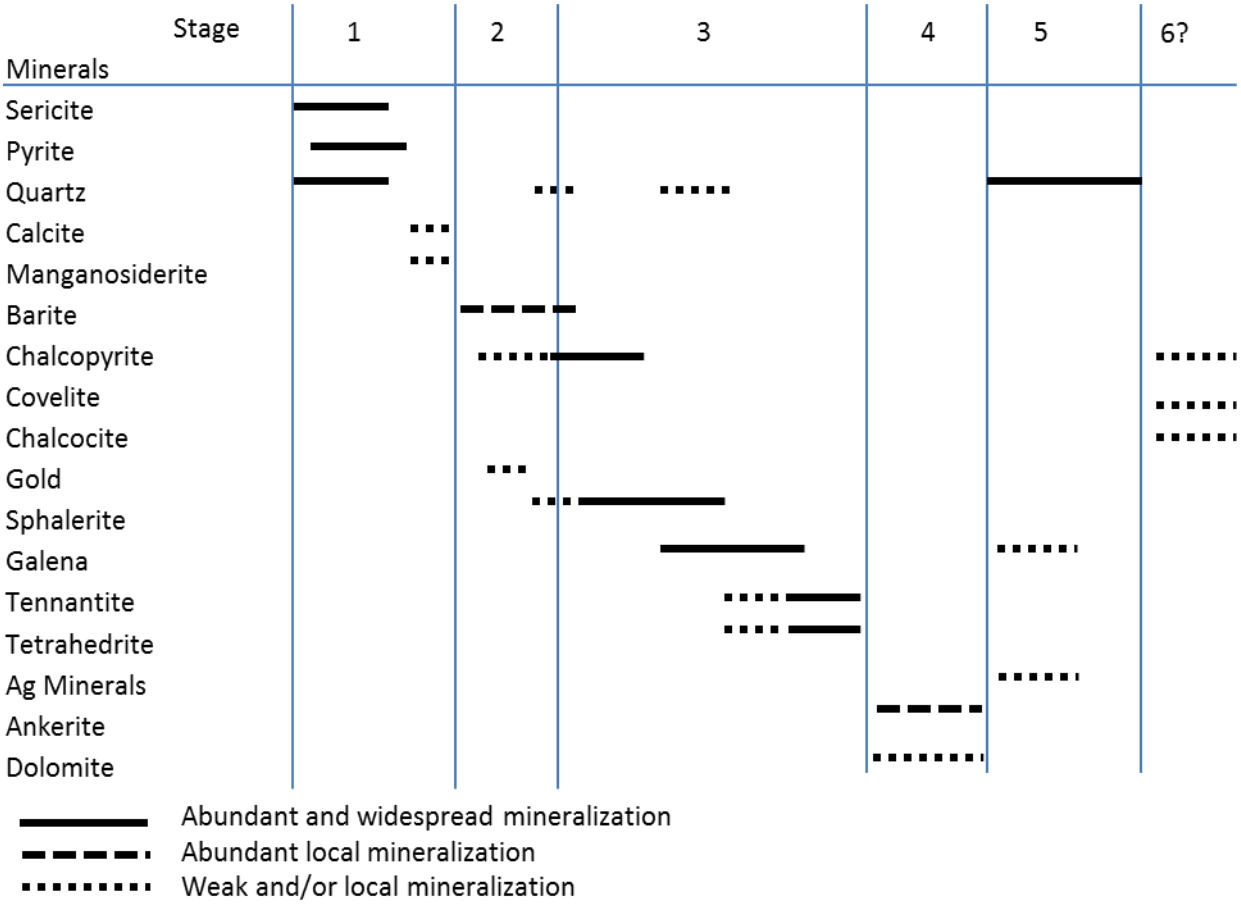

Figure 4.3.1 generalized paragenetic sequence for mineralized veins of the Montezuma mining district.

Table 4.3 list of mineral abbreviations from for photomicrograph annotations

Mineral or Minerals	**Abbreviation**
Quartz	qtz
Barite	ba
Pyrite	py
Tennantite-Tetrahedrite	ten-tet
Galena	gn
Sphalerite	sph
Carbonate	carb
Chalcocite	cc
Chalcopyrite	cpy
Proustite	pr
Plain polarized light	ppl
Cross polarized light	xpl

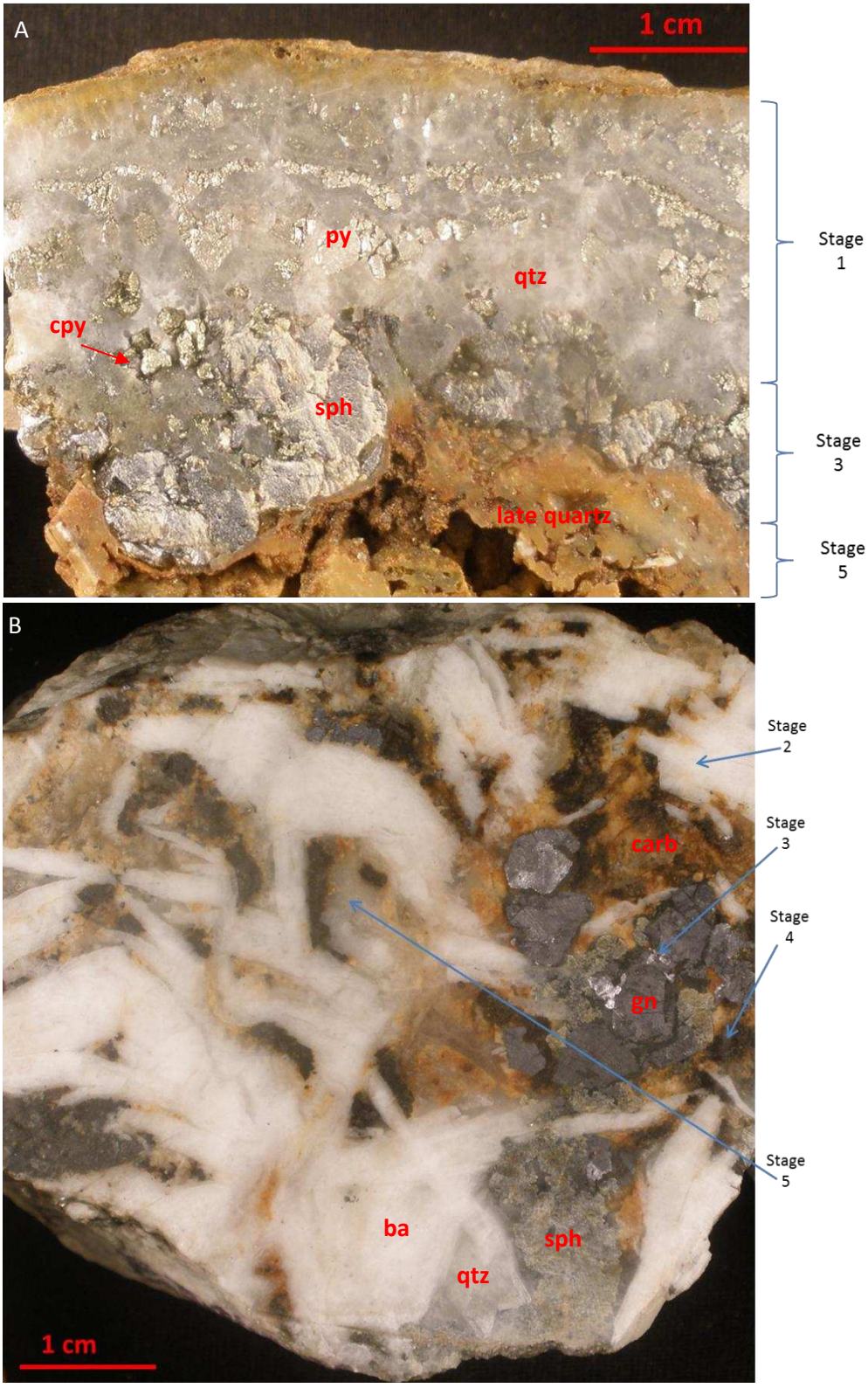

Figure 4.3.2 Example of the two vein types based on abundance of carbonate and barite. Numbered annotations indicate paragenetic stage. (A) Type 1 veins lack significant barite and carbonate. (B) Type 2 veins contain significant Stage 2 barite and/or Stage 4 carbonate.

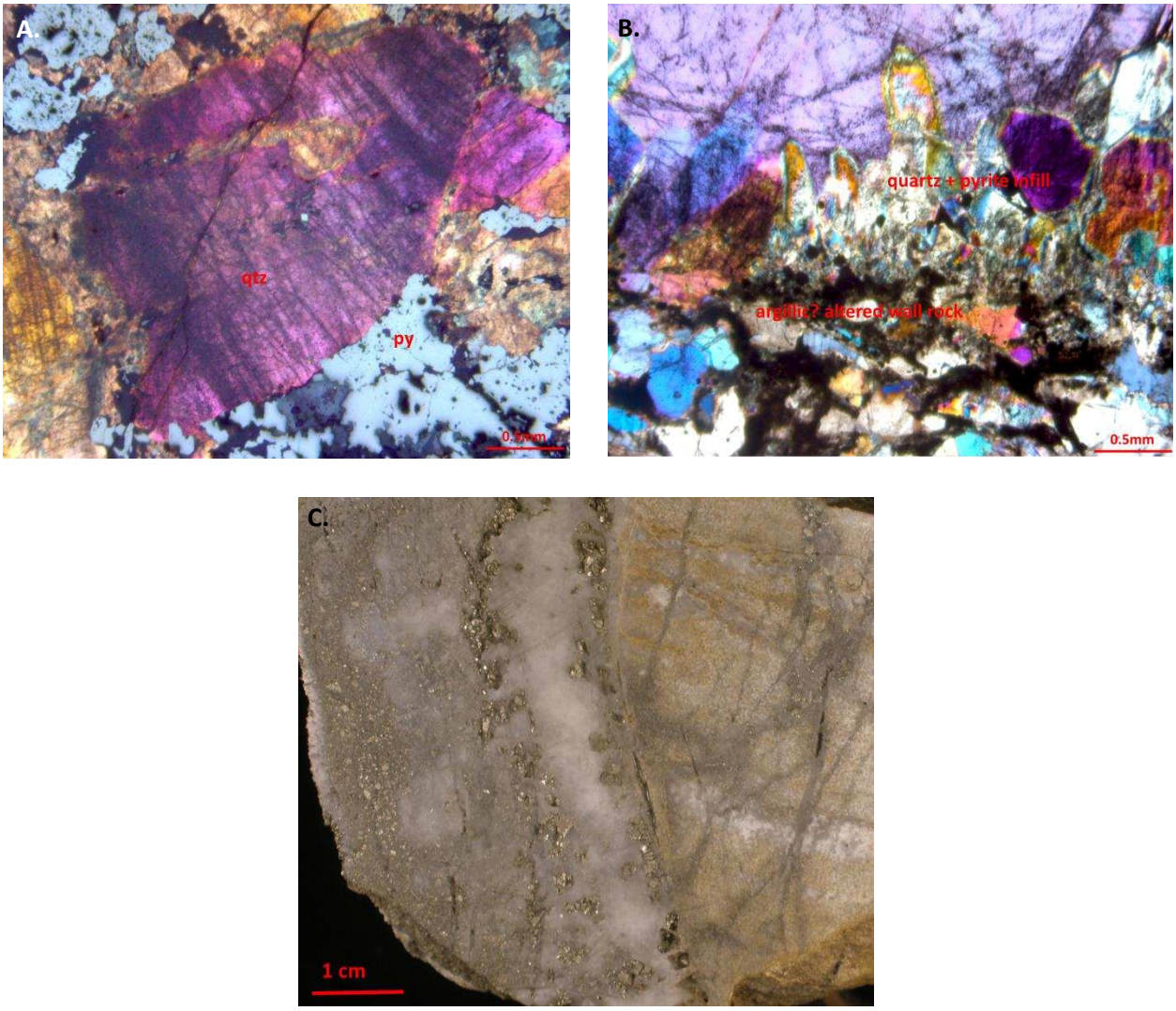

Figure 4.3.3 microphotographs and photograph exhibiting textures associated with the early quartz-pyrite found in Stage 1. (A) Sample from Sts. Johns mine dump (xpl). Evidence that some quartz grew before pyrite as indicated by fine pyrite growth along margins of coarse quartz grain . (B) Sample from Queen of the West mine dump (xpl). Example of intial euhedral quartz growth along an altered wall rock overgrowth. (C) Sample from the Revenue mine dump in Cinnamon Gulch**.** pyrite infill and pyrite replacement alteration (to the left of the figure), clear euhedral quartz infill and silicic alteration, fine grained pale buff orange carbonate (siderite?) alteration, textural retention of white clay replacing primary feldspars (argillic) along vein like fluid pathways. This sample also exibits D-type stockwork quartz-pyrite veining along the right portion of the figure.

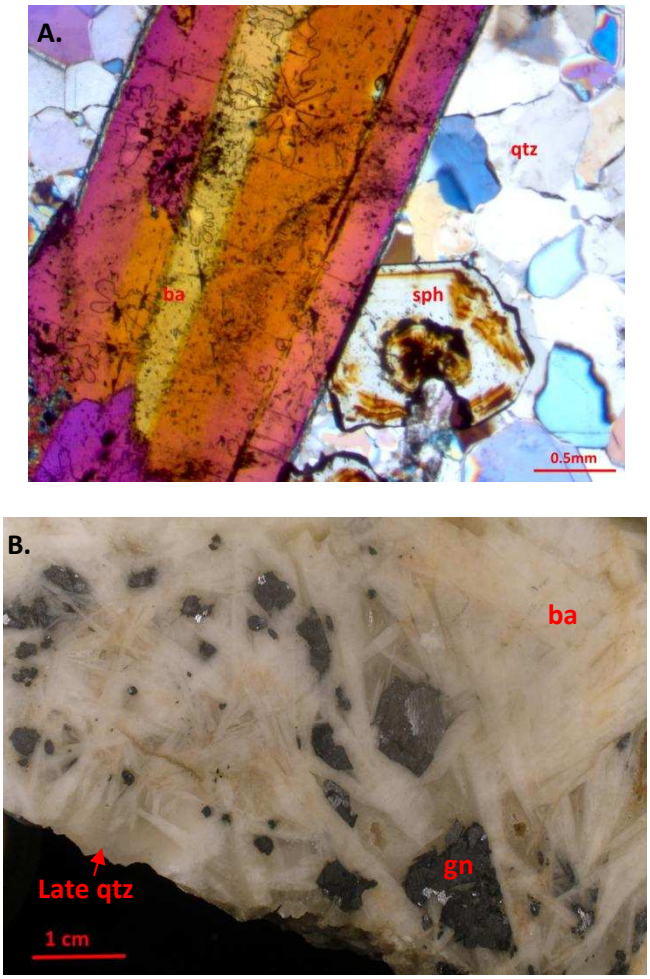

Figure 4.3.4 Stage 2 barite (A) sample from the More Work mine dump (xpl). Sphalerite growth after the growth of a coarse blade of barite. (B) Hand sample from the Star of the West mine dump along the west flank of Teller Mountain. Example of the coarse bladed nature of barite mineralization. Other phases include later galena infill before late clear quartz + microscopic proustite .

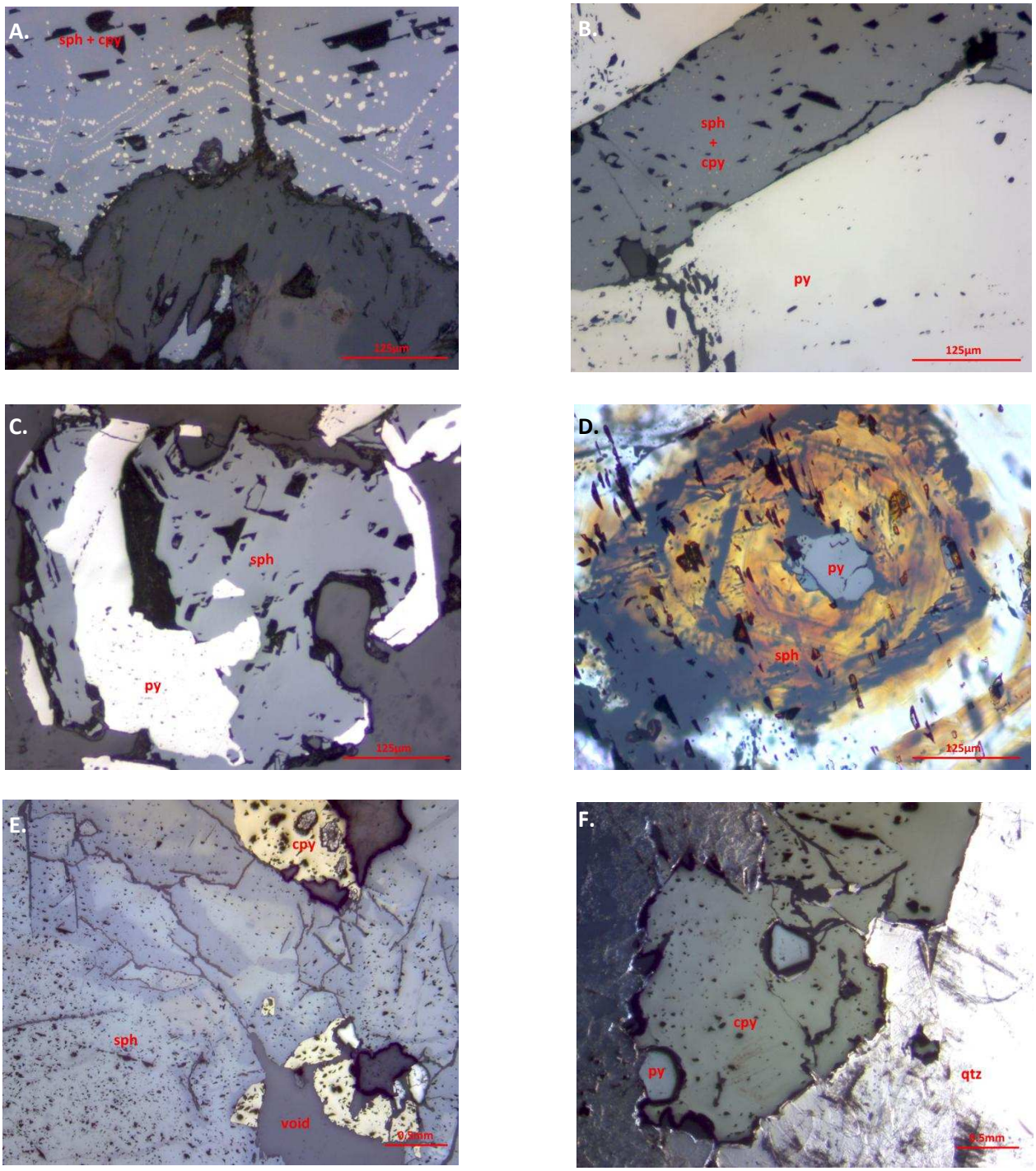

Figure 4.3.5 Stage 3 (A) sample from the Morgan mine (ppl). Oriented chalcopyrite disease indicating that sphalerite and chalcopyrite grew both as exsolution blebs and as intergrowths. (B) sample from the Brittle Silver mine (ppl). Less systematic chalcopyrite exsolution in sphalerite. Mineralization occurs as fill in a fractured pyrite grain. (C) sample from Quail mine dump (ppl). Common occurrence of sphalerite replacing early pyrite. Atoll texture is well developed in this specimen. (D) sample from Peruvian mine (ppl). Evidence for sphalerite nucleation on an earlier pyrite grain. (E) sample from the Sill mine (ppl). An additional habit of chalcopyrite growth along margins of sphalerite grains. (F) sample from the Sill mine (ppl). Chalcopyrite replacing earlier pyrite rendering a well developed relict islands of pyrite.

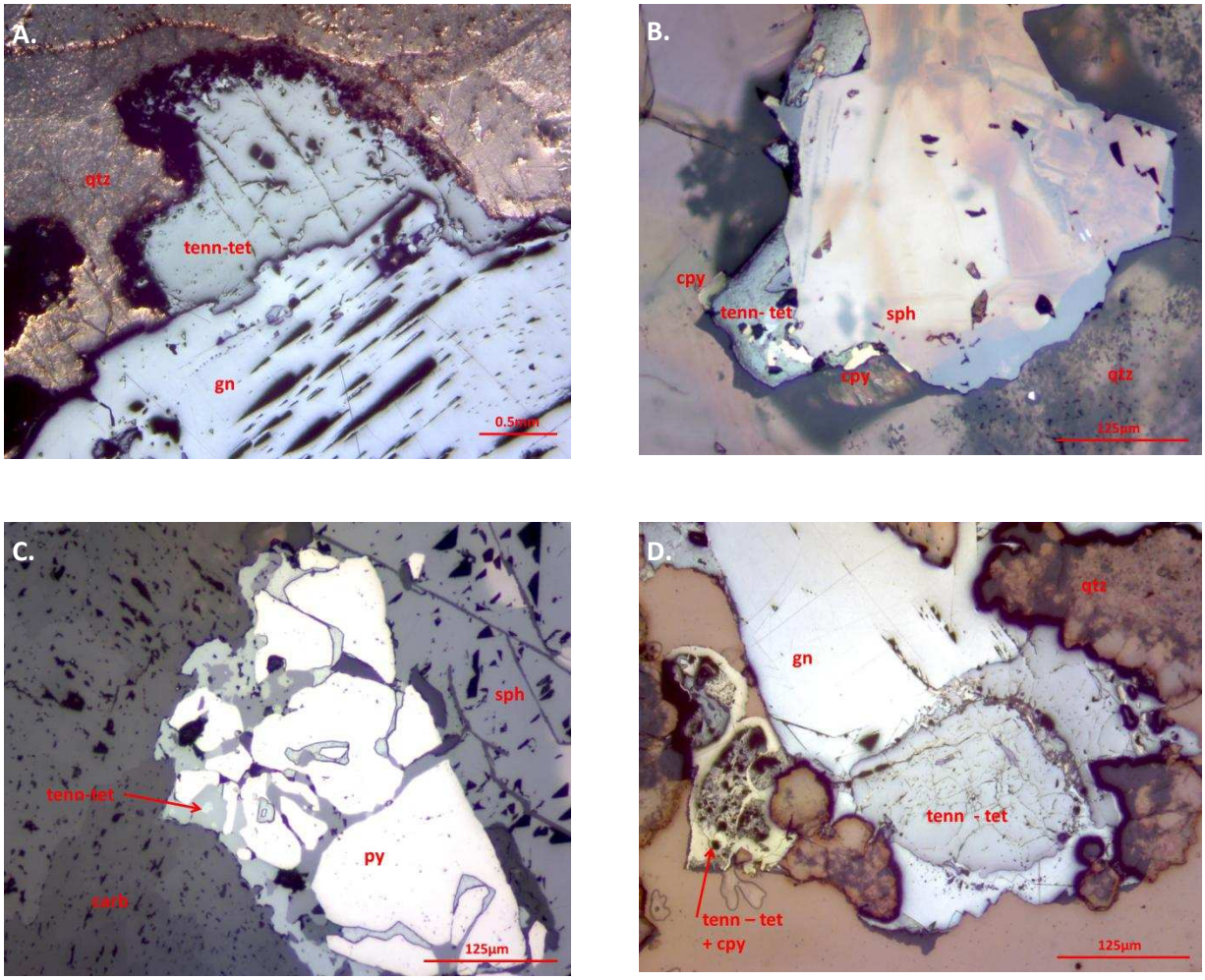

Figure 4.3.6 Stage 3 (A) Sample from Star of the West mine (ppl). Common occurrence of tennantitie-tetrahedrite along margins of galena. (B) Sample from Morework (ppl). Slightly later mineralization of tennantite-tetrahedrite and chalcopyrite than sphalerite (C) Sample from National Treasury mine (ppl). Tennantite-tetrahedrite replacing pyrite along fractures. (D) Sample from Chatauque mine (ppl). Complex association of galena-tennantitie-tetrahedrite-chalcopyrite hosted in early quartz.

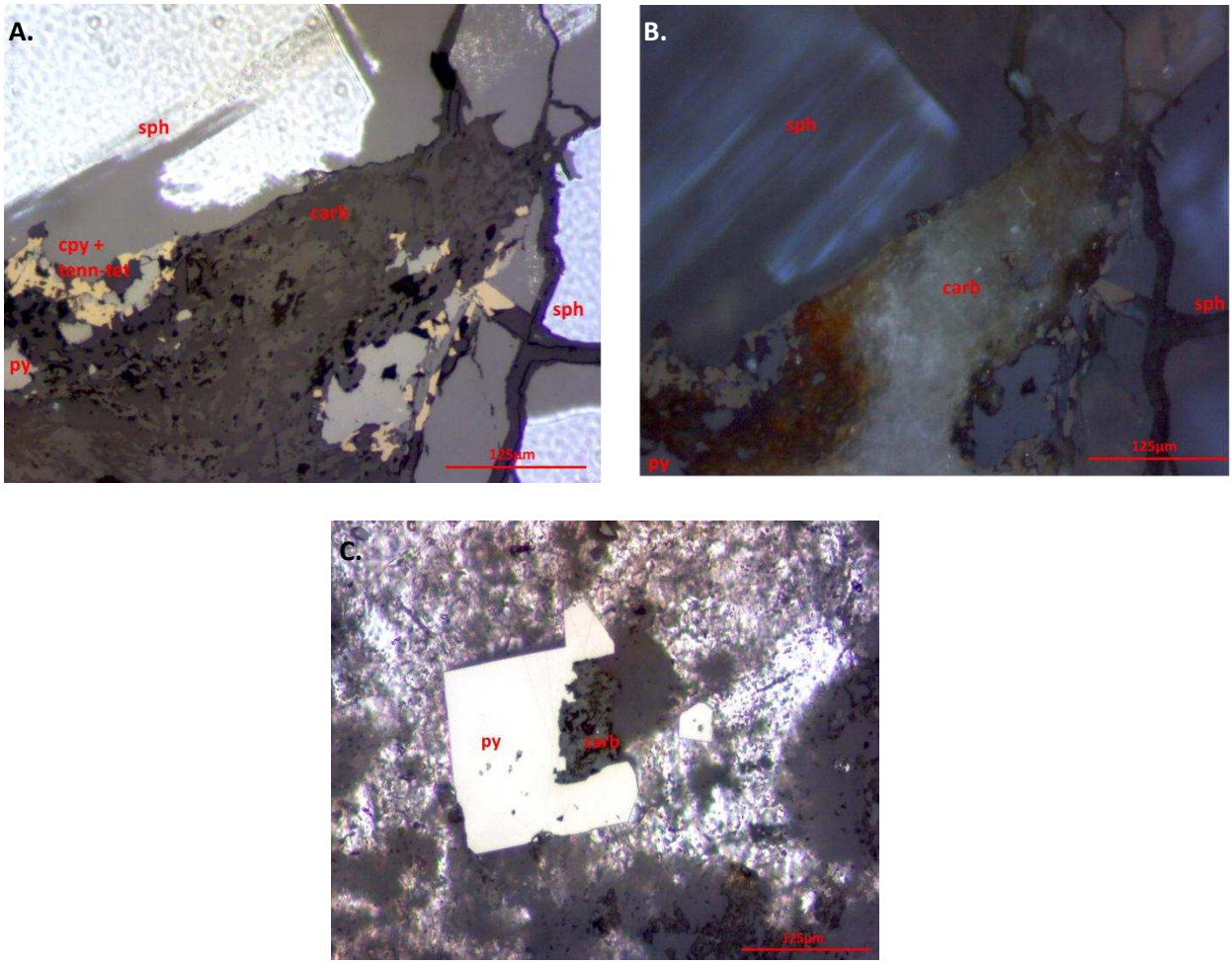

Figure 4.3.7 Stage 4 (A) sample from Equity mine dump (ppl). Carbonate infill after copper and zinc mineralization in plane reflected light. (B) sample from Equity mine dump. Same image as A, but with xpl. (C) sample from Sts. Johns mine dump (ppl). Carbonate possibly replacing early pyrite along alteration front.

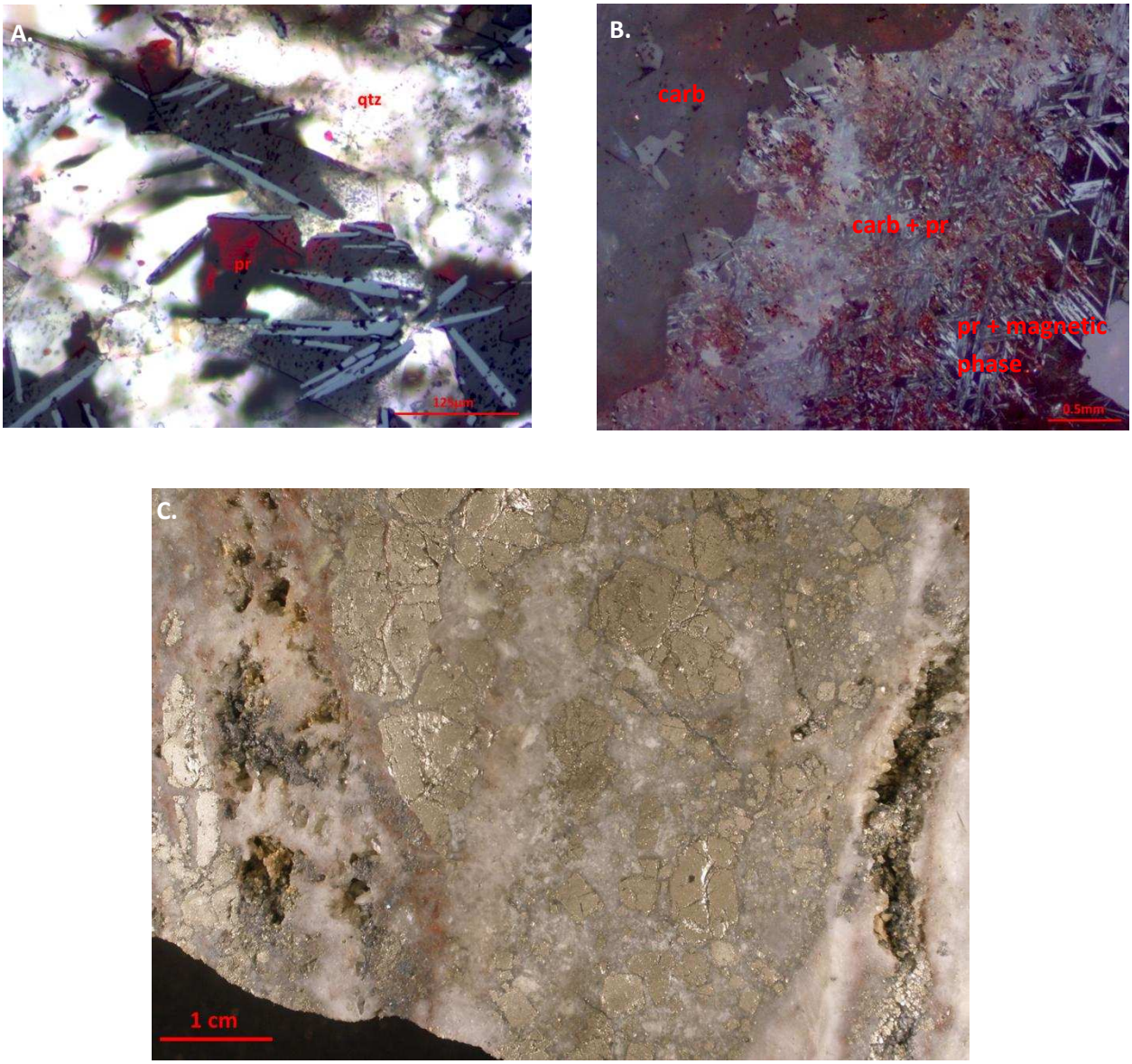

4.3.8 Stage 5 (A) doubly polished section from Brittle Silver mine (ppl). Ruby silver intergrown with quartz. (B) photomicrograph from the Quail mine (ppl). Proposed progressive replacement of carbonate by ruby silver and a magnetic phase from intense to total replacement to the lower right to lesser degrees of replacement to the upper right. (C) hand sample from the Brittle Silver mine. Two stage 5 banded quartz + ruby silver vein sets crosscutting earlier quartz pyrite stage mineralization (center and far left). Later mineralization is characterized by abundant vugs, red proustite and possible black stephanite.

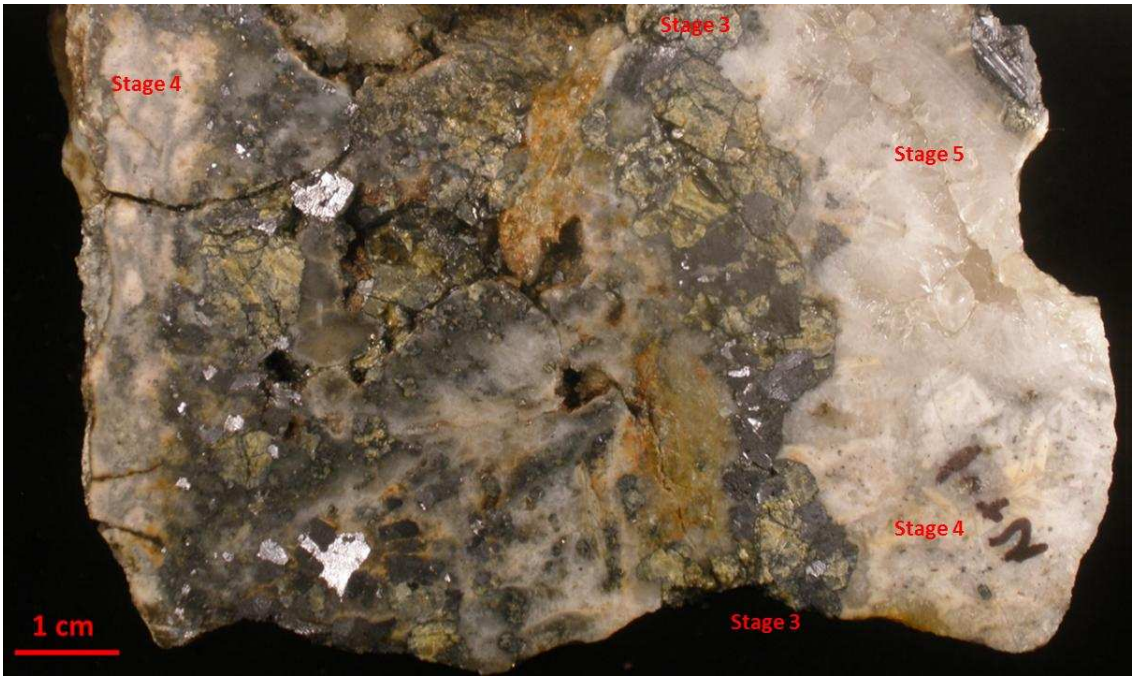

Figure 4.3.9 hand sample from National Treasury mine dump. Clear euhedral to polygranular comb quartz + silicification overprint before red-brown ankerite infill nucleated preferentially along margins of sulphides (lower left center of figure), as an impersistant channelway top to bottom center of figure, and as overprints after galena + sphalerite infill and replacing pyrite. The central left portion of the plate show a complex overprinting with galena before carbonate before quartz well displayed

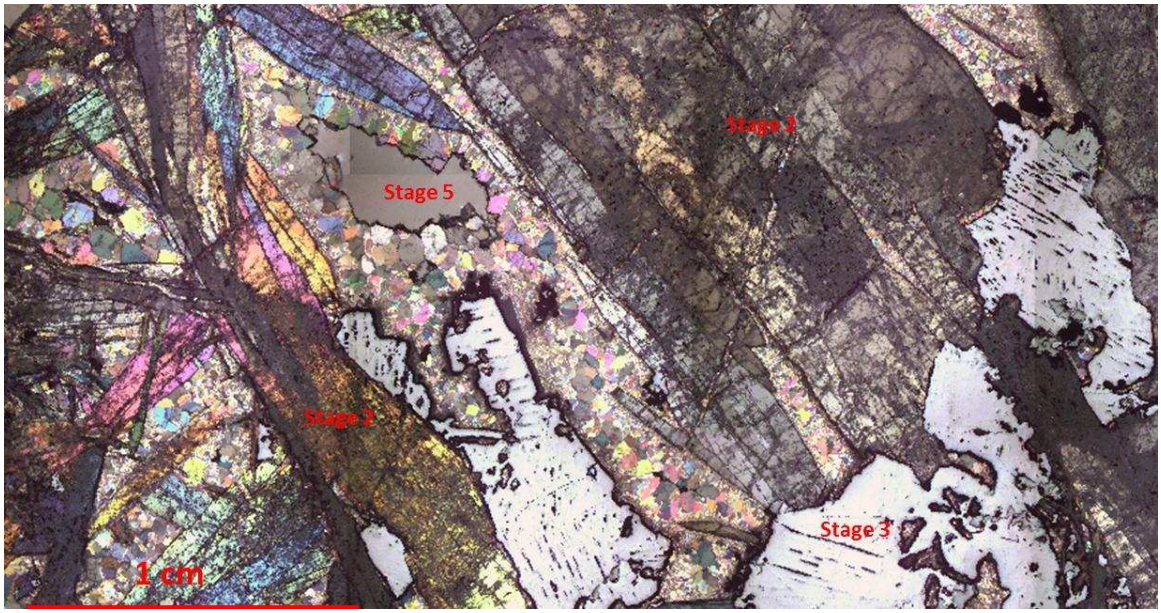

Figure 4.3.10 Doubly polished section from Star of the West mine dump (xpl). Stage 2 coarse bladed barite before Stage 3 base metals (galena + tennantitie-tetrahedrite) before late Stage 6 infill. Early barite grains are highly fractured rendering a darker color. Some of these microfractures have been healed by Stage 6 silver-quartz assemblages.

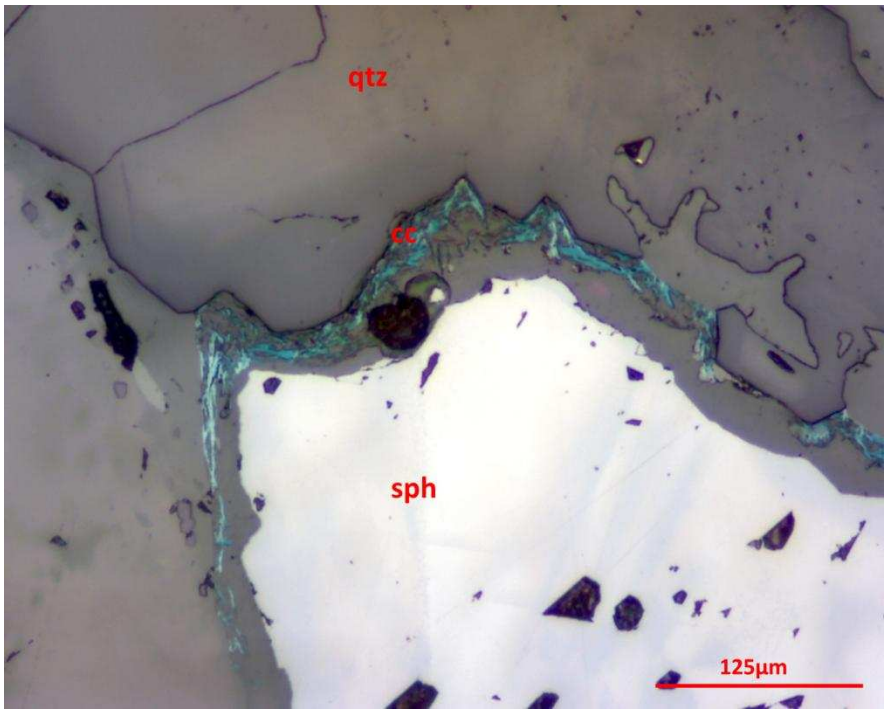

Figure 4.3.11 Doubly polished section from the Tiger mine on Glacier Mtn. Stage 6 copper? (ppl) Chalcocite in this stage is interpreted to be a product of supergene processes. Further investigations are required to verify this interpretation. Other possibilities include a resurgence of magmatic activity accompanied by copper mineralization of different oxidation states to account for chalcopyrite, covellite and chalcocite found in this stage.

5. Metal Ratios

5.1 Metal Ratios and District Scale Zonation Methods

A data base of metal production and grade was compiled from the work of previous authors (Lovering,1935) to define metallic zonation of the district. First, total productions of each metal were plotted on x-y graphs to identify relationships among metals. This allowed for the identification of a metal ratio suitable for zonation studies. Metal ratios from historic production values were used to account for the disparities in vein tonnage between mines. Comparing production values from a vein would render skewed results considering that size and tonnage of veins in the district are highly variable. Using metal ratios rather than metal production values also emphasises the relationship of three metals. For example, it is known that Cu precipitates from a hydrothermal fluid before Pb. Once Cu is depleted from a fluid, Pb then becomes the dominant metal precipitated by the fluid. Therefore an inverse relationship of Pb and Cu is hypothesized. Thus a comparison of Pb:Cu ratios for each vein are able to prove or disprove this hypothesis.

These ratios were then placed in a geospatial context to produce inverse distance weight multivariate interpolation maps with standardized configurations using MapInfo Professional 8.5 SCP. Maps from the above authors were rastered and digitized to support interpretations made from the production metal ratio interpolation maps.

The earliest data source was from Lovering, 1935. This record holds production values from 51 mines from the 1870s until the time of publication. The data is return from ore smelters, which may include recovery bias due to metallurgical practices of the time period or selective recovery due to economic conditions. Although these records are not entirely complete, they do contain workable data that can be used to gain insight into the district. The utilized production values were: gold (fine ounces),

silver (fine ounces), lead (wet assay pounds), copper (wet assay pounds) and zinc (pounds). The production values given for each year, were summed in order to better represent a full vein as a geospatial data point. Mines with available data are shown in Figure 5.1.1. Ratios were then made for each combination of Pb, Cu, Ag, and Au. These ratios were put on a log scale. There tends to be more data for the more productive mines of the district, which could reflect a higher level of professional book keeping practices than smaller operations. Also it is believed that more productive veins were mined out, while less economic veins may have only been partially mined then abandoned in some instances. Therefore production values for larger mines are believed to be more reliable. Another variable is that some smelters in operation during late 19^{th} century penalized for zinc ore (Botinelly, 1979), therefore data for this metal is considered highly inaccurate and is regarded as unreliable. Goodell and Petersen (1974) have proposed that Pb/Cu and Ag/Cu be used as ratios to evaluate zonation in polymetallic districts such as these, which were favoured ratios of this study.

In order to support interpretations of metal ratios, semi-quantitative mineral abundance data from Botinelly (1979) was digitized and integrated into the mapping data base. In his study, grid cells were given arbitrary values of abundant, moderate, sparse, trace, and not found with regard to minerals observed in particular grid cell. Abundances of galena, sphalerite, pyrite, tennantite-tetrahedrite, chalcopyrite, barite and carbonate minerals were made by inspection of 250 deposits. For the purposes of this research, this data is only used as supporting evidence, and not as concrete evidence of mineral distribution. Maps were also integrated from Neuerburg et al. (1974) to provide locations for the Montezuma Shear Zone, "rusty" alterations, vuggy quartz-sericite alteration and specularite vein occurrences. This data was used to support interpretations from the produced metal-ratio maps.

5.2 Metal Ratios and District Scale Zonation Results

Zonations on deposit and district scales have been identified in the district. Vertically, on a deposit scale, Lovering (1935) identified that in most veins there is an increase in sphalerite and pyrite

with depth, while galena is in higher abundances in upper portions of veins. In veins bearing copper, chalcopyrite increases in relative abundance to tennantite-tetrahedrite with depth. In this study, it was found that veins at Montezuma are zoned on a district scale based on relative copper abundance (Figure 5.2.8 and Figure 5.2.9). Two zones are identified from metal ratios studies and on generated metal ratio interpolation maps: a copper rich zone (CRZ) and a copper poor peripheral zone (CPZ). These zones are potentially supported by the abundance of particular gangue minerals: pyrite, carbonates and barite (5.2.10). There are no clear patterns in 5.2.10, yet it seems that pyrite is in higher abundance in the CRZ.

Metals

The first phase of assessment of metal production values in the Montezuma district was to create x-y plots of total production values for each metal (Figure 5.2.1). Au vs. Pb, Ag vs. Pb, Au vs. Cu and Au vs Ag all show a positive trends. Au vs. Cu shows a particularly good relationship for mines with high production values. These increasing trends would be expected as vein tonnage increases. However, only the Pb vs. Cu plot shows no apparent relationship. Therefore it is possible for a vein with high tonnage to contain high Pb and low Cu, or vice-versa. This invokes that veins in the district were subjected to varying ratios of the two metals. This is perhaps related to the contrasting precipitation conditions of the two metals in hydrothermal fluids. Thus the relationship of these two metals invokes further investigation.

Ag vs Cu in Figure 5.2.1.D does show a trend, however, this pattern seems to be weaker than those observed in Au vs. Pb, Ag vs. Pb and Au vs Ag plots. There is a linearly increasing relationship of the two metals, but there are significant outliers as compared to other metal relationship plots. The coefficient of correlation for Ag vs Cu is the second lowest, just above Pb vs Cu. This may indicate differing precipitation conditions, yet not as contrasting as Pb and Cu.

Figure 5.2.2 displays three metal relationships using ore grade rather than the log of total production values. Very few mines had complete ore tonnage records for the total duration of production,

and some veins rendered nil production of some metals. Therefore this study was highly limited by data points and should be interpreted with caution. The results show a negative relationship for Pb to Ag and Pb to Cu, while a positive relationship is observed for Cu to Ag.

Ag:Au ratios are used to differentiate Cordilleran-type veins and epithermal veins (Bendezú and Fontboté, 2009). Figure 5.2.3 depicts ratios of total production values of each metal on a log scale. The data shows a wide range of Ag:Au ratios from below average crustal levels to well above crustal ratios. This could be due to the variation in metallurgy practices among smelters or is perhaps a true reflection of these veins in nature. All veins in the district produce an order of magnitude greater amount of Ag than Au. Most veins contain Ag:Au ratios of Cordilleran-type veins, but some do contain low Ag:Au ratios that are more comparable to epithermal veins, which is detailed in chapter 7 section 7.1

Metal Ratios

Four figures contain a series metal ratio x-y plots using a common denominator for each plot; Figure 5.2.4 (Cu), Figure 5.2.4 (Pb), Figure 5.2.6 (Ag) and Figure 5.2.7 (Au). Blue points indicate that a mine contained data for all metals in the plot. Red and green points indicate mines that lack production of one metal used in the plot. Lack of production was substituted for 0.001. Lack of production of a particular metal may be due to lack of that metal in a vein or due to production biases as detailed above. These data are inserted to provide a complete data set, but interpretation of data with all metals is considered to be more reliable. All plots except 5.2.7.A (Ag/Au vs Pb/Au) and 5.2.5.B (Ag/Pb vs Au/Pb) show bimodal distribution. This distribution is an artefact of the insertion of data lacking production values for all metals.

Relationship analysis of these plots utilized an alpha level of 0.05. Figure 5.2.4 (A and B), Figure 5.2.5 (A, B and C) and Figure 5.2.7 (A and B) R^2 values above the alpha level of 0.05. It is interesting that when Cu is used as a denominator (Figure 5.2.4) all three plots show a positive relationship. Of the three plots in Figure 5.2.4, the Ag/Cu vs Pb/Cu plot (Figure 5.2.4.A) seems to show the strongest

relationship having the highest coefficient of correlation. This indicates that with relative increase in Pb+Ag there is a decrease in Cu in veins of the Montezuma district. The R^2 value in Figure 5.2.4.B (Ag/Cu vs Ag/Cu vs Au/Cu) is greater than the alpha level of 0.05, but only slightly. This does suggest that as Cu decreases in vein, Ag+Au increases, but the relationship is weak. All plots in Figure 5.2.5 using Pb as a common denominator were greater than the 0.05 alpha level, yet no correlation coefficients were as high as observed for Ag/Cu vs Pb/Cu (Figure 5.2.4.A).

Plots in Figure 5.2.6 using Ag as a denominator show no R^2 values above the alpha level of 0.05. Figure 5.2.6.A (Pb/Ag vs Cu/Ag) shows a very low R^2 value of 0.0558. There are over three orders of magnitude in variation for Pb/Ag. This may suggest that galena is a significant host to Ag in some veins while Ag in other veins are sourced from Ag sulphides and sulfosalts.

Figure 5.2.7 displays plots using Au as a denominator. The highest R^2 value is for Figure 5.2.7.A (Ag/Au vs Pb/Au), which is also the second highest for the entire study. This indicates that veins with high Ag+Pb contained low Au. If Ag+Pb has an inverse relationship to Cu and Ag+Pb also has an inverse relationship with Au, then Au and Cu may have a direct relationship as noted by Lovering, 1935. This is supported by Figure 5.2.5.C in which as Cu+Au increase, Pb decreases with a high R^2 of 0.4629. Yet Figure 5.2.7.B (Ag/Au vs Cu/Au) suggests that as Ag+Cu increases, Au decreases. However this may be a function of bias toward Ag production.

The maps in Figures 5.2.8 and 5.2.9 are based on relative metal abundances from historic production data, which is the same data set used in the metal ratio figures. The trends detailed above verify that the data set is valid in showing a spatial pattern for the inverse relationship between Pb and Cu, which is a consistent theme in analogue districts (Butte and Morrococha) and is consistent with known theory of metal precipitation relations to temperature decline (Reed et al., 2013; Woitsekhowskaya and Hemely, 1995). Pb:Cu has also been used as a proxy for metal zonation at the Julcani district (Goodell and Petersen, 1974). Therefore this ratio will be used as a proxy for zonation at the Montezuma district

based on use at analogue districts and supporting evidence from metal ratio studies. Ag + Pb is also hypothesized to have an inverse relationship with Cu. The coefficient of correlation is highest for Ag vs Pb in the total metal production x-y plots (Figure 5.2.1.B), therefore these two metals show the strongest direct relationship, however there is significant variation in the Pb/Ag ratio (Figure 5.2.6).. Additionally, R^2 values are the lowest for Pb vs Cu (Figure 5.2.1.F) and Ag vs Cu (Figure 5.2.1.C) of the 6 metal combinations. Also for all metal ratio combinations using a common denominator, the Ag/Cu vs Pb/Cu (Figure 5.2.4.A) has the highest coefficient of correlation of 0.7291.

District Scale Zonation: Cu-Rich Zone

The CRZ is defined by veins that bear high abundances of copper relative to lead and silver. The zone is roughly centred on a point which the propylitic alteration increases in east – west width. The exact centre is inferred to be at a point between Tiptop Peak, Santa Fe Peak and Silver Mountain. Veins with high abundances of pyrite are in higher densities in the CRZ (Figure 5.2.10.C). Gold production was also highest in marginal regions of the CRZ (Figure 5.2.10). Lovering (1935) recognized that gold is commonly in higher abundance in veins bearing copper minerals.

District Scale Zonation: Cu-Poor Zone

This zone is defined by veins bearing higher relative abundances of silver and lead to copper as compared to veins of the CRZ. In Figures 5.2.8 and 5.2.9 this zone is represented by regions of yellow and red. As mentioned, Au values and pyrite are generally lower in this zone than in the CRZ. Concentration of mineralized veins, distribution of propylitic alteration and clear concentric metal ratio zonation suggest that the region between Silver Mtn., Santa Fe Peak and Tiptop Peak is the main center of mineralization. Copper rich outliers exist outside the CRZ: south of Radical Hill (the Cashier and Whale Mines) and north of Glacier Mtn. (the Wild Irishman Mine). Outliers may be the result of several potential variables: 1. subsidiary magmatic intrusions providing a second fluid source, 2. outliers may mark a distal copper mineralization associated with well-developed structural weaknesses or 3. Outliers

may reflect the transition into epithermal style Au-Cu mineralization. The lack of abundant pyrite, present of barite and carbonate, distribution of propylitic alteration and finally the lack of high vein densities in these outlier regions suggests that they are not the result of a secondary fluid source and are more likely the result of one or multiple processes of fluid evolution.

Zonation of Gangue Minerals

The integration of mineral data from Botinelly (1979) has allowed an assessment of gangue mineral distribution in the district. This data set is based on a qualitative assessment of minerals mine dumps. The study applied a grid to the district in which each grid was assigned a value of abundant, moderate, sparse, trace or not found. Abundant values were integrated into this study. Figure 5.2.10.D is from Neuerburg et al. (1974) in which regions of maroon shading are reflect the presence of specularite in veins with no indication of abundance of the mineral.

The central portion of the CRZ has a high concentration of veins with pyrite (Figure 5.2.10.C). Likewise, veins bearing specularite seem to be concentrated in the CRZ. With distance from the center of the CRZ, there is a decrease in pyrite and specularite abundance reflecting early Fe precipitation. There is a narrow arc of sulfate mineralization (Figure 5.2.10.B). This arc is weak and segmented, but does seem to spread northeast along the Montezuma shear zone. Sulfate mineralization seems to be affected by the CRZ rendering a lensoid shape in the district. Sulfate is absent in the core, but is present in Cu-rich ores at the southern and northern parts of the district. Carbonate minerals in Figure 5.2.10.A show a similar pattern. Rather than a lensoid shape, the northeast trend of carbonate mineralization seems to be entirely deflected to the west by the central portion of the CRZ. Form these spatial observations, it should follow that Type 1 veins are dominant in the CRZ and Type 2 veins dominate in the CPZ. However, these inferences are only speculative as there are no clear patterns in these gangue mineral maps.

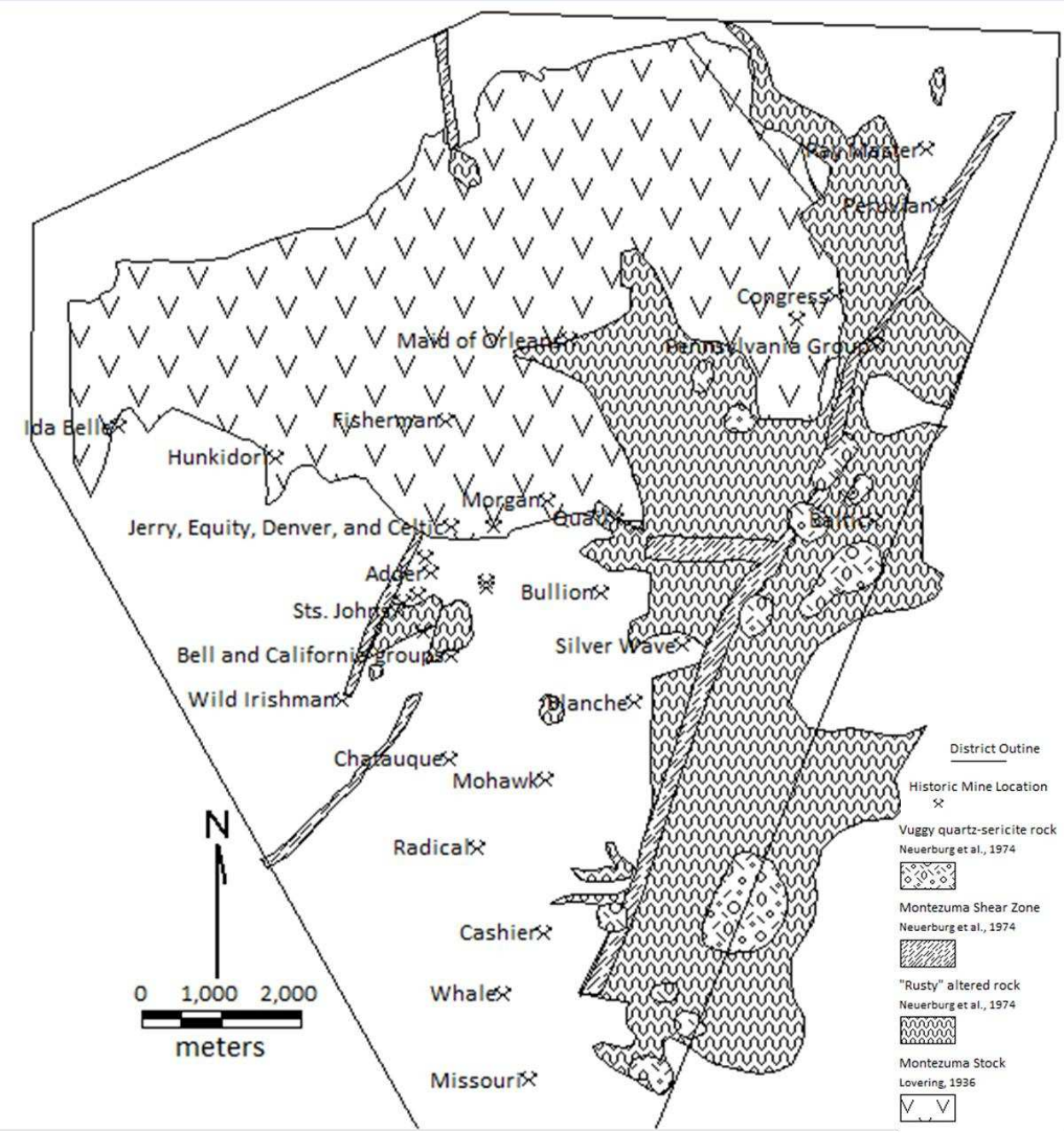

Figure 5.1.1 mines with production records in Lovering (1935). Production data from these mine were used in generating metal ratio interpolation maps. Note that these do not constitute all mined veins in the district, but are only mines with available production data. Untextured areas are Precambrian rocks.

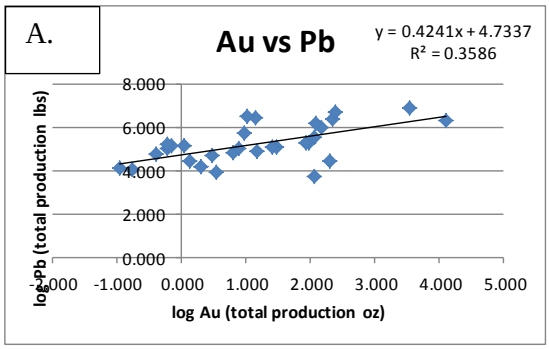

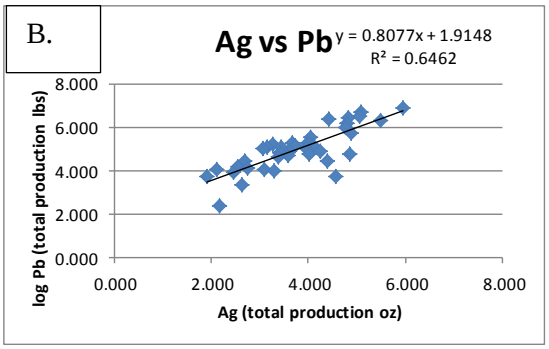

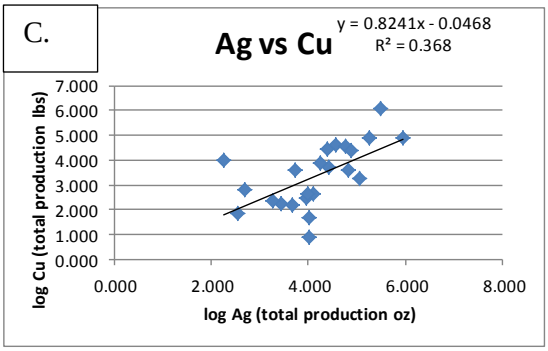

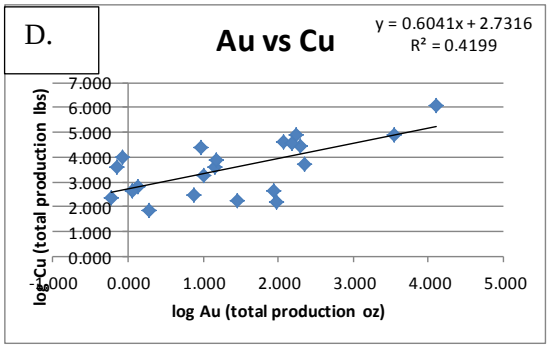

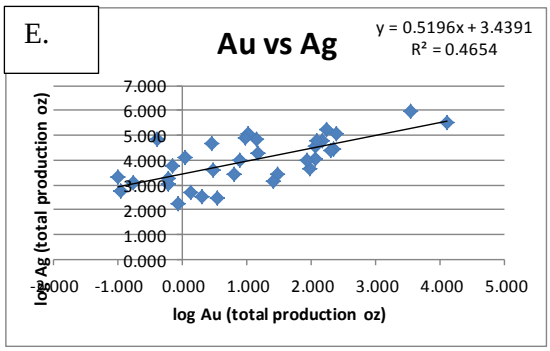

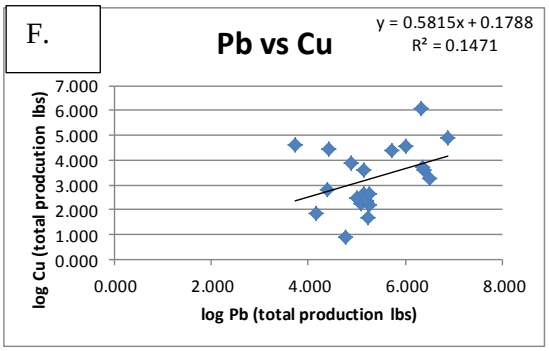

Figure 5.2.1 x-y metal plots by total production values on log scales. Pb vs Cu has the lowest r² value and shows no relationship with increased production values for the two metals.

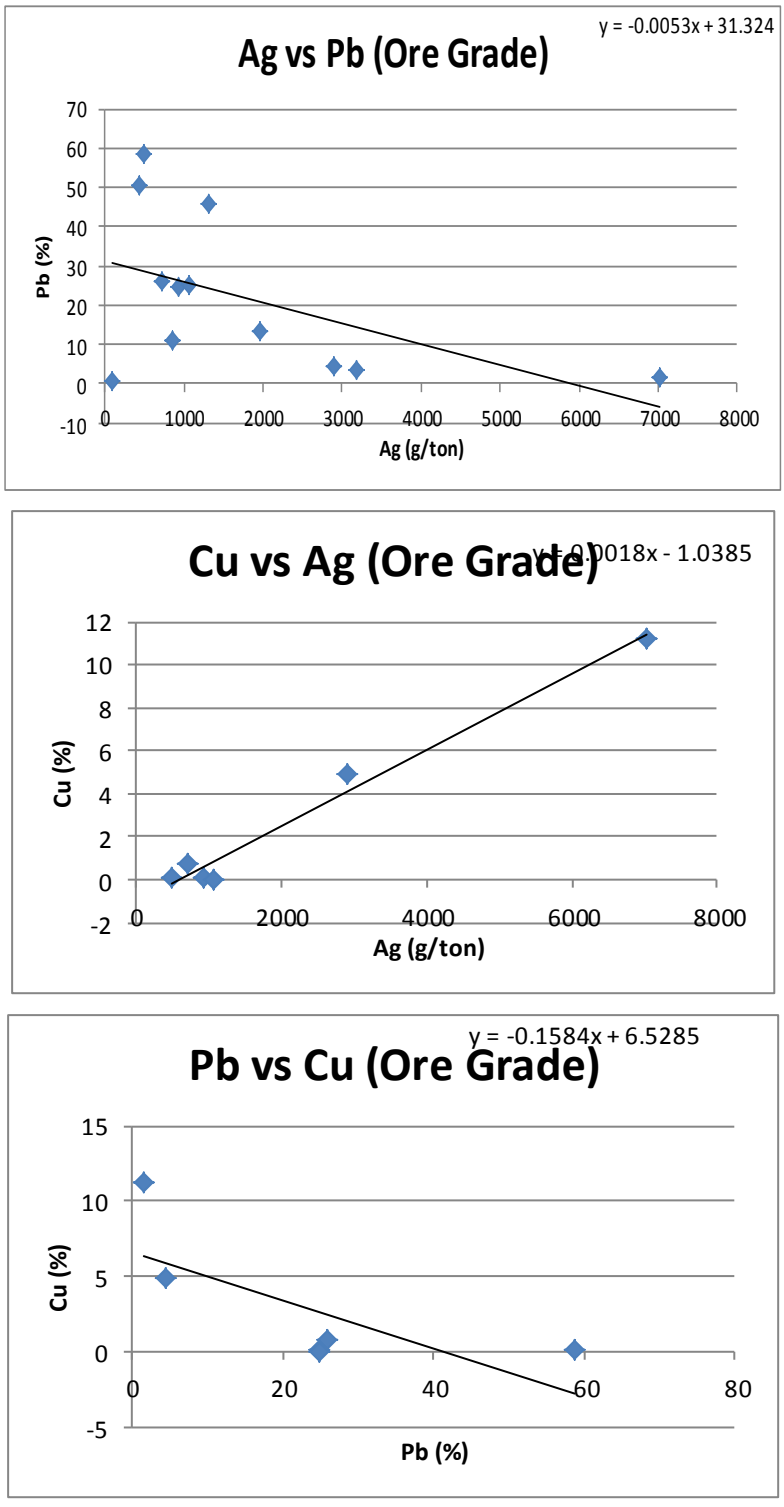

Figure 5.2.2 x-y metal plots by ore grade.

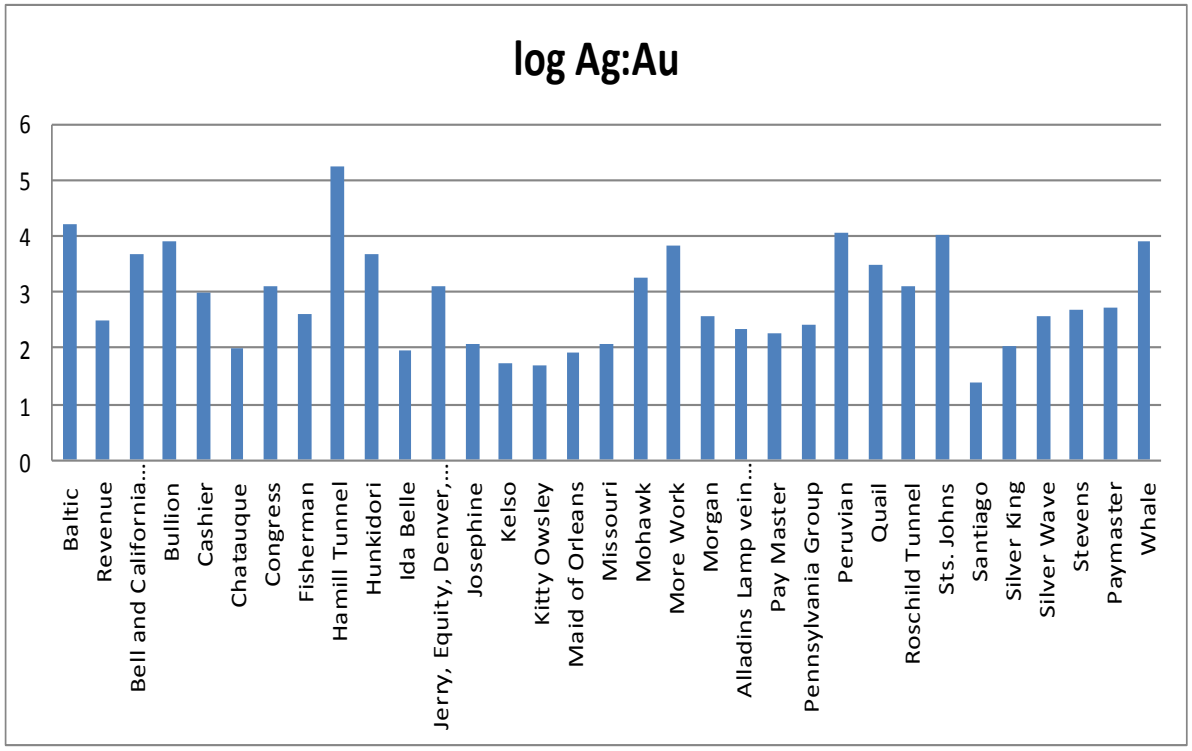

Figure 5.2.3 Ag:Au ratios for select mines of the Montezuma district. Production values from Lovering (1935). Note that all mines have at least an order of magnitude greater Ag than Au while many have several orders of magnitude greater amounts of Ag. Veins with low Ag:Au ratios may better fit the low sulfidation epithermal classification.

A.

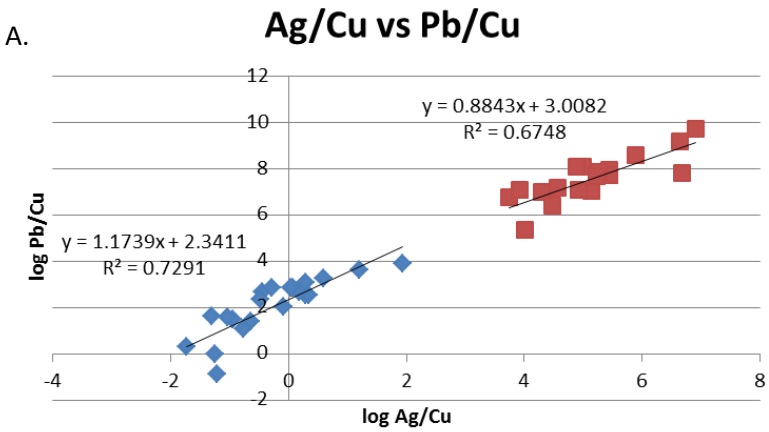

B.

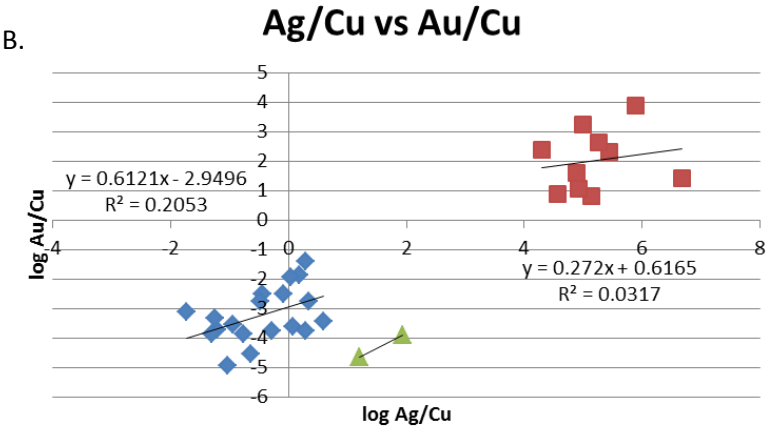

C.

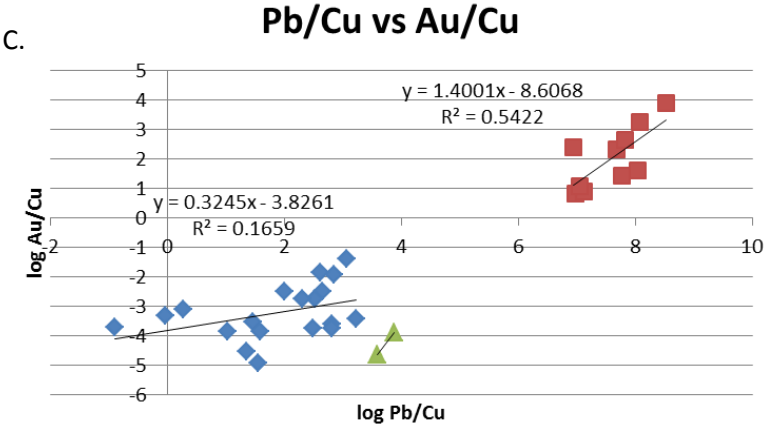

Figure 5.2.4 metal ratios with Cu as a common denominator. Blue data points are mines with production values for all three metals. Red data points are mines lacking production values for the denominators. Green data points are mines lacking production values for a numerator.

A.

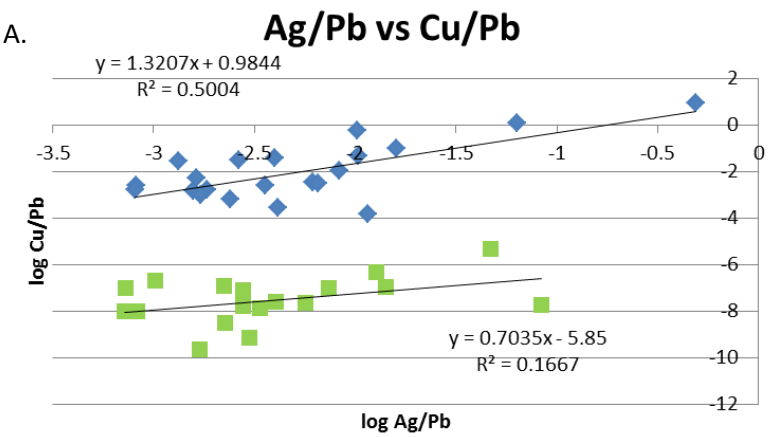

B.

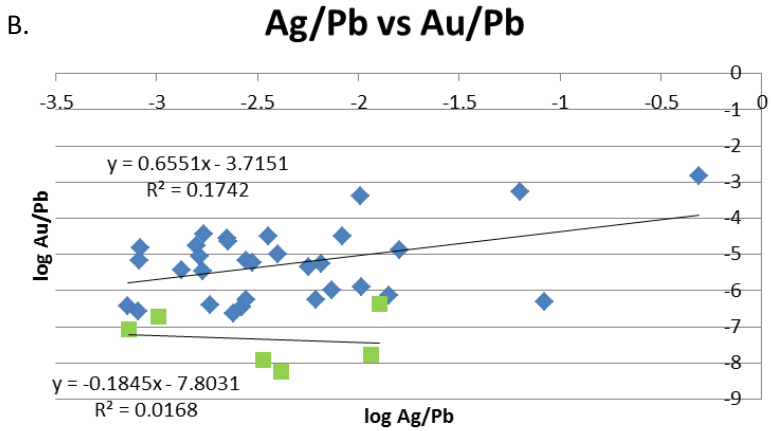

C.

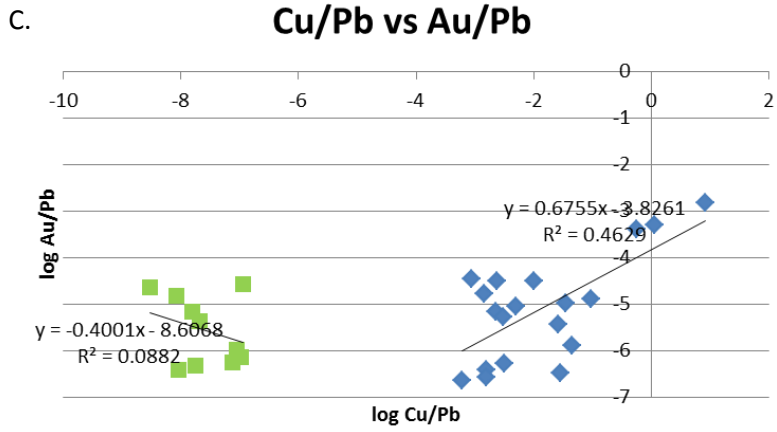

Figure 5.2.5 metal ratios with Pb as a common denominator. Blue data points are mines with production values for all three metals. Red data points are mines lacking production values for the denominators. Green data points are mines lacking production values for a numerator.

A.

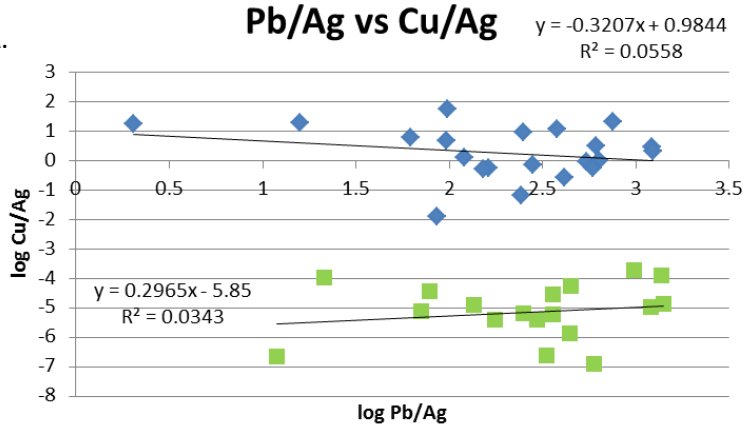

B.

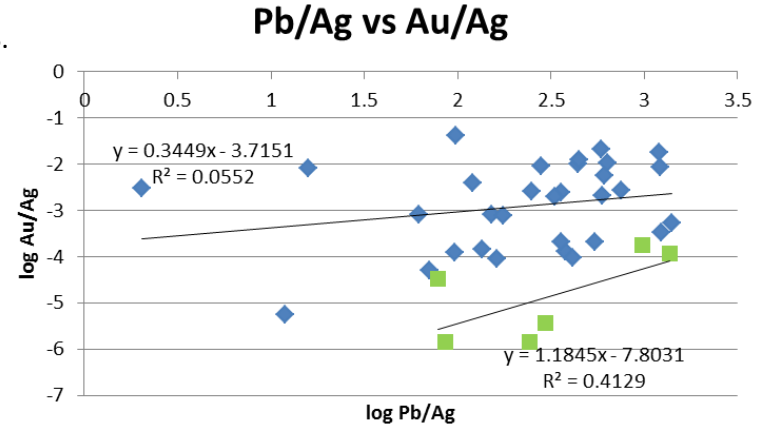

C.

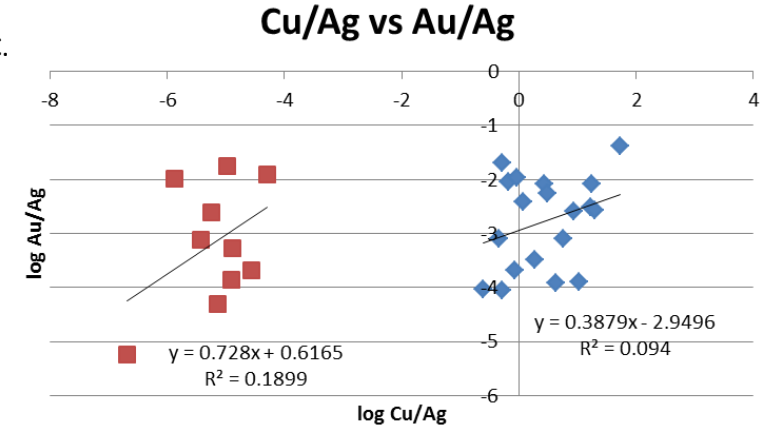

Figure 5.2.6 metal ratios with Ag as a common denominator. Blue data points are mines with production values for all three metals. Red data points are mines lacking production values for the denominators. Green data points are mines lacking production values for a numerator.

A.

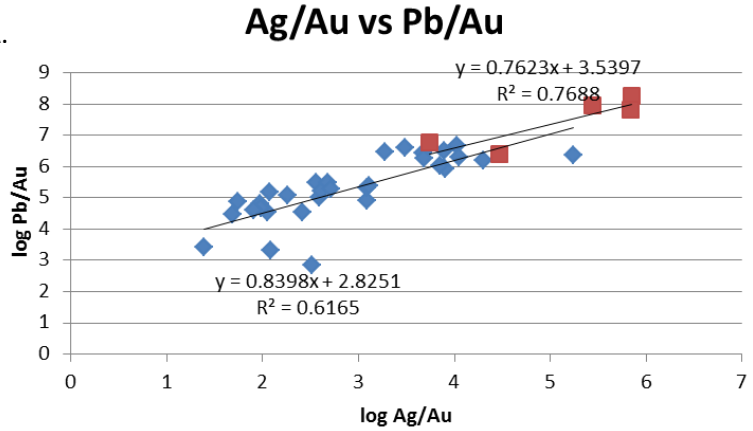

B.

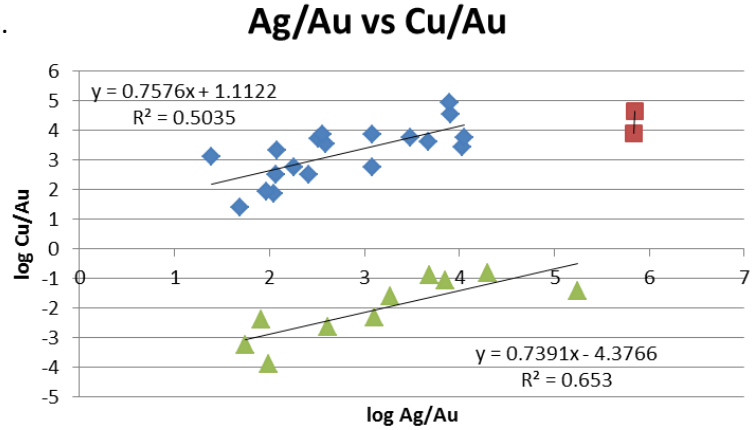

C.

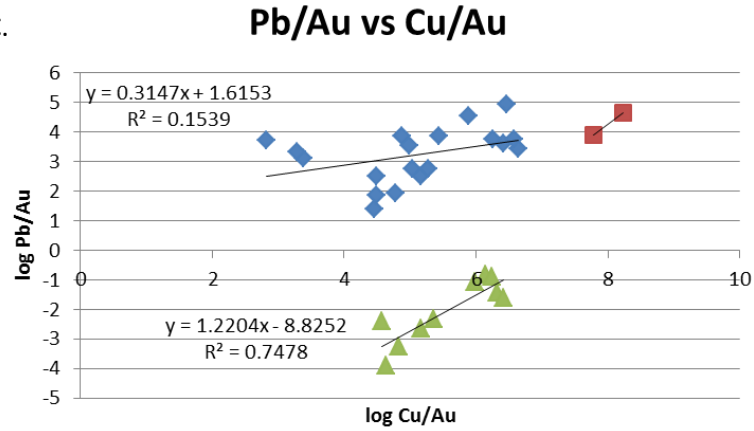

Figure 5.2.7 metal ratios with Au as a common denominator. Blue data points are mines with production values for all three metals. Red data points are mines lacking production values for the denominators. Green data points are mines lacking production values for a numerator.

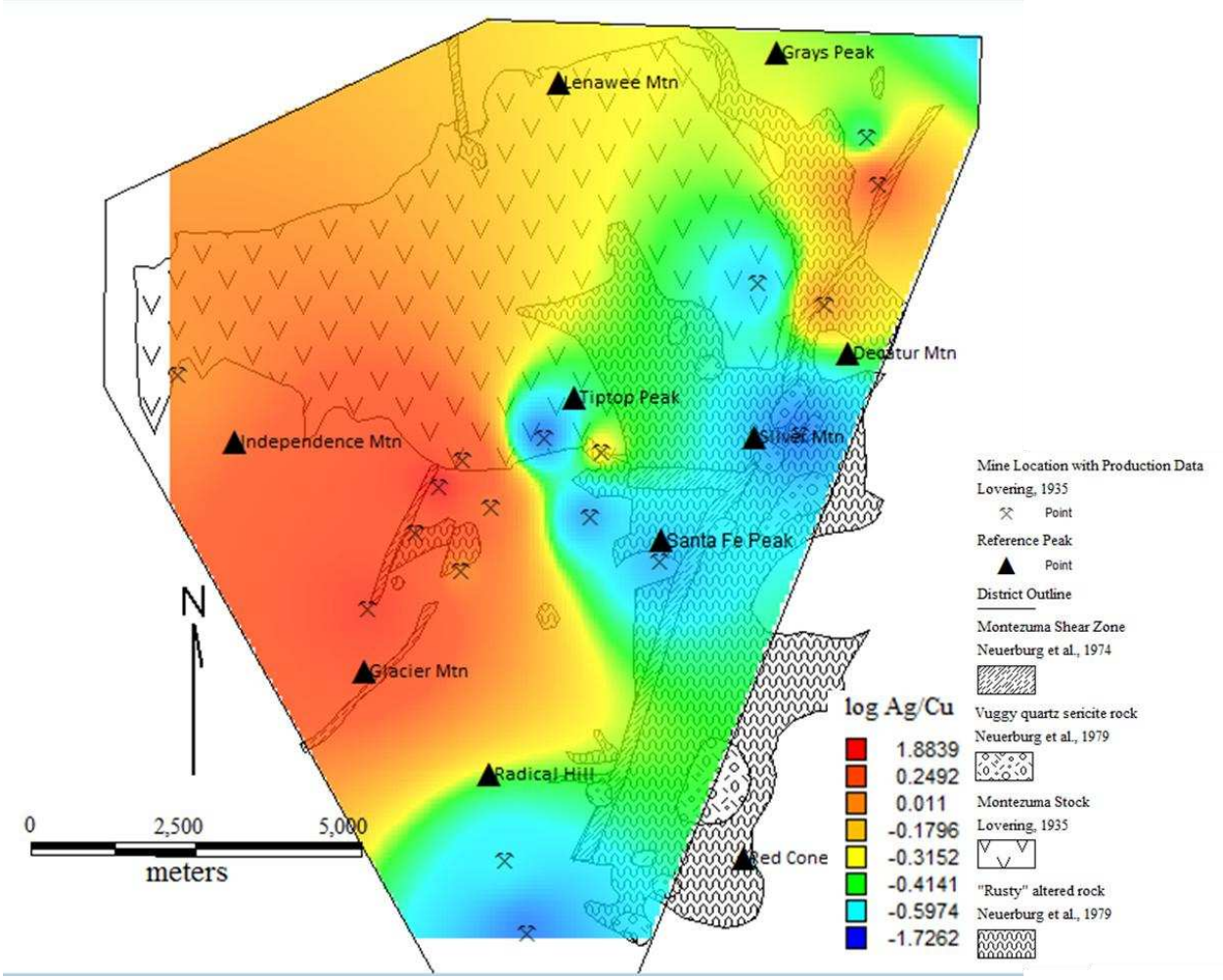

Figure 5.2.8 log Ag/Cu ratio interpolation map. Copper Rich Zone (CRZ) is indicated by cooler colors and the Copper Poor Zone is represented by warmer colors. Data points are represented by mine symbols. Note, data points are only for mines with production records. Ratios are used to account for production disparities among veins with high tonnage and veins with low tonnage.

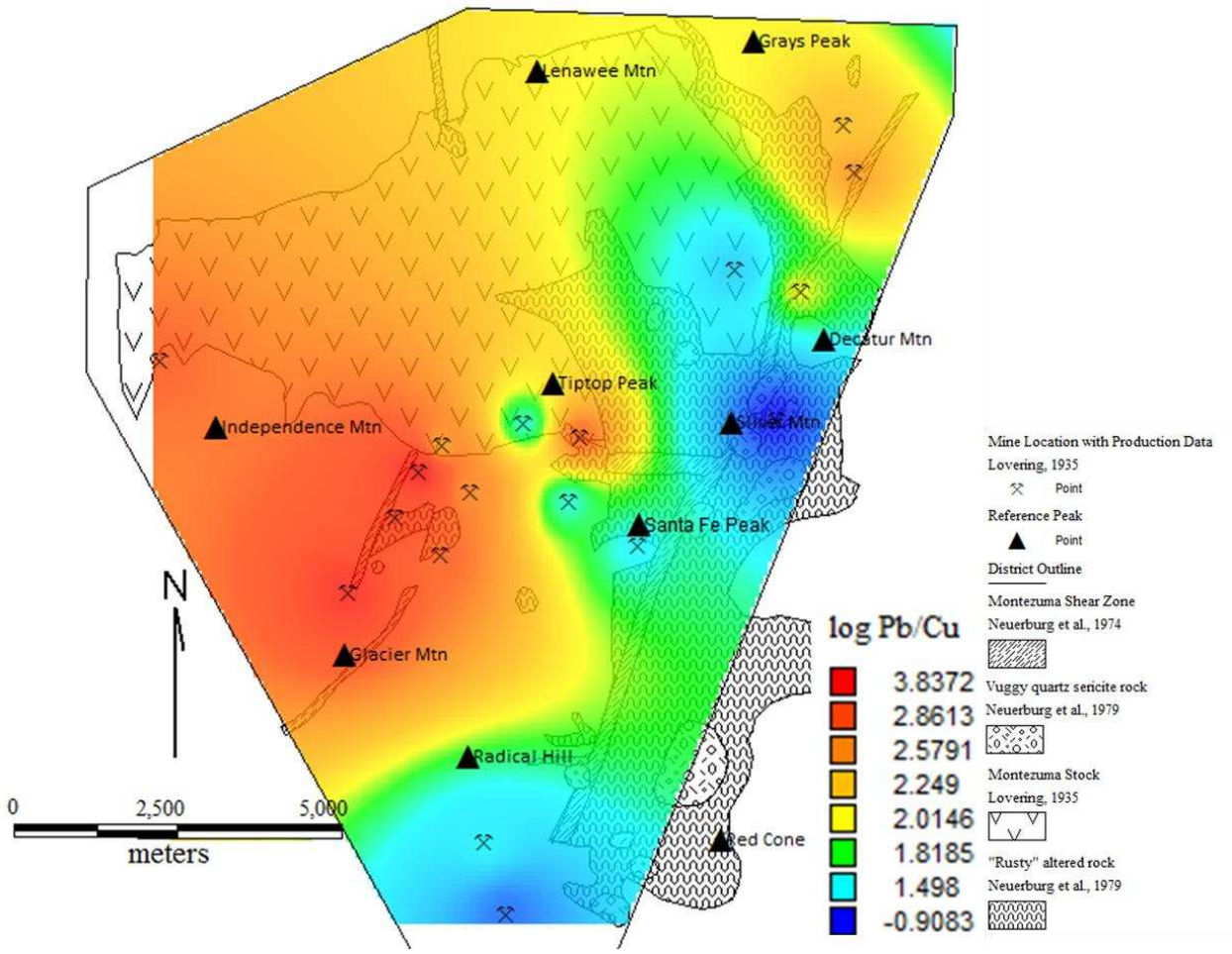

Figure 5.2.9 Pb/Cu metal ratio interpolation maps. Same data set as Figure 6.1.2 , but using Pb as a numerator.

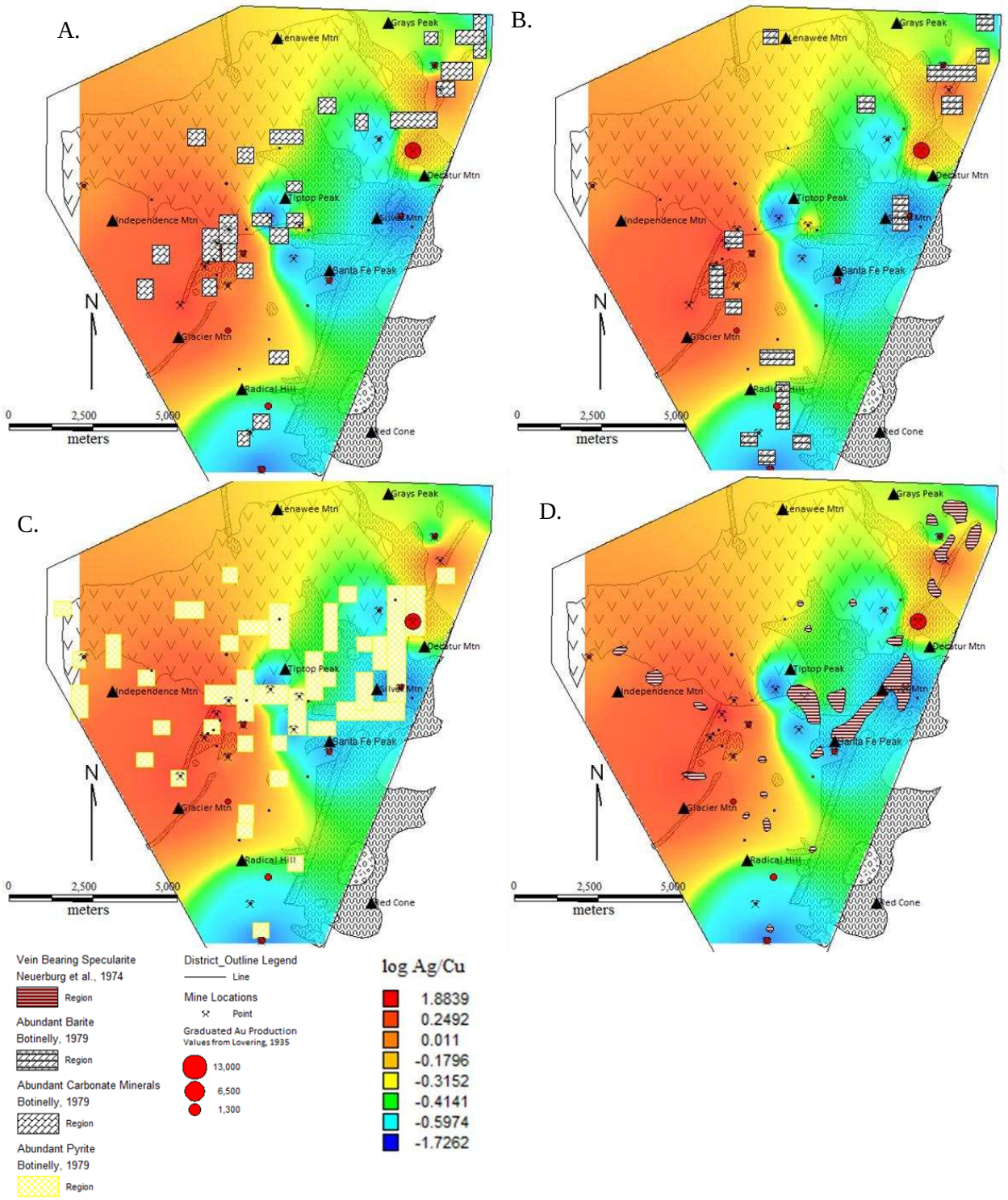

Figure 5.2.10 four maps depicting mineral distribution in the district A,B and C are based on qualitative abundances of minerals from Botinelly (1979) and D is from Neuerburg et al. (1974) simply mapping specularite presence in veins. All maps are superimposed on the log Ag/Cu map with the log gold production values as graduated red circles (A) Carbonate minerals in abundance. (B) Barite in abundance. (C) Pyrite in abundance. (D) Veins bearing specularite.

6. Fluid Inclusions

Polished sections from 16 different mines in both the CRZ and the CPZ were found to have suitable inclusions for microthermometry. The mount was stripped by submerging the sample in an acetone bath and remaining adhesive was removed with alcohol. The Linkham THMSG600 stage served to heat and cool the samples, and the Olympus BX51 microscope was used to observe phase changes. Total homogenization observations were easily observed by the author and were achieved at a temperature increase rate of 10°C/minute. The melting of ice was particularly difficult to observe. The majority of ice melting temperatures were achieved by observing motion in the gas phase in response to the inferred melting of ice. 91 approximations were made on this basis, but are supported by 21 measurements based on the empirical viewing of the solid ice phase melting. In total 112 measurements were made. Host crystals were quartz, sphalerite, barite and proustite.

6.1 Assessment of Microthermomety Data

Salinity Calculations

For two phase inclusions (liquid + gas), salinities were calculated by application of *Fluids BULK* (Bakker, 2003) to ice melting temperatures. The following procedures and equations were selected:

Component definition: (1) predefined systems

System: (2) H_2O – NaCl

Thermodynamic model for aqueous solution: (1) H_2O – Salts purely empirical, dissolved gasses and P neglected

Purely empirical equation: (4) Bodnar (1993) NaCl

Salinity of dissolved salts: (1) ice melting temperature

Equation of state of aqueous system: (4) Holmes et al. (1997)

Total Homogenization and Volume Fractions: (1) homogenization temperature

Mode of homogenization: (2) liquid

Since this study lacked geochemical knowledge of fluid inclusions, therefore the H_2O-NaCl system was assumed based on the knowledge that NaCl is the dominant salt in hydrothermal systems (Stanton, 1972). All fluid inclusions homogenized into the liquid phase.

Pressure and Isochore Calculations

Minimum pressure and temperatures of entrapment were determined from homogenization temperatures. For two fluid inclusions with two liquid phases at room temperature (double bubble). Computer modelling was applied to microthermometry data from samples QOW-1 2 A 1 and QOW-1 5 A 1. First the Q2 program was used to address the fluid composition and density using the following procedure:

Equilibrium of state to calculate fugacities in clathrate equilibria: (6) Duan et al. (1996)

Composition of homogeneous phase: 100% CO_2

Density of homogeneous CO_2-CH_4-N_2-C_2H_6 is obtained from: (3) homogenization temperature

Mode of homogenization: (1) vapor

Is the volume percentage of aqueous solution known direct after clathrate melting: (n)

The exact composition of the vapor phase was not known. 100% CO_2 was assumed because this phase is believed to be dominant in magmatic fluids (Stanton, 1972).

Results from Q2 were used to satisfy inputs required for the ISOC program. ISOC calculates isochores for fluid inclusions. The following procedure was applied to the CO_2 bearing samples:

Selection of fluid system: (1) amount-of-substance fractions of all components

Bulk fluid density: (1) value in cc/mol

Equation of state for isochore calculation: (2) Bakker (1999) Bowers and Helgeson (1983)

In which mineral group is the fluid trapped: (1) Quartz

The results from this program rendered temperature-pressure isochores for type B1 inclusion. The pressures for this inclusion were 41 Mpa and 47 Mpa, which indicates an addition of 20 – 30 °C for pressure corrections for two phase inclusions.

6.2 Fluid Inclusions Results

FI Types

Quartz, barite, sphalerite and proustite yielded workable fluid inclusions. Five types of workable fluid inclusions were reorganized based on FI morphology, relative location and phases present at 25°C (Figure 6.2.1). Other types exist but are unworkable due to either size or mineral refractive index issues.

Type A1 fluid inclusions (Figure 6.2.1.A) are rarely found in the Cordilleran-type vein system of Montezuma; rather they are more commonly found in fractured quartz in intrusive rocks. The inclusions include three phases: a liquid, gas and a cubic solid that is most likely halite. They tend to be slightly irregular with both smooth curved margins and sharp inflection points. They tend to be found in primary randomly oriented clusters or as isolated large inclusions only in quartz. FI of this type were only found in one Cordilleran-type sample from the Queen of the West mine in a Stage 1 quartz-pyrite vein (D-type vein). These inclusions were also found in a molybdenite-magnetite bearing leucogranite along the eastern flank of Teller Mountain. Unfortunately, once the sample was polished the trace molybdenite was removed from the section. Therefore petrographic relations of FI to the molybdenite were not possible. It is only speculated that this is Type A1 inclusion is related to molybdenite mineralization based on known FI relations to Mo mineralization in other deposits.

Three phase Type B1 inclusions are exclusively found in Stage 1 quartz. They are not common yet they are not as rare as Type A1 inclusions. The presence of three phases with two liquids and one vapor is the distinguishing feature of this type. Geometries are slightly irregular to sub-spherical with corresponding smooth to sharp inflection points similar to the morphologies found in Type A1. They are primary in nature occurring as random isolated inclusions or in randomly oriented clusters.

Type B2 inclusions are two phase liquid + vapor, are found in quartz and are very common. Consequently this type is well documented in this study. FIA are found as pseudosecondary trails, isolated large inclusions and randomly oriented clusters. Geometries are variable, but in quartz most are elongate pinching out or neck down along the long axis as exhibited in Figure 6.2.1.C. Type B2 inclusions in quartz are interpreted to represent Stage 1 quartz-pyrite mineralization.

Two phase, Type C1 inclusions are primary in barite and have been interpreted to be trapped during Stage 2 mineralization. These inclusions are two phase with variable proportions of liquid and gas at room temperatures. Morphologies can be similar to Type B2 inclusions or that of B1 inclusions.

Type D1 inclusions are exclusively found in sphalerite and are distinguished by their elongate geometries in which their long axis tends to be oriented parallel to growth zones. Clusters are also oriented along growth zones. These primary and pseudosecondary inclusions are interpreted to represent Stage 3 base metal mineralization. These are two phase liquid + vapor.

Type E1 inclusions are always secondary healing fracture planes in sphalerite, early quartz, barite and presumably opaque phases as well. In most instances the inclusions are two phase, but not uncommonly accidental proustite can be found as a solid phase in these inclusions (6.2.1.F). Inclusions are highly irregular in morphology and large in size relative to the other FI types. Surfaces of this FIA are also characterized by high degrees of asperities. The secondary nature and presence of daughter proustite suggest that these inclusions were trapped during Stage 5 Pb-Ag-quartz.

FI Relations to Stage of Mineralization

Figure 6.2.2 displays a scatter of all two phase FI temperature and salinity measurements with data points organized by host mineral and zone. Primary fluid inclusions from each mineral are interpreted to represent temperature and salinity conditions from a distinct stage: Type B2 in quartz are Stage 1, Type C1 in barite are Stage 2 and Type D1 in sphalerite are Stage 3. Fluid inclusions from the title heading Ag Minerals are both secondary Type E1 inclusions and primary in proustite, and these are

interpreted to represent Stage 5 mineralization. There is a high degree of scatter, but a cooling trend from Stage 1 quartz to Stage 5 Ag minerals is evident from inspection of this plot 6.2.2.

Figures 6.2.3 and 6.2.4 are box and whisker plots of results from two phase fluid inclusions (Types B2, C1 and D1). These plots are interpreted to give the range of salinities and temperatures during each stage using quartile 3 and quartile 1 values. Figure 6.2.3 displays host mineral vs pressure corrected homogenization temperatures. Temperatures are calculated from total homogenization temperatures plus 25°C for pressure isochore adjustments. Figure 6.2.4 exhibits salinity data as wt% equivalent NaCl. A systematic cooling is observed from Quartz (Stage 1) to Ag Minerals (Stage 5), while salinities are approximately constant except for barite. Stage 1 quartz-pyrite fluid temperatures were from 341 to 295°C with salinities from 11.09 to 7.58 wt.% equivalent NaCl. Stage 2 Barite temperatures were from 325 to 234°C with salinities from 9.16 to 3.70 wt.% equivalent NaCl. Stage 3 base metal temperatures were from 258 to 235°C with salinities from 11.45 to 6.73 wt.% equivalent NaCl. Stage 5 Pb-Ag-quartz fluid temperatures were from 172 to 151°C with salinities from 11.55 to 6.70 wt.% equivalent NaCl.

Figure 6.2.5 displays fluid salinity histograms. Stage 1 quartz salinities show a unimodal distribution from 8 – 12 wt.% eq. NaCl. Stage 2 barite shows a roughly bimodal distribution with high frequencies in the 2 – 4 wt.% eq. NaCl column and the 10 – 12 wt.% eq. NaCl column. Additionally, gas rich and liquid rich inclusions were found to coexist as primary inclusions in barite (Figure 6.2.6). Salinities from Stage 3 exhibit a weak bimodal distribution with a heights at 4 – 8 wt.% eq. NaCl and at 10 – 12 wt.% eq. NaCl.

Interpretation and Evaluation of Boiling in Barite

Figure 6.2.6 displays two Type C1 inclusions in barite with notably different gas: liquid ratios at 25°C. The coexistence of these two inclusions suggests that two phases (liquid and vapor) may have been present during the mineralization of this barite crystal. The gas rich inclusion (NT-13B2) homogenized at 352°C with a salinity of 3.866 wt.% eq. NaCl, and the liquid rich inclusion (NT-13B1) homogenized at

229°C with a salinity of 4.95 wt.% eq. NaCl. Figure 6.2.7 depicts isotherms at which gasses and liquids can coexist with given salinities. If the above two inclusions are the result of phase separation, then this would have occurred at around 35 MPa and at roughly 425°C (reference the horizontal blue tie line in Figure 6.2.7). These two fluid would then rise in the vein until their final crystallization temperatures indicated by total homogenization. The gas rich inclusion total homogenization temperature is higher than the liquid rich inclusion, which is expected as a liquid phase would most likely travel slower and thus be subjected to greater degrees of cooling.

6.3 Fluid Inclusion Relations to District Scale Zonation

Data from fluid inclusions were separated into two groups based on the zone in which the sample originated: CPZ or CRZ. This segregation has allowed for temperature and salinity comparisons of the two zones. The division of minerals into zones rendered particularly small populations for each grouping: Ag CPZ (6), Ag CRZ (10), Sphalerite CPZ (24), Sphalerite CRZ (5), Quartz CPZ(9) and Quartz CRZ (36). Note that all data from barite samples were from the CPZ therefore this mineral was not used in the comparison. Figure 6.3.1 displays fluid temperatures. There is little zonal difference in quartz. However, it is evident that fluid temperatures are greater in the CRZ for sphalerite and silver minerals than their CPZ counterparts. Salinities from quartz and sphalerite show no apparent difference in zones (Figure 6.3.2). Salinities in Ag minerals do show zonal differences. Salinities for Ag minerals in the CRZ are greater than salinities in the CPZ. However, this relationship is based on very few data points.

Figure 6.3.3 displays histograms of salinity and temperatures for each mineral with color shading according to CPZ and CRZ. These histograms were produced to determine if any patterns existed in this system in order to evaluate the validity of mean relations of among the zones. Salinities and temperatures for both CPZ and CRZ in quartz show a unimodal distribution, with no zonal differences. Temperatures for sphalerite in the CPZ show unimodal distribution while the sphalerite in the CRZ are also unimodal. Also, based on Figure 6.3.3.C it is clear that temperatures were hotter in the CRZ. Salinities during

sphalerite mineralization are bimodal for both the CPZ and the CRZ and show no zonal differences. Temperatures during Ag mineralization are likely hotter, yet not conclusively, hotter in the CRZ based on Figure 6.3.3.E. Salinities are also greater in the CRZ during Stage 5 Ag mineralization.

Figure 6.3.4 charts the means with confidences for salinities and temperatures for each host mineral by zone. This is displayed to simplify and generalize the analysis. All mean salinities and temperatures for the CRZ are higher. However, only sphalerite showed no overlap at 90% confidence for temperatures, and the normal distribution of data for this mineral (6.3.3.C) indicate that this is a robust relationship. Therefore it is proposed that a thermal gradient was a factor in metal zonation, at least during Stage 3 base metal mineralization. Temperatures for Stage 1 quartz show significant overlap in 90% confidence among the CPZ and the CRZ and therefore it is proposed that district scale thermal gradients did not affect mineralization during this stage. Stage 5 Ag mineralization indicates that there was little thermal differences among zones, but there were greater salinities in the CRZ than the CPZ based on 90% confidence intervals.

Figure 6.3.5 charts the means with confidence indices of all fluid inclusions separated only by zone. The CRZ temperatures are hotter with no overlap at 90% confidence. Salinities are also greater in the CRZ with only a minor overlap at 90% confidence as compared to the CPZ. This may indicate a higher degree of meteoric water dilution in the distal CPZ regions of the district. Figure 6.2.2 displays a scatter of all FI measurements with data points organized by host mineral and zone. This figure shows that the system is actually more complex than the above interpretation. Perhaps the high degree of scatter with regard to single stages is a function of time in addition to the spatial component. An additional possibility is that the district has been subjected to multiple fluid sources. One conclusion can be made from this data: that fluid cooling is a significant control on mineral paragenetic sequence in this system and metallic zonation.

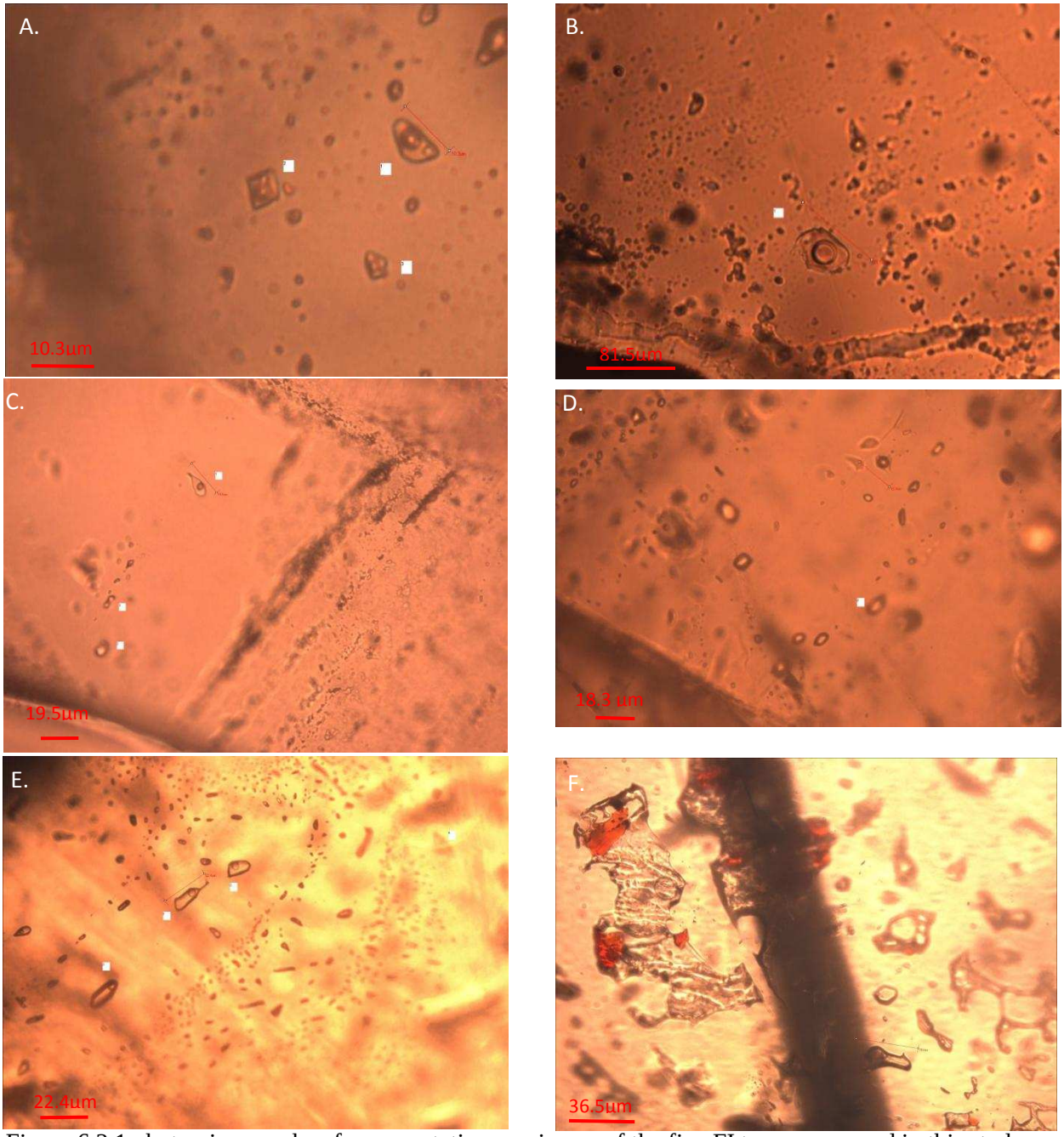

Figure 6.2.1 photomicrographs of representative specimens of the five FI types measured in this study. The types were interpreted to represent fluid conditions of particular stages. (A) Rare type A1 inclusions found in early quartz and in intrusives. Three phase inclusions: liquid, gas and a cubic solid most likely halite. (B) Type B1 inclusions in early quartz. Three phase: gas, gas (Double bubble) and liquid. (C) Type B2 inclusions in early quartz. Two phase inclusions: gas and liquid. (D) Type C1 inclusions in barite two phase with variable liquid gas ratios (E) Type D1 inclusions in sphalerite. Two phase inclusions with liquid and gas. (F) Type E1 inclusions are secondary in sphalerite, early quartz and barite. Primary inclusions in proustite yield similar results. These are two or three phase: liquid and gas or liquid, gas and accidental solid (red material in image is proustite).

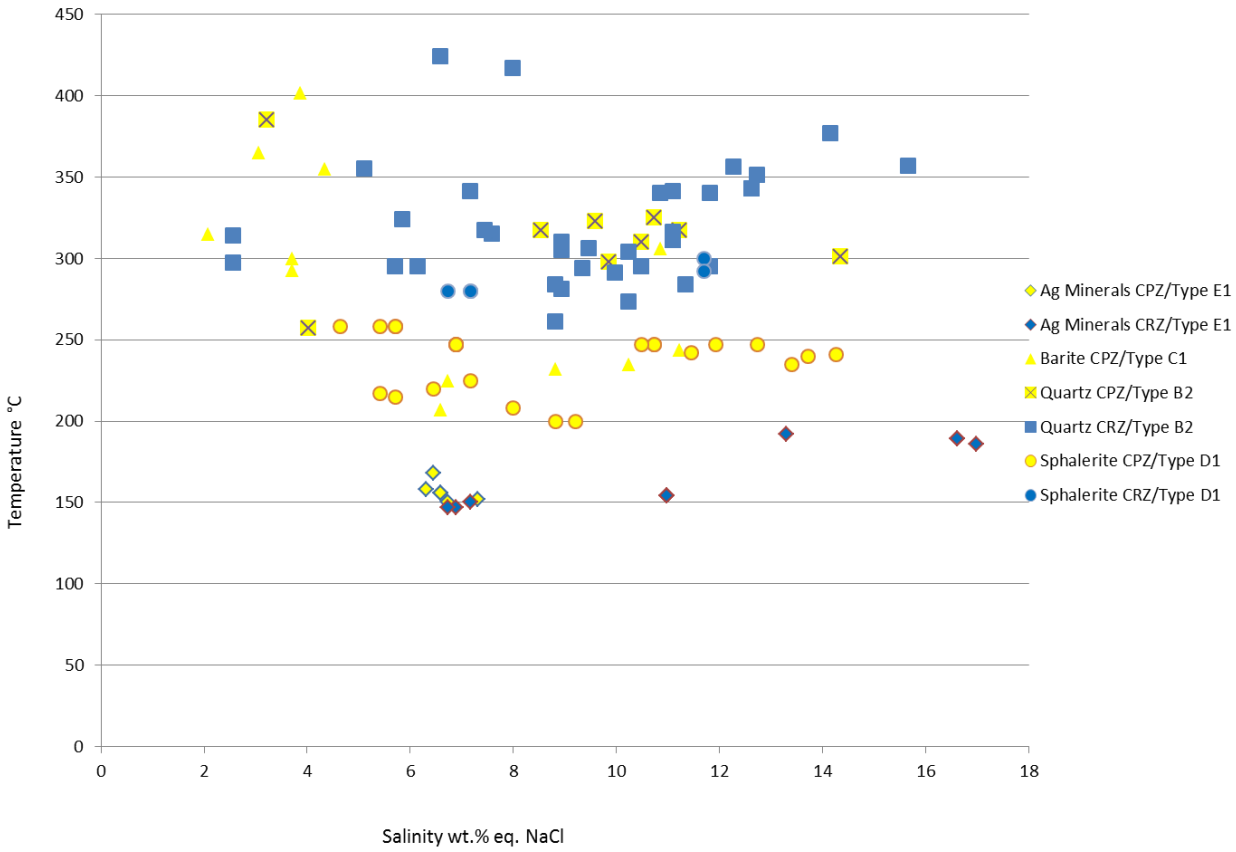

Figure 6.2.2 Salinity vs temperature plot with data points organized by mineral and zone. There is a clear cooling trend from quartz to sphalerite to Ag minerals, while salinities values are less systematic. Quartz/Type B2 is Stage 1, Barite/Type C1 is Stage 2, Sphalerite/Type D1 is Stage 3 and Ag Minerals/Type E1 is Stage 5.

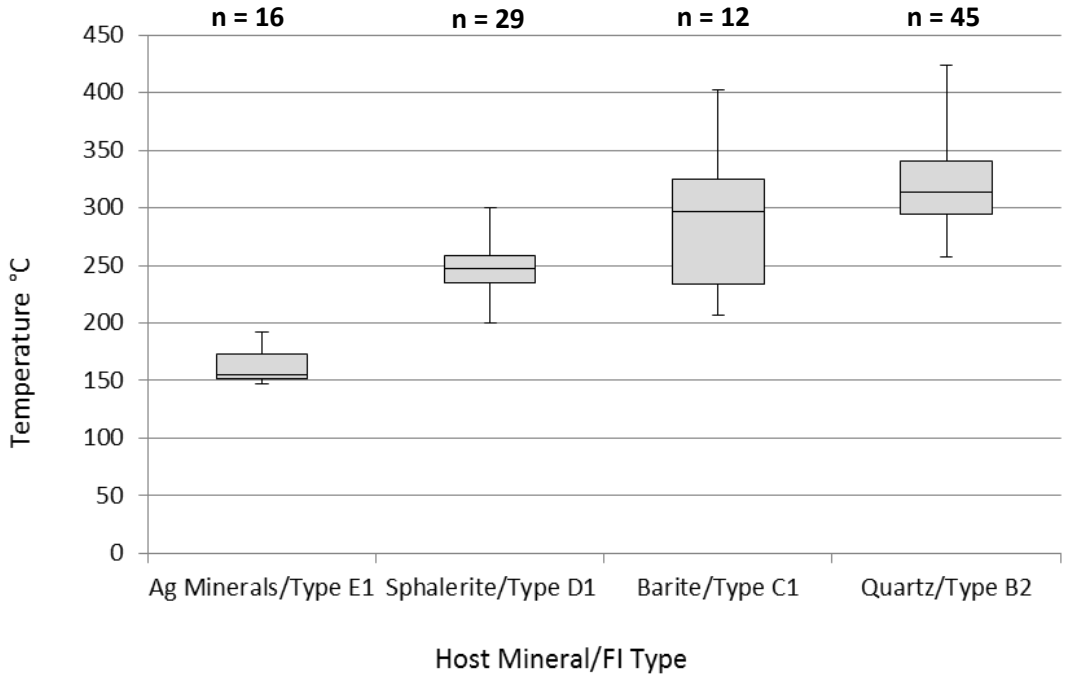

Figure 6.2.3 Box and whisker plot of total homogenization temperatures in two phase inclusions plus temperature adjustments for pressure. Temperatures have been adjusted to pressure conditions of 41—47 MPa isochores adding 25°C. A cooling trend is apparent from Stage 1 Quartz to Stage 5 Ag Minerals.

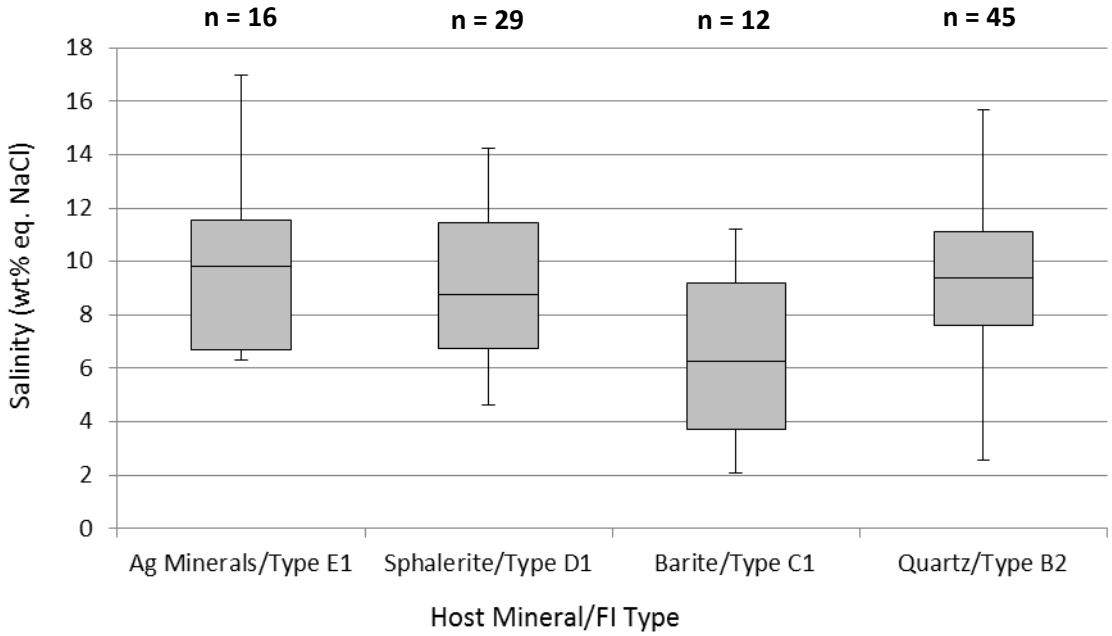

Figure 6.2.4 Box and whisker plot of calculated salinities from final ice melting temperature and *BULK* modeling program. Salinities are roughly consistent through the paragenetic sequence with the exception of Barite.

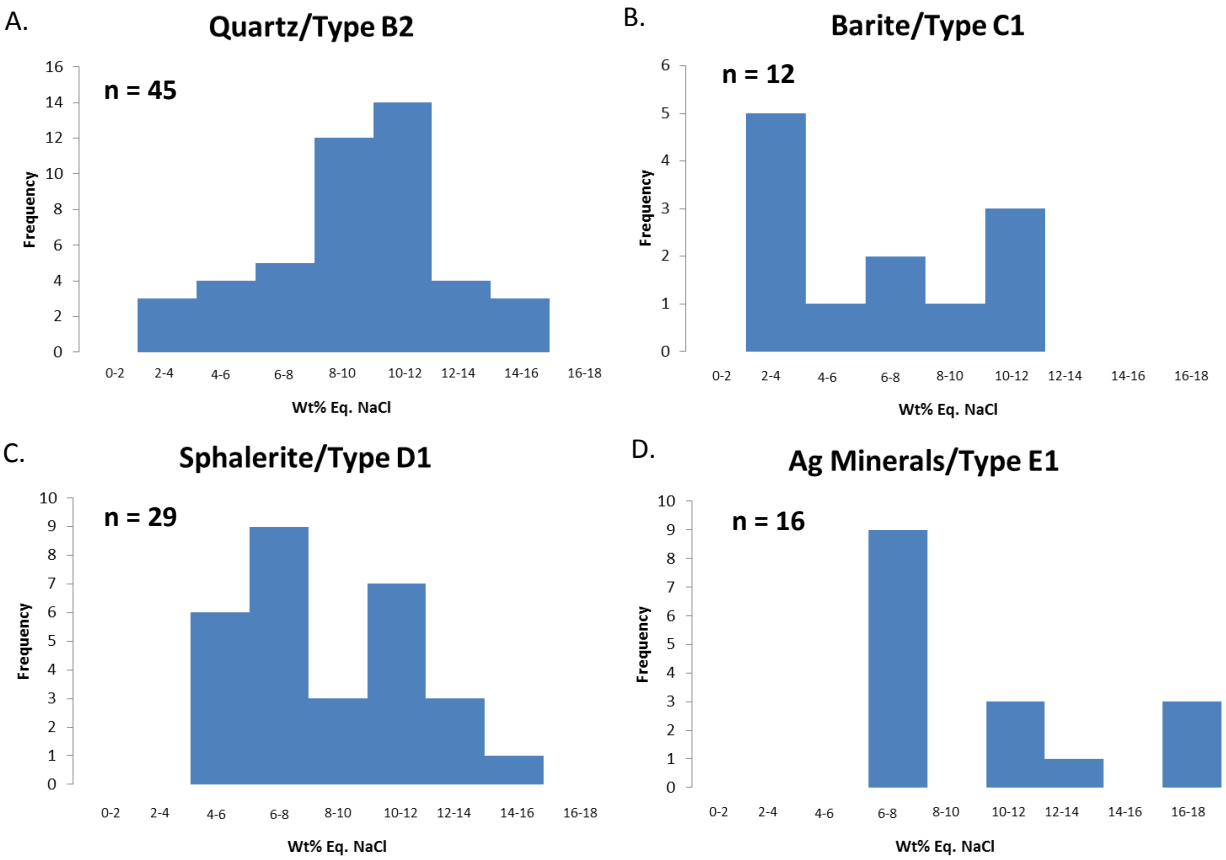

Figure 6.2.5 Histogram representations of approximate salinities for each mineral (A) Quartz salinities show a prak distribution from 8—12 wt.% eq. NaCl. (B) Barite indicates a bimodal distribution pattern. (C) Sphalerite data shows a very weak bimodal distribution within a large range from 4—12 wt.% NaCl. (D) Ag Mineral distribution peaks from 8—10 wt.% NaCl.

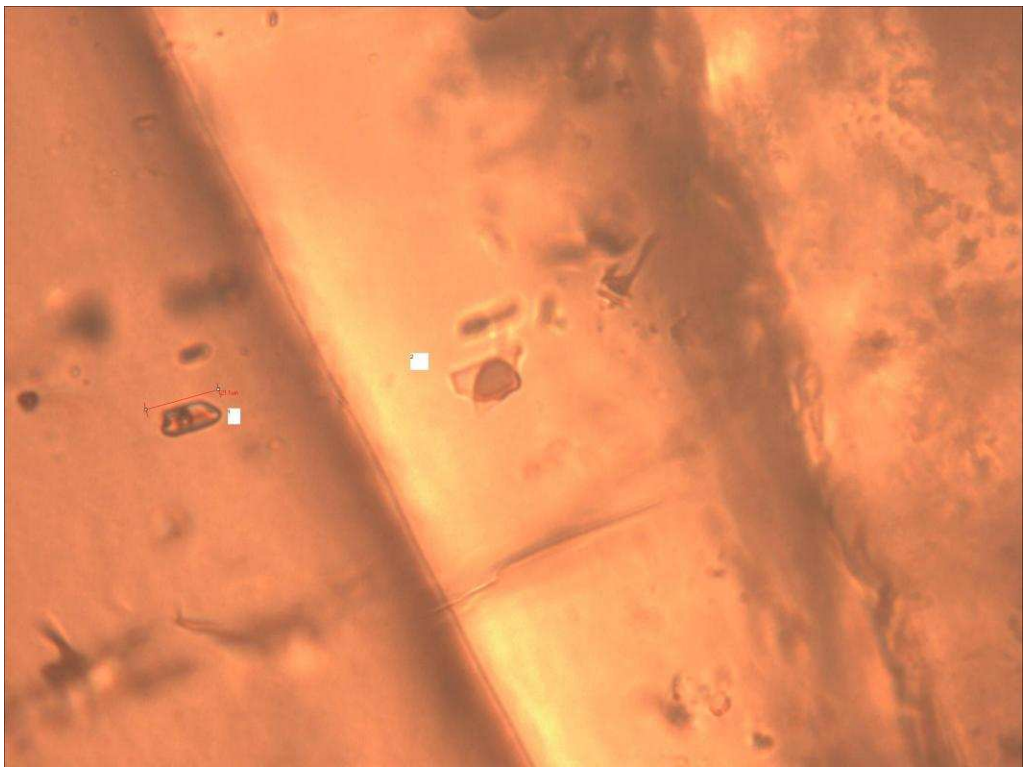

Figure 6.2.6 FI in barite from the National Treasury Mine (NT-1). Both labeled inclusions are interpreted to be primary, yet fluid/gas ratios are vasty different among the two. Additionally, the inlusion on the right seems to have a gas phase with a higher refractive index than the inclusion on the left, which suggest these two inclusion are of different compositions.

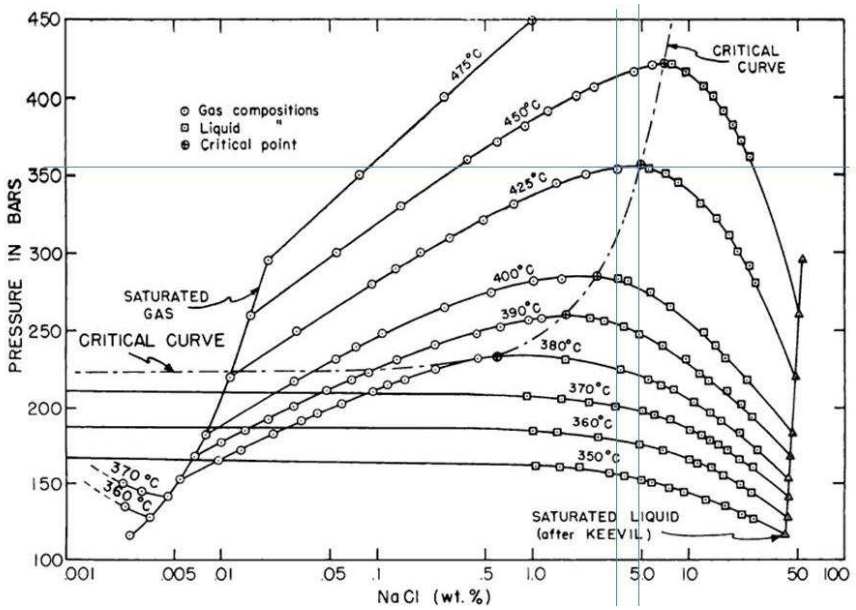

Figure 6.2.7 modified from Sourirajan and Kennedy (1962). Isotherms 350—450°C showing composition of coexisting gasses and liquids at the pressures shown on the x-axis.

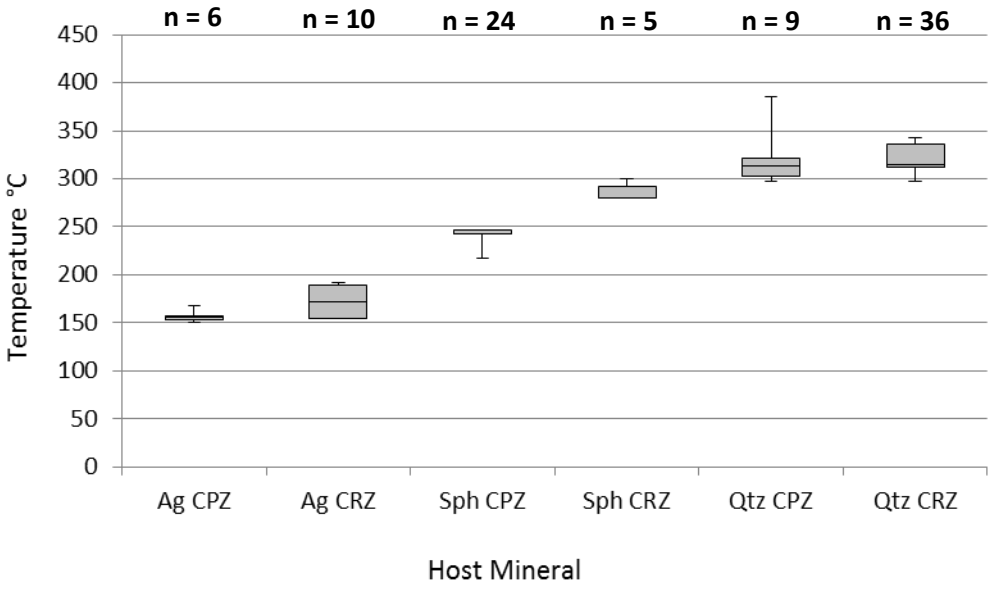

Figure 6.3.1 Box and whisker plot of fluid temperatures by host mineral and location with in district scale zonation: Copper poor zone (CPZ) or copper rich zone (CRZ). CRZ temperatures are consistently hotter than their CPZ counterparts.

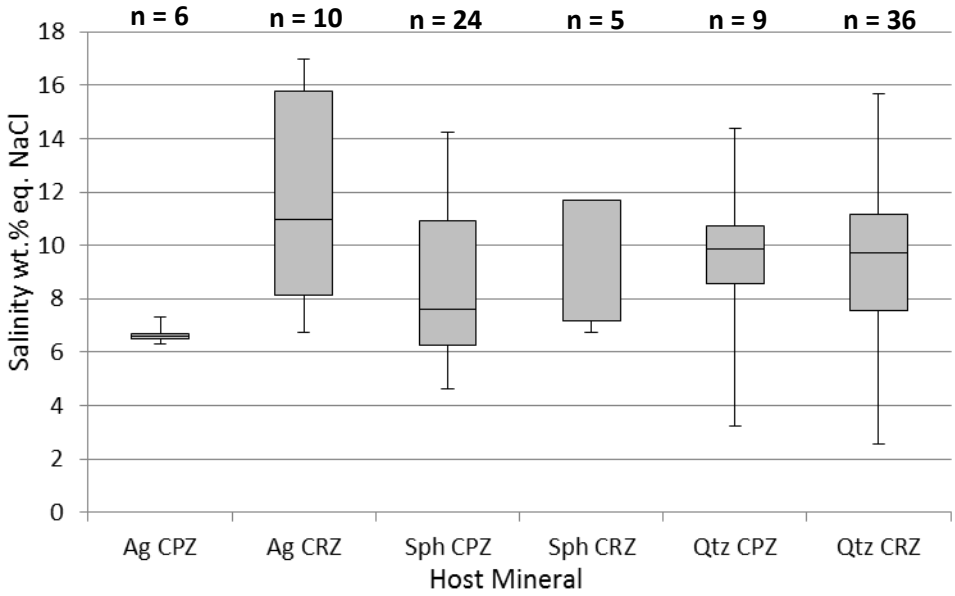

Figure 6.3.2 Box and whisker plot of fluid salinities by host mineral and location with in district scale zonation: Copper poor zone (CPZ) or copper rich zone (CRZ) except for the quartz stage.

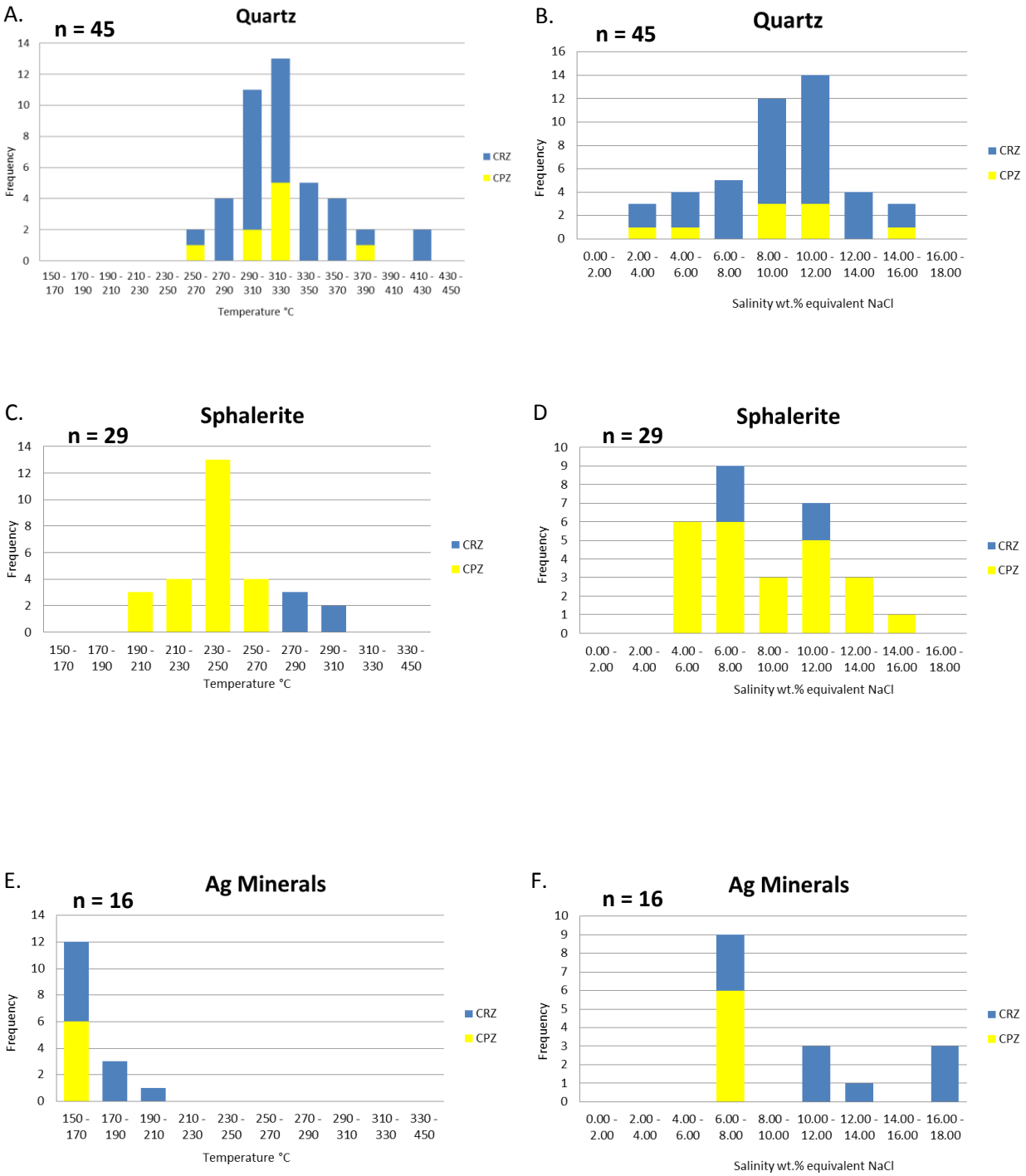

Figure 6.3.3 temperature and salinity histograms organized by minerals and divided into zones.

Mineral and Zone	Quartz CRZ	Quartz CPZ	Sphalerite CRZ	Sphalerite CPZ	Ag Minerals CRZ	Ag Minerals CPZ
Mean Temperature/ 90% confidence (°C)	321 331—310	314 335—294	286 293—278	237 243—231	166 177—154	156 161—151
Mean Salinity/90% confidence (wt.% eq. NaCl)	9.42 10.25—8.59	9.11 11.25—6.98	8.89 10.99—6.79	8.71 9.76—7.66	11.72 14.07—9.36	6.66 6.92—6.40

Figure 6.3.4 Mean with 90% confidence for salinities and temperatures organized by mineral and zone.

Zone	CRZ (Quartz, Sphalerite and Ag Minerals)	CPZ (Quartz, Sphalerite, and Ag Minerals)
Mean Temperature/ 90% confidence (°C)	287 303—271	242 257—228
Mean Salinity/90% confidence (wt.% eq. NaCl)	9.82 10.59 — 9.05	8.49 9.29 —7.69

Figure 6.3.5 Mean with 90% confidence for salinities and temperatures for all fluid inclusions by zone.

7. Discussion

The Cordilleran-type classification of veins at Montezuma allows the district to be compared to better studied analogue districts. The evolution of hydrothermal fluids responsible for alteration and fissure fill in these Cordilleran veins are highly variable from district to district, which reflects the open system in which they operate. Contrasting genetic interpretations of fluid evolution mechanisms and ore deposition have been proposed by researchers of such ore deposits worldwide (Beuchat et al., 2004). This suggests that there are indeed a wide array of variables that act on hydrothermal fluids of this ore type. However, unifying characters are that a low-salinity magmatic ore fluid has been variably mixed with meteoric waters, while P-T-X parameters are responsible for precipitation of compositionally and spatially variable ore minerals (Catchpole et al., 2012). Reed et al. (2013) have determined that a single evolving magmatic fluid has the capability to render effectively all characteristic alteration and mineral assemblages found in theses deposits. The dominant controls on fluid evolution are variations in temperature, extent of fluid-wall rock interaction along fluid pathway and inevitable pressure decrease on fluid flow upwards through the crust. Additionally meteoric water interactions can also play an important role in these systems (Catchpole et al. 2012; Bendezú and Fontboté, 2009; and others). At Montezuma, temperature decline is the dominant precipitation mechanism of ore and gangue minerals in veins as discussed later in this chapter.

At Montezuma, district scale zonation and temperature decline over the paragenetic sequence in veins indicate a waning pluton as the source for heat in the district. Under the assumption that these Cordilleran-vein deposits are magmatic in origin, a connection to porphyry Cu-Mo systems can be speculated. In the Cordilleran-porphyry system a general succession of four consistent hydrothermal fluid periods are identified at deposits globally: 1. an early quartz-chalcopyrite with biotite-potassium feldspar alteration, 2. a quartz-molybdenite fluid with little or no alteration, 3. a later pyrite-quartz fluid with

intense sericitic alteration and finally 4. an overprinting base metal vein stage (Reed et al., 2013; Seedorf et al., 2005; Sillitoe, 2010). Stages three and four are the fluids in Cordilleran vein fields and are well developed in the Montezuma district. This connection between fluid events and styles of mineralization is well documented at Butte, USA (Reed et al., 2013) and Morococha (Catchpole et al., 2011), which exemplify the model for Cordilleran veins and porphyries. Based on data presented in this study, an evaluation of a Mo-Cu porphyry connection at Montezuma will be attempted in Section 7.5.

7.1 Cordilleran-type classification

The veins of the Montezuma mining district fit the eight criteria laid out by Fontboté and Bendezú (2009) for Cordilleran veins. The mineralized veins of the Montezuma district are spatially related to the sub-alkaline Montezuma stock, which satisfies criterion 1. Although a mineralized porphyry has not been identified in the district, Cordilleran veins are observed cross cutting the Montezuma stock (eg. the American Eagle, Winning Card, Fisherman and Congress veins). This indicates that the mineralized veins are later than the associated magmatic body satisfying criterion 2. Additionally, D-type stockwork veins in the district were found to be hotter than later base and precious metal mineralization suggesting a later timing for Pb-Zn-Cu-(Ag-Au) veins. Criterion 3 requires that these veins are deposited under shallow crustal conditions. Data from three phase fluid inclusions indicate that these vein were deposited at 47 to 41 Mpa, which correlates to less than 2 km depth based on average pressure gradients in the crust. Criterion 4 states that Cu-Zn-Pb-W-Sn-(Ag-Au-Bi) are the metal suites found in these veins with more than 50 wt.% as sulphides. Cu-Zn-Pb-(Ag-Au) were the commodities mined from the Montezuma district. Bi is noted to occur as bismite, bismuthinite, bismutite, beegerite, cuprobismutite and other minerals (Lovering, 1935). W is found as wolframite and is associated with bismuth ores at the Missouri mine (Lovering, 1935). Sn is not observed in this district, thus criterion 4 is only partially satisfied. District scale zonation was identified based on relative copper abundances satisfying criterion 5 of zonation in ores of this type. Criterion 6 requires that that mineralization occurs as open space fillings. At Montezuma, this is evidenced by ore textures of coarse

grained euhedral minerals, comb texture, abundant vughs and triangular acute infill and other indicative textures. Criterion 7 states that Ag:Au ratios are significantly higher than high-sulfidation epithermal Au-(Ag) deposits. Figure 5.2.3 shows the Ag:Au ratios for mines of the district. All mines have at least an order of magnitude greater Ag than Au while many have several orders of magnitude more Ag than Au. Most high sulfidation state epithermal veins only have Ag:Au ratios of 1:1 to 100:1 (Figure 7.1.1). The median Ag:Au ratio at Montezuma is 480:1 and the average is 7,800:1 which is significantly higher than ratios found at epithermal deposits. However, there are several veins in the district (Maid of Orleans, Ida Belle and Chatauque) and several directly marginal to Montezuma (Santiago, Kitty Owsley, Kelso and Josephine) that indicate Ag:Au ratios within the epithermal range. This only acts to support the idea that the classification of veins in a magmatic-hydrothermal system lie along a spectrum. Fluid inclusion total homogenization temperatures ranged from 156°C to 341°C. Salinities range from 11.69 to 3.70 wt.% eq. NaCl, which constitute low to moderate salinities. These fluid inclusion data satisfy criterion 8.

7.2 Framework and Setting of the Cordilleran Veins in the Montezuma District

Component and Fluid Source

Data from this study cannot prove conclusively that metals are from a magmatic source. The zonation and paragenetic sequence observed in veins are typical of sulphide ore bodies around centrally located stocks (Sillitoe et al., 2010; and others). It is predicted that an ICP-MS fluid inclusion geochemistry study would prove a systematic depletion of Cu from the CRZ to the CPZ indicating a single fluid source. The proven classification of these veins as Cordilleran-type favors the interpretation that metals are magmatic in origin, but does not provide a definitive answer.

Assimilation of sulfur from evaporate country rock is a proposed sulfur source for Pb-Zn-Cu-Ag mineralization at Sultan Mountain mine (San Juan Mountains, Colorado, USA) based on $\delta^{34}S$ values (Musgrave and Thompson, 1991). Contrastingly, it has also been inferred that sulfur is from a magmatic source as inferred from $\delta^{34}S$ values (Sweet Home mine, Lüders et al., 2009). The Montezuma district

lacks evaporates and other sulfur rich host rocks, which renders the possibility of assimilation of sulfur from country rock unlikely. Most researchers (eg. Catchpole et al., 2011) have found that sulfur in sulfides and sulfates are from a magmatic source in the Cordilleran environment, and this will be the favored interpretation for this study.

Acidity in hydrothermal solutions is dominantly sourced from CO_2, Cl and S-derived species. Most reduced S-species acids are weak acids, and the precipitation of sulphides further reduces the influence of these species rendering the CO_2 and HCl as primary acidity generators (Giggenbach, 1997) in addition to disproportionation of SO_2. CO_2 is presumably derived from magmatic H_2CO_3, and HCl is most likely magmatic as well. In epithermal and Cordilleran systems, CO_2 is from a magmatic source based on carbon-oxygen isotope signatures in carbonate (Zukowski et al., 2014). Other components are likely to exist in the Montezuma district, but HCO_3^- and Cl^- will be assumed as dominant anions. CO_2 was found in Type B1 inclusions in early quartz therefore this anion is known to exist in the hydrothermal fluid.

Timing

Several authors (Bendezú et al., 2003; Rice et al., 1982; Cunningham et al., 1994) have found through quantitative studies that spatially related intrusives are older in age than associated polymetallic vein fields. In many ore fields, veins can be observed crosscutting associated intrusives as found in the Montezuma mining district and others. These Cordilleran-type veins also post-date stockwork porphyry type mineralization. The classic example of this relationship is found at Butte, Montana where the Main Stage veins can be observed overprinting porphyry stockwork copper mineralization (Reed, 1999). Muntean and Einaudi (2001) found that Cordilleran-type veins formed after D-veins in the porphyry system. D-veins serve as a time line that is taken to indicate the cessation of igneous activity in porphyry systems. As mentioned, the American Eagle, Winning Card, Fisherman and Congress veins all crosscut the Montezuma stock indicating they are younger relative age to magmatism in the area.

Pressure and Depth of Emplacement

Pressure is an important variable considering the range in depth from cupola source to the Cordilleran environment and considering the range of temperatures. Two controls on fluid pressure in veins are: 1. depth of emplacement of the system and 2. vertical movement of the brittle-ductile transition. Greater paleo depths of emplacement and greater temperatures correlate to greater pressures and more ductile conditions. Brittle fracture of rock is essential in the Cordilleran-type environment; shallower cooler conditions will promote the development of larger structures that provide the necessary conduits for hydrothermal fluid flow. More ductile conditions can limit the volume of structures. As a pluton cools, the country rock also cools leading to more brittle conditions. The transition to a brittle regime leads to the potential for greater volume in fractures, which result in lower pressure conditions for passing hydrothermal fluids. An additional pressure reduction control is progressive weathering and removal of overburden of a deposit with time, which will decrease country rock lithostatic pressures.

Entering a brittle regime can have several influences in a district. Lower fluid pressures enact to decrease the concentration of ionic species by favouring disasociation reactions while the association reactions are favoured by pressure increase. This can aid in reducing the stability of chlorides complexes for example (Seward and Barnes, 1997):

$$FeCl^{2+} \rightarrow Fe^{3+} + Cl^{-} \qquad \text{(Eq. 7.1)}$$

In this disassociation reaction, Fe is now available to bond with sulfur forming pyrite depending on sulfur fugacity. Additional physical precipitation mechanisms such as boiling may also be induced by pressure decline. A brittle regime may also enhance meteoric water dilution by increasing the volume of structural weaknesses and permitting these fluids to enter the magmatic hydrothermal system.

Pressures in veins at Montezuma were obtained from Stage 1 quartz three-phase fluid inclusions. These veins were deposited at pressures of 47 to 41 Mpa. Depth of emplacement values are not available for the Montezuma stock. However, paleodepths of emplacement are available for the neighboring Urad-

Henderson and Climax porphyries, which will be used for a lack of geobarometric for the Montezuma Stocks. Geraghty et al. (1988) have determined that both the Climax and Urad-Henderson were emplaced at depths of 2.8 to 3.1 km at lithostatic pressures of 72 to 80 MPa. The upper limits of these measurements will be assumed due to the slightly earlier pre-Rio Grande rifting ages of the Montezuma Stock (40 to 35 Ma, while rifting began at 33 Ma). Therefore it will be assumed that the source cupola for hydrothermal fluids was emplaced at a paleo depth of 3.1 km at an approximate lithostatic pressure of 80 Mpa. Subsequent Cordilleran-type veins were emplaced at pressures between 41 MPa – 47 MPa, which corresponds to vein fluid pressures, not pluton emplacement pressures. This pressure reduction from 80 Mpa to 41 MPa – 47 MPa is a function of increased volume in due to fracturing, shallower depth of emplacement of Cordilleran veins and general lowering of the brittle-ductile transition linked to waning of plutonism. The latter control is perhaps the most influential. The brittle ductile transition in these systems is at about 400°C (Fournier, 1991). Temperatures of Cordilleran vein mineralization began at 341°C suggesting that deformation conditions were brittle during Cordilleran vein mineralization. Additionally, the speculative phase separation during barite mineralization (Figure 6.2.6 and Figure 6.2.7) indicates that this occurred at 425°C, which correlates to 35 MPa. This is indicates a pressure drop from 47 – 41 MPa during Stage 1 quartz-pyrite to 35 MPa during Stage 2 barite.

7.3 Hydrothermal Fluid Temperature Decline and Zonation

A commonality among Cordilleran vein fields is that fluid temperatures decrease with distance from fluid source and with time (barring the variable of magmatic resurgence). Progressive overprinting of a deposit is linked to temperature decline with time. Thermal decline is perhaps the best understood variable in these veins and is proposed here to be the dominant control on ore deposition at Montezuma. A decline in fluid temperature with time is evident in the Montezuma district by analysis of fluid inclusions through the paragenetic sequence. A temperature decline with distance from fluid source is indicated by interpretations of metal ratios and by district scale zonations. Fluid temperatures decrease by means of conduction equilibration with wall rock, by means of mixing with cooler meteoric water or by

decompression. Temperature decline can cause precipitation by: 1. affecting the solubility products of ore minerals, 2. affecting the formation and stability of ions transporting metals and 3. by influencing the hydrolysis constants of ligands (Skinner, 1997). For example the stability of $PbCl^{+}$ decreases by an order of 2.5 magnitudes from 300°C to 25°C (Seward and Barnes, 1997). The trend is similar for other metals (Figure 7.2.1) with the exception of AgCl. The disassociation of ligands like Cl^{-} and HS^{-} frommetals in solution is enhanced by temperature decrease. Figure 3.3.1 serves as a model depicting temperature gradients as a fluid cools away from a source cupola. Additionally a general cooling with time leads to progressive inward migration of these gradients. In this scenario, lower temperature assemblages overprint earlier higher temperature assemblages as the entire system becomes cooler. This retrograde sequence is most likely found at Montezuma as indicated by zonation maps and vein paragenesis.

District Scale Zonation at Montezuma and Hydrothermal Fluid Flow Paths

This succession of metal precipitation is reflected in the zonation and in the paragenetic sequence found at Montezuma. District scale zonation at Montezuma is controlled by thermal gradients across the district. Average temperatures are consistently higher in the CRZ than the CPZ in quartz, sphalerite and Ag minerals (Figure 6.3.4 and 6.3.5). Based on the knowledge of metal solubilities as a function of temperature it is possible to infer the flow path of hydrothermal fluids at Montezuma. This is particularly useful when applied to Stage 3 base metals. The first metals to precipitate out on cooling are Cu and Fe in the form of sulphides and sulfo-salts, which explains the quantity of pyrite and copper minerals found in the CRZ at Montezuma and in copper cores at analogue deposits. As the fluid cooled along the flow path, zinc began to precipitate out with copper becoming increasingly depleted from solution. Lead became the next metal to precipitate out as galena. At Julcani, a monotonic increase in Pb/Cu values along the path of mineralization were observed (Goodell and Petersen, 1974), which supports the general paragenetic sequence and systematic zonation found at most deposits including Montezuma. At the point of significant lead precipitation, copper has become a subordinate metal in the system. For this reason, the Pb/Cu ratio has been used by several authors (Sims and Barton, 1962; Goodell and Petersen, 1974) as an

indicator of zonation in a Cordilleran vein fields. Figure 5.2.1.F proves that the Pb and Cu do not have a direct relationship with regard to total production values. Production values for Au and Ag both increase with an increase in Cu production. Pb production values do not increase with increased Cu production values at Montezuma. Additionally, Figure 5.2.2.C proves that there is an inverse relationship between Pb and Cu grade. These data are consistent with temperature decline and sequential precipitation of metals. Therefore, as the fluid became cooler with distance, copper became progressively less soluble at higher temperatures than Zn, Pb and Ag. This indicates that the fluid source is traced to regions of high copper.

The proposed centre of mineralization in the Montezuma district is at a point along the flank west of Silver Mountain, which is a rough center of the CRZ. In addition to the hydrothermal fluid geochemistry detailed in the above paragraph, this center is supported by the distribution of propylitic alteration (Figure 4.2.2), veins with abundant carbonate and barite (Figure 5.2.10) and concentration of abandoned mines (Figure 1.1). To begin with, the majority of abandoned mines lie between Glacier Mtn, Tiptop Peak, and Santa Fe Peak (Figure 1.1). Since the bulk of ore bearing fluids passed through this part of the district, it is probable that this is the dominant center of the district. Neuerburg et al. (1974) proposed that there may be several cupola mineralization centers. This may be true, but all other centers are subordinate to the one under Silver Mountain. An alternative hypothesis to subsidiary cupolas is that the northeast and southeast extensions of the CRZ can be accounted for by means of structural control or by the specific evolution to an epithermal fluid. The presence of Silver Plume Granite to the east may act as a buttress to mineralization fluids. Accordingly, fluids are deflected to the west and along the strike of the contact of the Silver Plume Granite. Fluids flowing along the strike of the granite are afforded an efficient structural control rendering higher fluid temperatures to distal locations from the fluid source. This model is somewhat supported by the fact that carbonates and barite are present in these CRZ outliers. This suggests that these outlier portions of the CRZ were subjected to similar portions of meteoric waters

and/or boiling as the veins in the CPZ. Additionally, the propylitic alteration zone is centered at Silver Mountain, which suggests a central fluid source.

It is hypothesized here that the Cu-core is not exposed at the surface in this district. Based on fluid inclusion homogenization temperatures and metal tenor in veins, the CRZ is most likely equivalent to the Cu-Zn transition zone of current literature, and the Cu-core is not exposed at the surface. This is proposed because zinc is high in this zone and copper minerals are not dominant in this zone. Also bulk temperatures in this intermediate zone are 250 – 350°C (Bendezú and Fontboté, 2009), which is comparable to the temperatures observed in the CRZ at Montezuma, 303 – 271 (Figure 6.3.5). Temperatures of the outer Pb-Zn-Ag zone are 250 - 150°C in Cordilleran veins fields (Bendezú and Fontboté, 2009), which fits the CPZ at 257 - 228°C (Figure 6.3.5). It is proposed here that a true copper core may lie directly under the center of the CRZ roughly under Silver Mountain. A cupola environment would also be found under this point in the district. Subsidiary copper cores may exist to the south east along the Montezuma shear zone, but lack of production data in the southern portion of the district limits this assessment. An additional possibility is that these distal regions of high Cu reflect a transition into an epithermal environment. Figure 5.2.3 indicates that there is a large range of Ag:Au ratios and that some could be classified as epithermal veins. Therefore, it is more likely that these distal CPZ veins are transitional to epithermal Au-Cu veins.

As a pluton wanes, cooler fluids will invade what once were zones of hotter hydrothermal fluids. This process is called overprinting. Overprinting is most likely evident at Montezuma due to the presence of Pb and Ag minerals within the CRZ. As the system cooled, these lower temperature metals precipitated in central regions of the district.

7.4 Cordilleran Vein Paragenetic Sequence and Fluid Evolution Model

Abundant chalcophile metals can be carried in solution by a fluid with abundant chloride ions, a pH slightly on the acid side of neutral and at moderately elevated temperature (Stanton, 1972).

Accordingly, a reduction of chloride ions (or other ligands), a pH increase and temperature decrease will favor ore mineral precipitation. Additionally, a pressure drop can also cause precipitation (Heinrich, 2005). Temperature decline has been identified in this study as a major precipitation mechanism for ore minerals at Montezuma based on zonation and fluid inclusion studies. This section will link additional precipitation mechanisms to stages of mineralization.

Stage 1 Quartz-Pyrite

Mineralization temperatures for quartz and pyrite from this stage are from 341 to 295°C, with negligible temperature difference between in the CPZ and the CRZ. Since mineralization occurred below 400°C, it is likely that this stage was deposited under brittle conditions. This stage is most likely a distal equivalent to the D-type veins of the porphyry system.

Iron and sulfur can mineralize as pyrrhotite or as pyrite during early stages of mineralization in Cordilleran veins. Figure 7.4.1 summarizes the stability relationships of magnetite, hematite, pyrrhotite and pyrite with regard to Eh, pH and partial pressure of sulfur. The presence of pyrite at Montezuma indicates a higher sulfidation state or lower pH than deposits that contain pyrrhotite (eg. Julcani, Goodell and Petersen, 1974). Woitsekhowskaya and Hemley (1995) have investigated the effects of total sulfur and pH on the Butte-type hydrothermal systems through computer simulations. Higher total sulfur will enable pyrite to become stable at higher temperature whereas pyrrhotite would be stable with lower total sulfur. They also found that as the activity of H^+ increases S_2 is favored regardless of oxidation state. In summary, the presence of pyrite over pyrrhotite is the result of higher H^+ and/or higher total sulfur. Based on the knowledge that as a magmatic fluid cools, the activity of H^+ increases (Reed et al. 2013), it is proposed that pH is the primary control on pyrite stability. At constant total sulfur and fO_2, an increase in H^+ will always favor an increase in S_2 fugacity through reaction with HS^- or HSO_4^- disproportionate. The following reactions summarize the increase in H^+ and thus S_2 increase (Woitsekhowskaya and Hemley, 1995):

$$2HS^- + O_2 + 2H^+ \rightarrow S_2 + 2H_2O \quad \text{(Eq. 7.2)}$$

and

$$HSO_4^- + H^+ \rightarrow 0.5S_2 + 1.5O_2 + H_2O \quad \text{(Eq. 7.3)}$$

and

$$SO_4^{2-} + 2H^+ \rightarrow 0.5S_2 + 4H_2O \quad \text{(Eq. 7.4)}$$

The following reaction is a summary of the action of H^+ in the FeS system (Woitsekhowskaya and Hemley, 1995):

$$4FeS + 4H^+ + 3HS^- + HSO_4 \rightarrow 4FeS_2 + 4H_2O \quad \text{(Eq. 7.5)}$$

This pH variable may also explain why pyrrhotite is more common in carbonate replacement and skarn ores as the hydrothermal fluid is neutralized by reactive wall rocks lowering the activity of H^+. Conversely, the buffering capacity in the Cordilleran vein environment is significantly less, which would favor pyrite stability.

Lovering (1935) notes that minor carbonate was precipitated at the end of this stage. This may be evidence of minor meteoric water contamination. Heating of CO_2^- rich meteoric waters by magmatic fluid mixing can induce carbonate precipitation (Rimstidt, 1997). Alternatively, since CO_2 was observed in early fluid inclusions, it may be that carbonates were precipitated directly from the magmatic fluid. Additionally, cooling of a CO_2-bearing fluid may induce carbonate precipitation. Precipitation mechanisms for these minor carbonates are unknown since this stage was not observed in this study.

Stage 2 Barite

In regions of abundant barite mineralization, the aqueous sulfur species shifted from H_2S or HS^- to SO_4^{2-} or barium was added to the fluid. Figure 7.4.2 depicts stabilities of aqueous sulfur-bearing species in the H-S-O system with regard to Eh and pH. Phase relationships in this diagram indicate that sulfate stability can be achieved by means of an Eh increase and/or a pH increase. A dilution may be

indicated from a decrease in salinities from 11.09 – 7.58 wt.% eq. NaCl during the quartz-pyrite stage to 9.57- 3.70 wt.% eq. NaCl during the barite stage, however this salinity decline may alternatively be a function of phase separation. From Figure 6.2.5.B it is observed that salinities during barite mineralization are strongly bimodal. The bimodal salinities and coarse bladed textures suggest that boiling was a significant precipitation mechanism of barite. Additionally, gas rich and fluid rich primary fluid inclusions are observed in barite crystals (Figure 6.2.6). These data may indicate a complex interaction of phase separation and increased meteoric water dilution.

The location of the brittle-ductile transition can control fluid pressure variables in these systems. The transition in these systems is at about 400°C (Fournier, 1991). As a system cools this initiates a progressive deepening of the brittle ductile transition. This deepening would enhance the affect of hydrostatic fluid-pressure relative to lithostatic pressure, and would increase the potential to widen fractures. This volume increase in veins could induce a slow downward migration of a boiling horizon across the district. Depressurization of the hydrothermal system can enrich a vapor in SO_2 (Rye, 1993), which favors sulfate deposition. The widening of veins would also promote greater degrees of meteoric water influence. This meteoric water would cool and condense into the vapor plume. This would alter the dominant sulfate species in solution in a magmatic vapor by means of the following reaction (Giggenbach, 1997):

$$4SO_2(aq) + 4H_2O(l) \rightarrow \quad \text{(Eq. 7.6)}$$
$$H_2S(aq) + 3H_2SO_4(aq)$$

A modification to this equation to reflect the above scenario would be the following:

$$4SO_2(va) + 4H_2O(l) \rightarrow \quad \text{(Eq. 7.7)}$$
$$H_2S(aq) + 3H_2SO_4(aq)$$

A way to test which meteoric water induced barite precipitation would be a Cs/Na ratio analysis. Tracking Cs/Na ratio across an ore field have been used to detect meteoric water influence (Catchpole et

al., 2011) as this value will decrease several orders of magnitude from the original magmatic fluid values once mixed with a Cs poor meteoric water (Audétat and Pettke, 2003; Audétat et al., 2008).

A second possibility is that the bulk chemistry of the hydrothermal fluid changed during this stage of mineralization. Ba^{2+} may have been enriched in a hydrothermal fluid by release from k-feldspar alteration. An addition of barium to a fluid can induce barite precipitation without an increase in SO_4^{2-}. Figure 7.4.3 shows how $BaSO_4$ is stable in a wide range of pH and Eh conditions at 25°C. If this graph is appropriate for elevated temperatures (310 to 233°C), then it is possible that a simple addition of Ba from altered feldspars has induced the precipitation of barite in this system.

Stage 3 Base Metals

Temperature decline with significant overlap from Stage 2 (310 to 233°C) to Stage 3 (258 to 220°C) is indicated from fluid inclusion data. This is consistent with textural relationships illustrated in Chapter 4 as most barite grew before base metal sulfides. Salinities in Stage 3 are greater than Stage 2, but are roughly equal to Stage 1. However quartile 1 and quartile 3 values for Stage 3 have greater disparities than Stage 1 (Figure 6.2.4). This large disparity in salinities may indicate a slight increase in meteoric water proportions or phase separation. However, temperature decline is most likely the dominant ore precipitation mechanism. This temperature decline is proposed to be linked to the progressive waning of the source pluton. The waning of a pluton also implies the lowering of the lithostatic to hydrostatic transition. This lowering is possibly evidenced by boiling in Stage 2 barite. At the Crnac Pb-Zn-Ag deposit (Kosovo), it is proposed that ore fluids lost additional heat to escaping vapor phase thereby inducing main stage precipitation (Šoštarić et al., 2013). This process is proposed in the Montezuma district and is supported by the weakly bimodal distribution of salinities in Figures 6.2.5.C.

The variety of copper mineral species observed in the district may be explained by variation of sulfur and oxygen fugacities. These affect the resulting mineral species in vein assemblages and in alteration assemblages. Advanced argillic alteration can be associated with high sulfidation assemblages

including covellite, enargite, digenite and pyrite. This alteration-mineralization association is linked to hydrothermal fluids with a low pH. Copper in an acid solution can precipitate by means of increasing the sulfidation state of the fluid and copper need not be in high concentrations to achieve this (Reed et al., 2013). These high sulfidation assemblages are found in Cordilleran vein fields, but tend to be subordinate to lower sulfidation state minerals like chalcopyrite or tennantite-tetrahedrite. Increasing meteoric water input can render lower sulfidation states, which may explain the assemblage found in many Cordilleran vein fields and at Montezuma. The relation between copper minerals of different sulfidation states are exemplified by the following reaction (Meyer and Hemley, 1967):

$$4Cu_3AsS_4\ (en) + 3H_2O\ (aq) \rightarrow \qquad \text{(Eq. 7.8)}$$

$$Cu_{12}As_4S_{13}\ (tn) + 1\tfrac{1}{2}H^+\ (aq) + 2\tfrac{1}{4}H_2S\ (aq) + \tfrac{3}{4}SO_4^{2-}\ (aq)$$

Tennantite is found in the Montezuma district while the district lacks enargite. This reaction shows how an enargite stable system becomes a tennantite stable system with the addition of water. Since magmatic fluids become acidic with cooling (Reed et al., 2013), it is inferred that there must be some degree of meteoric water influence at Montezuma considering the observed dominance of chalcopyrite and tennantite over bornite and covellite. However, it is proposed here that meteoric to magmatic ratios only increased slightly from Stage 1. An additional equation shows how removal of S_2 will favour lower sulfidation state minerals (Ridley, 2013):

$$Cu_5FeS_4 + 4FeS_2 \rightarrow 5CuFeS_2 + S_2 \qquad \text{(Eq. 7.9)}$$

A similar equation exists for tennantite and enargite (Ridley, 2013). The precipitation for large quantities of pyrite and barite may have reduced sulfur quantities to an extent that later mineralization may only support lower sulfidation states. Perhaps a combination of the two above equations has led to the presence of lower sulfidation state copper minerals at Montezuma.

At Morococha, sulfidation states decrease from intermediate-high in the Cu-core to low-intermediate in the distal Zn-Pb-Ag zones (Catchpole et al., 2012). An interpretation may be that

increasing degrees of meteoric water mixing with distance from the source pluton have rendered this chemical change. At Montezuma, average salinities for this stage do not indicate this trend. Additionally, it was found that sphalerite generally decreases in Fe content with time, which suggests an increase in sulfidation state with time. A spatial assessment of Fe in sphalerite was not made in this study. A quantitative spatial and temporal assessment of Fe content in sphalerite would be a good approach in addressing this question since this can be used to determine sulfur fugacity if the temperature is known (Scott and Barnes, 1971; Czamanske, 1974). However, since sphalerite commonly replaces early pyrite local enrichment of iron in sphalerite at nucleation sites may occur as described in Eq. 4.1, thereby complicating Fe-Zn studies.

Stage 4 Carbonates

Workable fluid inclusions in ankerite were not found due to the nearly opaque nature of crystals. Assuming a consistent cooling of the fluid from Stage 3 to Stage 5, Stage 4 carbonates would have precipitated in the temperature range from 220 to 156°C. Rimstidt (1997) notes four ways in which carbonates can be precipitated from a hydrothermal fluid: 1. heating the solution at low salinities and/or temperatures, 2. degassing CO_2, 3. decreasing salinity and 4. increasing the pH.

The existence of this carbonate stage suggests that either magmatic degassing of CO_2 occurred changing the composition of the fluid or that CO_2 was present through the evolution and that previous stages contained CO_2 below detectable limits in fluid inclusion studies. The latter case is more likely considering that CO_2 was identified in Stage 1 quartz-pyrite (5.2.2.B). The lack of visible CO_2 in Stage 3 and Stage 2 inclusions indicates that the concentration is less than 4.4 wt% (Cooke and Bloom, 1990). Therefore, saturation of CO_2 was not achieved by addition from a second fluid, rather evolution of single aqueous fluid induced precipitation of carbonates.

The massive habit of carbonates at Montezuma indicates rapid precipitation under high degrees of super saturation. CO_2 saturated waters can be generated by absorption of vapors separated from deeper

Cl waters into a cooler ground water (Hedenquist, 1990). Additionally, "isenthalpic expansion of steam, separated from a deeper liquid phase, to close to atmospheric pressures is accompanied by a drop in temperature to about 160°C" (Giggenbach, 1997). Interestingly, subsequent Stage 5 silver precipitates out at 171 to 151°C.

Boiling or isenthalpic expansion can be initiated by simple vertical movement of the fluids through the crust or progressive unroofing of a deposit. The precipitation of carbonates is commonly linked to these processes. CO_2 is removed from solution during depressurization by the following reaction (Rimstidt, 1997):

$$H^+ + HCO_3^- \rightarrow CO_2 + H_2O \qquad \text{(Eq. 7.10)}$$

Removal of CO_2 raises the solution's pH and renders a dissociation of HCO_3^- to H^+ and CO_3^{2-}. At Morococha, Catchpole et al. (2011), have interpreted a salinity increase and corresponding carbonate precipitation to be a result of phase separation. Salinity data from this stage would have been particularly valuable in the evaluation of phase separation as a potential precipitation mechanism. Since workable fluid inclusions were not found in this stage, textural and paragenetic evidence were used to evaluate carbonate precipitation. Lack of large platy carbonates and subsequent silicification in this stage suggests that these ankerite and dolomite phases were not precipitated by means of boiling (Simmons and Christenson, 1994), therefore isenthalpic expansion is favored.

Stage 5 Ag-Pb Quartz

The transition of Stage 3 base metal mineralization into Stage 4 carbonates indicates a removal of CO_2 from the hydrothermal fluid. This removal decreases the proton concentration of the solution by several orders of magnitude, which further increases the pH of the solution (Drummond and Ohmoto, 1985). This pH increase and rapid temperature decrease may have been instrumental in the deposition of subsequent Stage 5 silver. A pH increase along with a temperature decline is the favored mechanisms for Stage 5 Ag-Pb mineralization.

Significantly higher salinities in the CRZ indicate that meteoric water did cause greater dilution in veins of the CPZ than in the core of the district during this stage of mineralization (Figure 6.3.4). This is perhaps due to significant lowering of the brittle-ductile transition linked to waning of the source pluton, which allowed substantial degrees of meteoric water into the system during this time.

7.5 Implications for Mo Exploration

In many instances, Mo porphyries are associated with silver-rich polymetallic veins (Ludington and Plumlee, 2009; Richards et al., 2010; Lang and Eastoe, 1988; Stein and Hannah, 1985; and others). Anderson et al. (1989) assayed (PIXE and PIGE) fluid inclusions from the core of the Bingham Canyon Cu-Mo porphyry where only molybdenite and no Cu minerals are present in veins. Despite the fact that only Mo was mineralized in this region of the porphyry, fluid inclusions proved to contain significant amounts of Cu, Pb, Zn and Fe. A mass balance calculation of the amount of these base metals in inclusions was found to be sufficient for adjacent Cu stockwork mineralization and distal Pb-Zn fissure fill mineralization. This proves that base metals can be transported through barren potassic cores with selective precipitation, and that magmatic fluids are the source of metals in both porphyries and adjacent polymetallic veins.

Results from this study have concluded that Cordilleran veins in the Montezuma district are sourced from a waning pluton. A brief evaluation of porphyry type base metal mineralization is a second question in this study. The majority of research addressing this connection has focused on the connection of Cordilleran veins and Cu porphyries (Catchpole et al., 2011; Catchpole et al., 2012; Einaudi, 1977; Meyer and Sales, 1968; Bendezú and Fontbote, 2009; Bendezu et al., 2003; Sillitoe, 2010; Sillitoe, 1973; Reed et al., 2013; and others), while the connection between polymetallic veins and Mo porphyries has received less attention (Rice et al., 1985). At Montezuma, it is inferred that Mo mineralization is more likely than Cu mineralization based on proximity to active Mo porphyry mines (Climax and Henderson) of similar age.

Temperature

Molybdenum bearing veins form from 400° to 600°C (Bloom, 1981; Cline and Vanko, 1995; Seedorf and Einaudi, 2004) in the porphyry system. Hypersaline Type A1 inclusions (Figure 6.2.1.A) in fractured quartz in a molybdenite bearing leucogranite (Figure 7.5.1) homogenized from 567 to 347°C with an average of 415°C from six samples. Salinities ranged from 48 to 36 wt.% eq. NaCl . These temperatures and salinities are similar to stockwork Mo mineralization occurring during potassic stages of alteration, and prove that some portions of the Montezuma district were subjected to these elevated fluid temperatures. Stage 1 quartz-pyrite fluid temperatures were from 341 to 295°C, which suggests that this stage came after this possible Mo mineralizing event. This is consistent with the succession observed at Mo porphyry deposits: B-type veins (molybdenite+quartz) being overprinted by D-type veins (quartz+pyrite) (Sillitoe, 2010).

Porphyry Mo Types and the Montezuma District

Wallace (1995) defines four types of Mo porphyries, of which only the Climax-type and Quartz monzonite-type are candidates for potential mineralization under the Montezuma district. Considering the current economics of Mo in Colorado, only Climax-type are of interest for exploration. Wallace (1995) defines several characteristics of the Climax-type Mo porphyry system based on commonalities of known deposits of this type. These characteristics are that they: 1. contain the highest grade of any Mo deposit type, while boasting adequate tonnage 2. are associated with highly evolved porphyryitic felsic rocks, 3. are in highest abundance in the COMB, 4. Have high fluorine anomalies as well as other incompatible lithophile elements, 5. can be associated with rare lamprophyres and 6. are uncommon in occurrence. Ludington and Plumlee (2009) note that only 13 deposits of this type are known, with all occurring in the North American Cordillera. Conversely, the Quartz monzonite-type is the most abundant Mo porphyry type in the Western Cordillera and is lower grade. Wallace (1995) has included a third

category called Sub-Climax type deposits to exemplify that there is a spectrum from Climax-type to Quartz monazite-type.

From historical research and this study, there are few clues available to address this question. Although, from what has been compiled and analyzed, it is predicted that if Mo mineralization does exist under the Montezuma district, it would fail to be a Climax-type and would most likely be a Sub-Climax type based on exploration criteria presented in Wallace (1995).

To begin with, porphyries tend to cluster along trends with a predictable orientation dictated by a variety of tectonic and petrogenetic trends. Identification of these trends is a powerful exploration tool. The Montezuma district lies directly on the margin of the "Climax Line" (Figure 7.5.2) as defined by Wallace (1995). The Climax Line is not a definite geologic feature, but based on locations of the Urad-Henderson, Climax, Mt. Emmons and Silver Creek, there does seem to be a pattern. Wallace (1995) details his theories on the development of this trend. Regardless, the Montezuma district lies directly on the margin of this zone. Assuming the Climax Line is valid and considering the location of the Montezuma District with regard to the Climax Line, there is an increased possibility of underlying stockwork Mo mineralization.

Both the Climax and Urad-Henderson porphyries both contain anomalously high Ni and Cr (Wallace 1995) (Figure 7.5.3.A), which is unusual for a highly evolved melt. Figure 7.5.3.B shows the Ni and Cr concentrations in the Montezuma Stock. These values are more comparable to the concentrations found in Sub-Climax type deposits. The exact reason of high Ni and Cr in the stocks of the two Climax-type deposits is not well understood. Wallace (1995) speculates that this may be a function of high crustal temperature and associated higher degrees of crustal assimilation. Increased assimilation is favored by the thick Laramide crust. He furthers in noting that the Silver Plume Granite contains high Ni and Cr, which may be the source for elevated Ni and Cr in Climax-type melts. In summary, these metals are of interest and can provide another clue as to the nature of Mo mineralization in the Montezuma stock;

yet, the reliability of the markers is uncertain. It is possible that magmatism under the Montezuma District did incorporate the Silver Plume Granite and thus did not assimilate high degrees of Ni and Cr. Alternatively, anomalously high heat flows associated with Climax-type were not present in the district, and thus underlying Mo mineralization at Montezuma is most likely Sub-Climax type.

Timining and Tectonic Constraints

Climax-type deposits are tectonically similar in that all deposits of this type formed during extension subsequent to cessation of subduction of the Kula and Farallon plates beneath western North America (Ludington and Plumlee, 2009). Intrusive activity at Urad-Henderson spans from 29.9 to 26.95 Ma (Geissman et al., 1992), magmatism at Climax spans from 33 to 24.5 Ma (White et al., 1981), and 17 to 16 Ma at Mt Emmons (Thomas and Galey, 1982). These dates presumably correlate to progressive migration of Rio Grande rifting and associated magma generation. If this rift related magmatism occurred from 33 to 27 Ma in the region of Climax and Urad-Henderson then it follows that the 40 to 35 Ma Montezuma Stock slightly predates extensional tectonics. Therefore, the Montezuma stock may only be an earlier premineralization intrusive, and later syn-mineralization intrusives may still lie below.

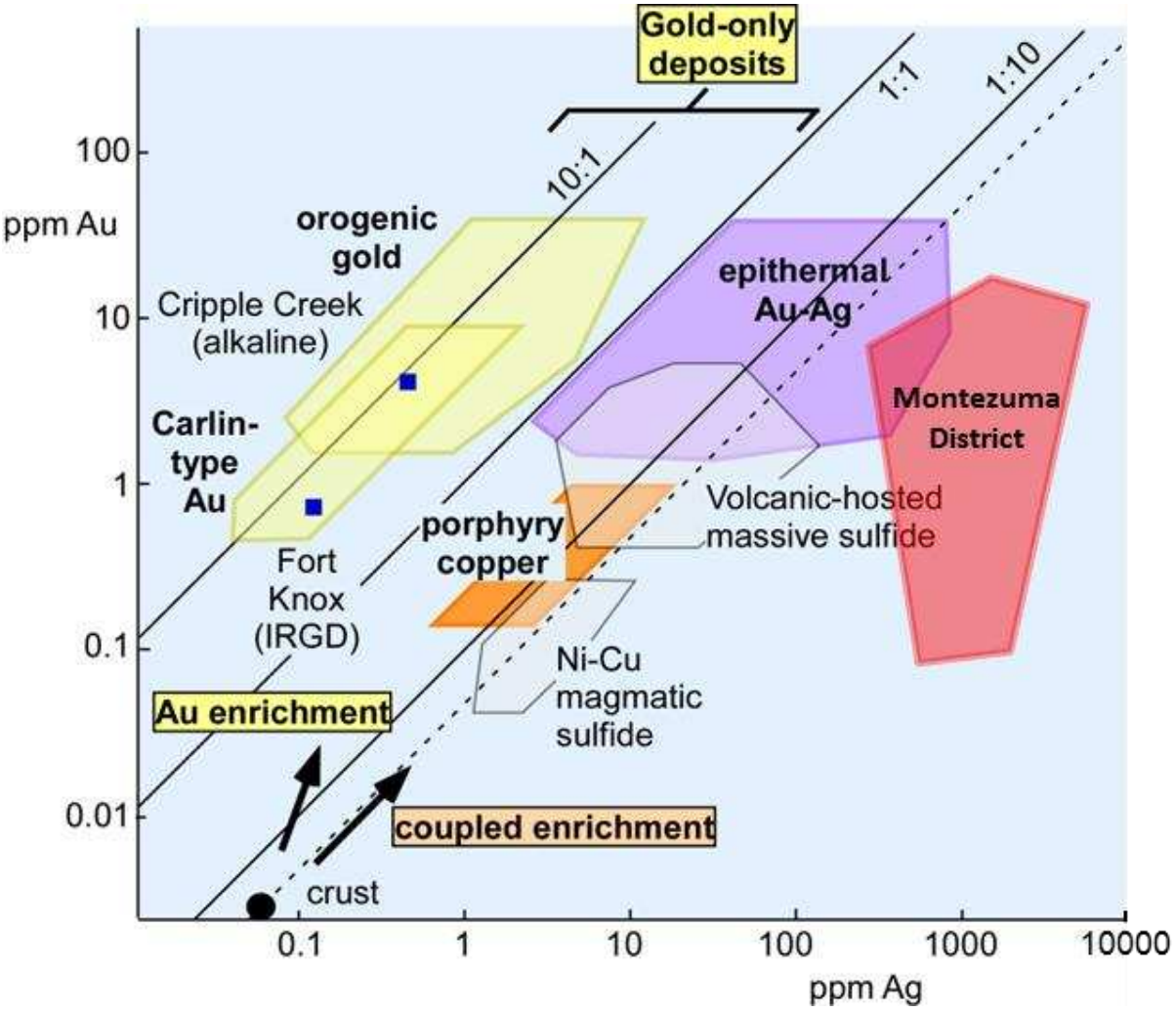

Figure 7.1.2 modified from Ridley, unpublished. Diagram of various deposit types with relation to Au:Ag. Notice a minor overlap of the Montezuma District and epithermal Au-Ag. This suggests that both Cordilleran veins and epithermal veins exist in the district. This exemplifies the gradational nature of classification of deposits related to felsic igneous centers.

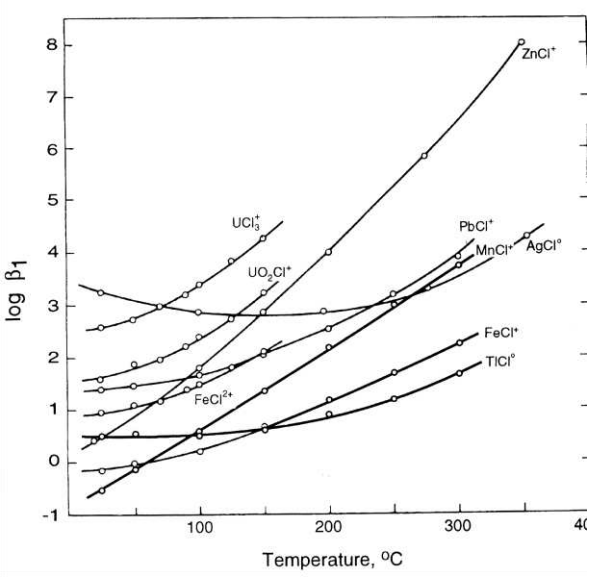

Figure 7.2.1 from Seward and Barnes (1997). Variation of the equilibrium formation constant β_1 (as log β_1), with temperature for simple chloride complexes at the saturated vapor pressure.

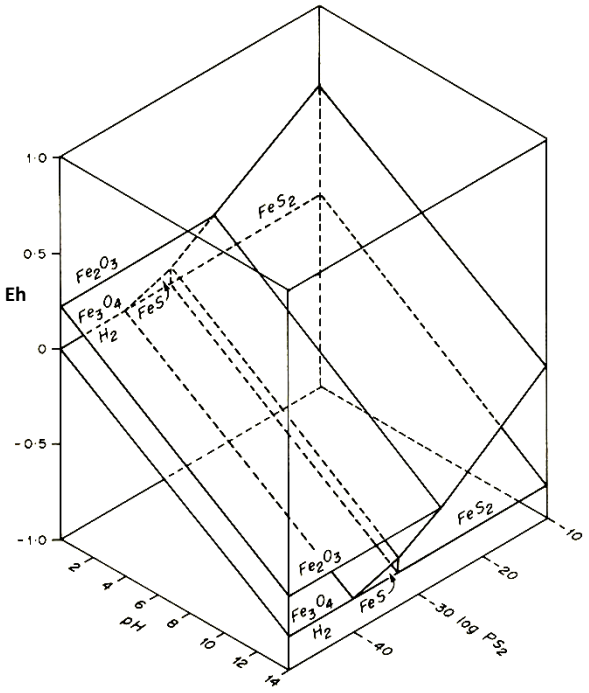

Figure 7.4.1 from Stanton (1972). Stability relations of hematite, magnetite, pyrrhotite and pyrite in terms of Eh, pH and partial pressure of sulfur (log Ps_2) at 1 atm total pressure in the presence of water.

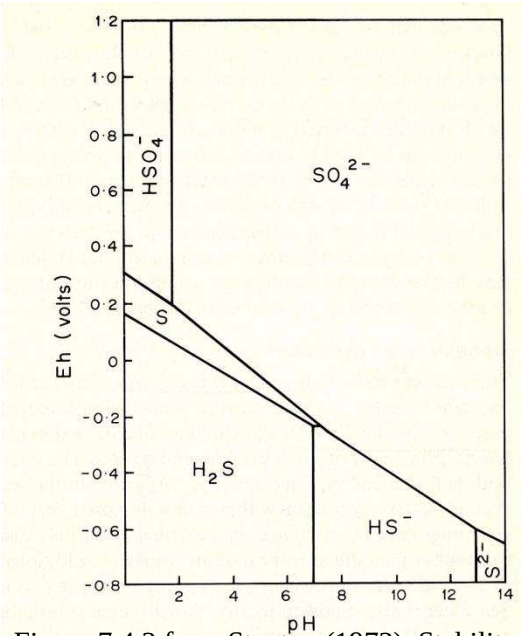

Figure 7.4.2 from Stanton (1972). Stability relations of the principal aqueous species in the H-S-O system in terms of Eh and pH at 25°C.

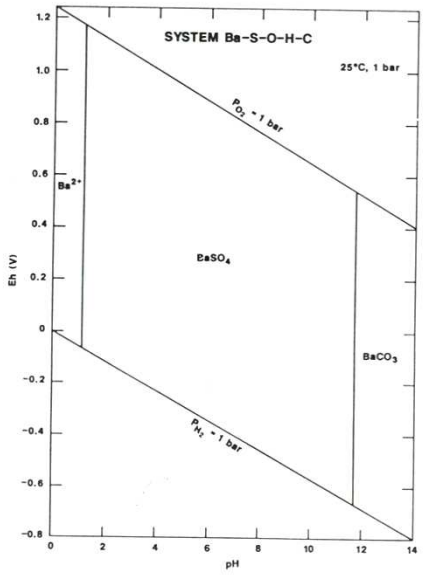

Figure 7.4.3 from Brookins (1988) Eh-pH diagram for part of the system Ba-S-O-H-C. Assumed activities for dissolved species are: Ba = 10^{-6}, C = $^{-3}$.

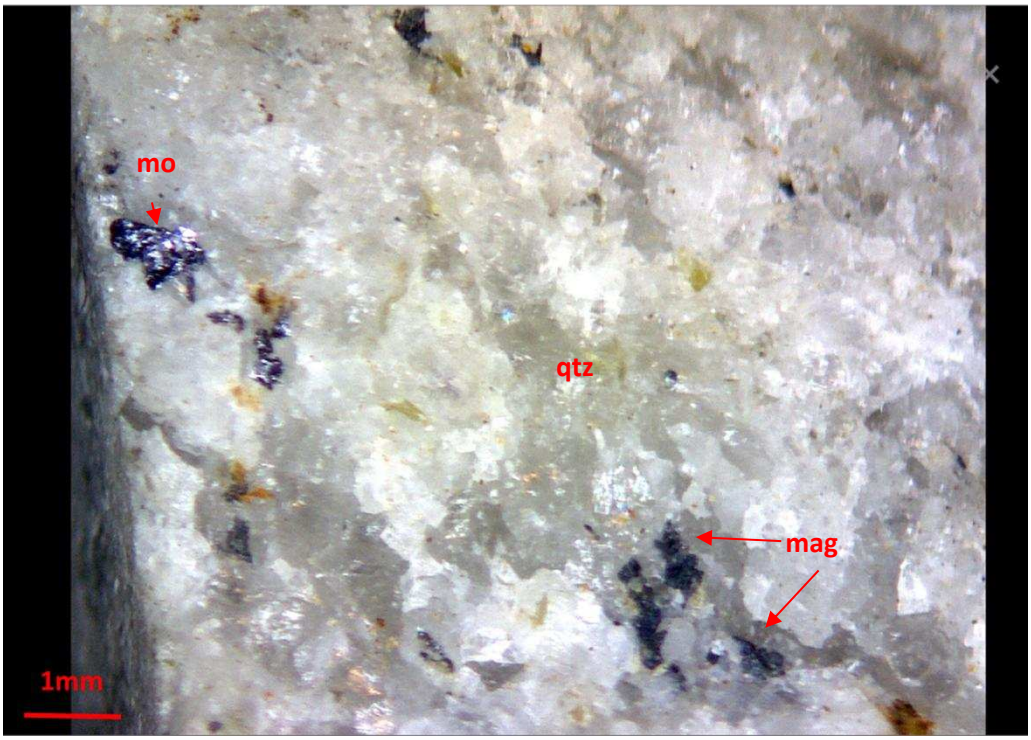

Figure 7.5.1 molybdenite-magnetite bearing leucogranite from Teller Mountain (SRC-8). Microthermometry results from this sample revealed high temperature hypersaline fluid inclusions in fractured quartz. (mo = molybdenite; mag = magnetite; qtz = quartz)

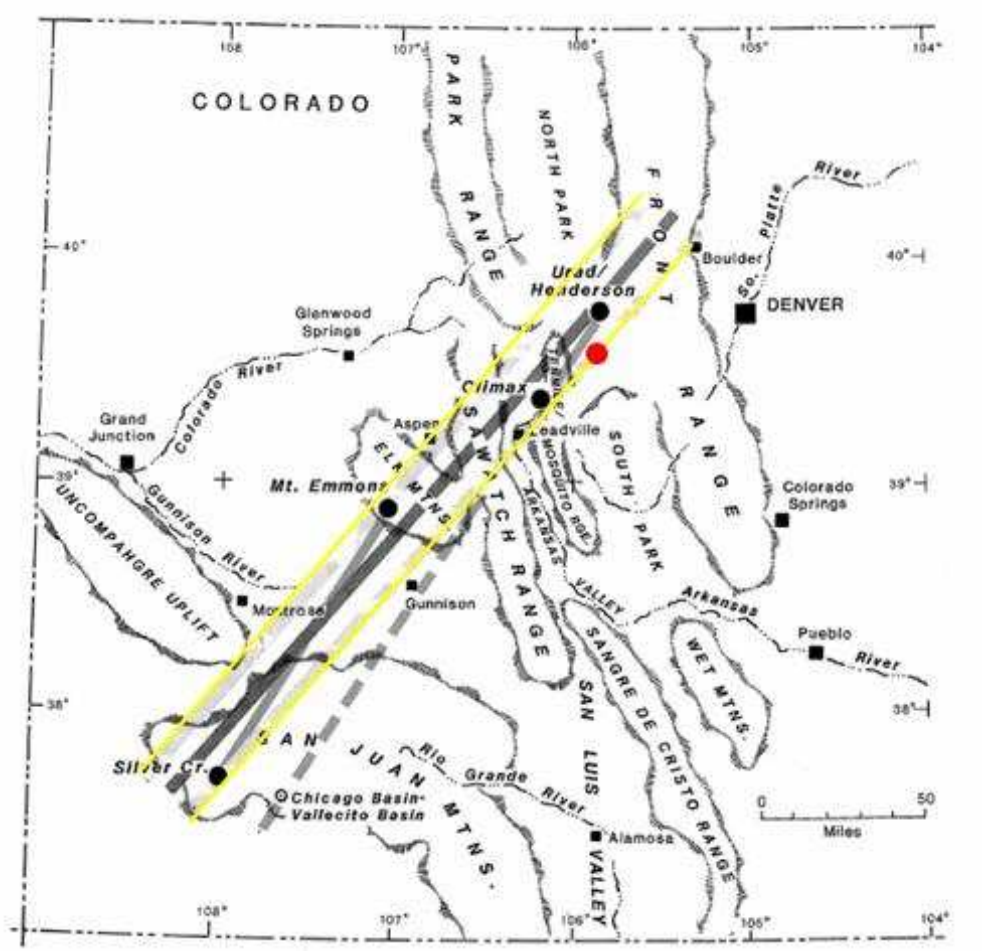

Figure 7.5.2 modified from Wallace (1995) the Climax line (within yellow lines). The Montezuma district lies directly on the margin of the hypothetical Climax Line. The line is constructed based on known Climax-type deposit locations of Silver Creek, Mt Emmons, Climax and Urad-Henderson.

(A)

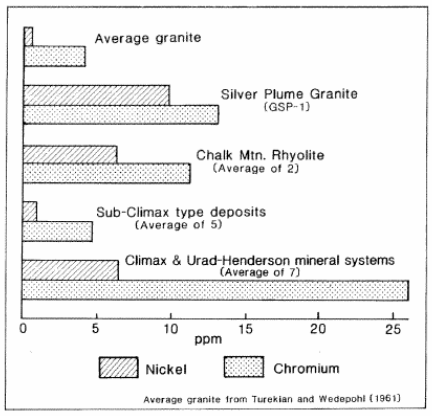

(B)

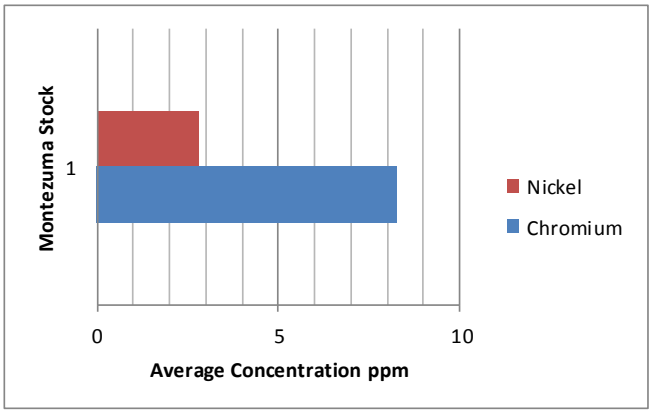

Figure 7.5.3 Ni and Cr concentrations in Mo bearing granites (A) from Wallace (1995) comparison of Nr and Cr concentrations in various other granites to that found in the Climax and Urad-Henderson deposits. (B) Ni and Cr concentrations found in the Montezuma Stock. The Montezuma stock contains similar amounts of Ni and Cr to Sub-climax type deposits. The Montezuma stock does have higher Ni and Cr than the average granite.

8. Conclusion

The metallogeny, associated magmatism, district scale zonation, ore textures, late timing relationship to associated magmatism and hydrothermal temperature ranges indicate that the veins of the Montezuma District are of the Cordilleran vein type according to criteria proposed by Bendezú and Fontboté (2009). Evidence from this study in conjunction with data from previous studies in the region (Lovering, 1935; Neuerburg, 1974; Botinelly, 1979; and others) serve to support this classification. This classification acts to link veins of the Montezuma District to analogous mineralization (eg. Butte, Montana; Morococha, Peru; and others).

District scale zonation and fluid inclusion data from Cordilleran Pb-Zn-Cu-(Ag-Au) veins of the Montezuma district suggest mineralization is linked to the waning of a central pluton or cupola. A radial zonation pattern from a copper rich core to a copper poor distal zone suggests that a single dominant fluid source in the district was responsible for vein mineralization. Fluid inclusion temperatures support that the copper rich zone was subjected to hotter bulk fluid temperatures that the copper poor zone, which suggests that the fluid source in this district lies somewhere under the CRZ near Silver Mountain. Homogenization temperatures through the paragenetic sequence indicate a cooling trend in the district with time: Stage 1 quartz-pyrite at 341 to 295°C, Stage 2 barite and incipient base metals at 325 to 234°C, Stage 3 base metals at 258 to 235°C, and finally to Stage 5 Pb-Ag-quartz at 172 to 151°C. During Stage 3 base metal mineralization, temperatures were hotter in the CRZ than in the CPZ, which provides an explanation for a Cu core in the district. Stage 1 quartz-pyrite did not indicate any thermal differences among zones, thus distinct thermal gradients must have developed after this stage. Approximate salinities from fluid inclusions are less consistent, and can be interpreted that phase separation and meteoric water interactions were factors during vein fill. A progressive lowering of the brittle ductile transition linked to waning of the source pluton is the proposed primary control for these additional variables. Finally, it is

likely that the Cordilleran veins are genetically related to stockwork Mo mineralization that would most likely exist under the copper rich zone. However it is probable that this stockwork mineralization is Sub-Climax in nature, and may be sub economic by current mining standards.

The following additional projects in the district would serve to better understand mineralization in the district. A Cs/Na ratio study would solve the question of weather meteoric waters played a significant role in the zonation patterns of the district. A comparison of Cs/Na ratios from samples from the CRZ and the CPZ linked to specific stages of mineralization would answer two questions: 1. did meteoric water render greater cooling in the CPZ? And 2. If meteoric water did induce greater cooling in the CPZ, then at which stage of mineralization was this influence the greatest? Based on this study and comparison with analogous districts, it is likely that ore bearing fluids are from a magmatic source, but a targeted fluid source study would provide a conclusion to this hypothesis. Several approaches may be taken to identify a fluid source for the district. δD values from Stage 1 quartz-pyrite could prove that this early fluid is from a magmatic source. Variations δD values from subsequent stages may indicate increased proportions of meteoric water influence or conversely lack of variation may indicate no meteoric water dilution. An ICP-MS metal analysis of fluid inclusions could determine if the district is subjected to a single or multiple fluids. If Pb-Zn-Cu-Ag are high in fluid inclusions of the Stage 1 quartz-pyrite, then it would be suspected that one fluid rendered all metals in the district, and that each metal precipitated out at different times and locations in the district. Also a comparison of metals in sphalerite FI of the CRZ and the CPZ could also support a single fluid theory. It is hypothesized that this study would reveal higher Pb+Ag in inclusions of the CRZ than in the distal CPZ. If each of these studies indicate a magmatic source for metals, and that the district was subjected to a single dominant fluid, then a drilling program along the flanks of Silver Mountain may prove stockwork style porphyry mineralization under the CRZ.

9. References

Anderson, A.J., Clark, A.H., Ma, X., Palmer, G.R. and MaCarthur, J.D. (1989). Proton-induced X-ray and gamma-ray emission analysis of unopened fluid inclusions. *Economic Geology* **84**, 924 – 939.

Audétat, A., Günther, D. and Heinrich, C.A. (2000). Causes for large-scale metal zoneation around mineralized plutons: fluid inclusion LA-ICP-MS evidence from the Mole Granite, Australia. *Ecomomic Geology* **95**, 1563 – 1581.

Audétat, A., Pettke, T. (2003). The magmatic-hydrothermal evolution of two barren granites: a melt and fluid inclusion study of the Rito del Medio and Cañada Pinabete plutons in northern New Mexico (USA). *Geochimica et Cosmochimica Acta* **67**, 97 – 121.

Audétat, A., Pettke, T., Heinrich, C.A. and Bodnar, R.J. (2008). The composition of magmatic-hydrothermal fluid in barren and mineralized intrusions. *Economic Geology* **103**, 877 – 908.

Cline, J.S., and Vanko, D.A. (1995). Magmatically generated saline brines related to molybdenum at Questa, New Mexico, USA. In, *Magmas, fluids, and ore deposits - Mineralogical Association of Canada short course series,* Thompson, J.F. (ed), Victoria, Mineralogical Association of Canada, 53 – 174.

Babcock, R.C., Ballantyne, G.H. and Phillips, C.H. (1995). Summary of the geology of the Bingham district. *Arizona Geological Society Digest* **20**, 316 – 335.

Bakker, R.J. (2003). Package *FLUIDS* 1. Computer programs for analysis of fluid inclusion data and for modelling bulk fluid properties. *Chemical Geology* **194**, 3 – 23.

Bartos, P.J. (1987). Quiruvilca, Peru: Mineral zoning and timing of wall-rock alteration relative to Cu-Pb-Zn-Ag vein-fill deposition. *Economic Geology* **58**, 538 – 569.

Bartos, P.J. (1989). Prograde and retrograde base metal lode deposits and their relationship to underlying porphyry copper deposits. *Economic Geology* **84**, 1671 – 1683.

Bates, R.L. and Jackson, J.A. (1985). *The Dictionary of Geological Terms Third Edition*, New York, Anchor Books.

Bendezú, R., Fontboté, L. and Cosca, M. (2003). Relative age of Cordilleran base metal lode and replacement deposits and high sulfidation Au-(Ag) epithermal mineralization in the Colquijirca mining district, central Peru. *Mineralium Deposita* **38**, 683 – 694.

Bendezú, R. and Fontboté, L., 2009. Cordilleran epithermal Cu-Zn-Pb-(Au-Ag) mineralization in the Colquijirca district, central Peru: deposit-scale mineralogical patterns. *Economic Geology* **104**, 905 – 944.

Beuchat, S., Moritz, R. and Pettke, T. (2004). Fluid evolution in the W-Cu-Zn-Pb San Cristobal vein, Peru: fluid inclusion and stable isotope evidence. *Chemical Geology* **210**, 201 – 224.

Bloom, M.S. (1981). Chemistry of inclusion fluids – stockwork molybdenum deposits from Questa, New Mexico, Hudson Bay Mountain and Endako, British Columbia. *Economic Geology* **76**, 1906 – 1920.

Bodnar, R.J. (1993). Revised equation and table for determining the freezing point depression of H_2O-NaCl solutions. *Geochimica et Cosmochimica Acta* **57**, 683 – 684.

Bodnar, R.J. (1995). Fluid inclusion evidence for a magmatic source for metals in porphyry copper deposits, in Thompson, J., ed., Magmas, fluids, and ore deposits. *Mineralogical Association of Canada Short Course* **23**, 139 – 152.

Bookstrom, A.A. (1981). Tectonic setting and generation of Rocky Mountain porphyry molybdenum deposits. in *Relations of tectonics to ore deposits in the southern cordillera*, Arizona Geological Society Digest **14**, 215 – 225.

Bookstrom, A.A., Naeser, C.W., and Shannon, J.R. (1987). Isotopic age determinations, unaltered and hydrothermally altered igneous rocks, north-central Colorado Mineral Belt: Isochron/West **49**, 13 – 20.

Botinelly, T. (1979). Mineralogy as a guide for exploration in the Montezuma District, central Colorado. *US Geologic Survey Open-File Report* **79-1177**.

Bove, D.J., Caine, J.S. and Lowers, H.A. (2012). Geologic and mineralogic controls on acid and metal-rich rock drainage in an alpine watershed, Handcart Gulch, Colorado. *US Geologic Survey Scientific Investigations Report* **2012-5067**.

Brchan, C., Cappa, J. and Keller, J. (2003). Gold! Gold! Gold! *Colorado Geologic Survey Rock Talk* **6**, 2.

Brookins, D. (1988). *Eh-pH Diagrams for Geochemistry*, New York, NY, Springer-Verlag.

Bryant, D.G. and Metz, H.E. (1966). Geology and ore deposits of the Warren mining district. In *Geology of the porphyry copper deposits, southwestern North America,* Titley, S.R. and Hicks, C.L. (eds), University of Arizona Press, Tucson, 189 – 203.

Caine, J.S., Manning, A.H., Verplanck, P.L., Bove, D.J., Kahn, K.G. and Ge, S. (2006). Well construction information, lithologic logs, water level data, and overview of research in Handcart Gulch, Colorado: an alpine watershed affected by metalliferous hydrothermal alteration. *United States Geologic Survey Open-File Report* **2006-1189**.

Caine, J.S., Ridley, J. and Wessel, Z.R. (2010). To reactivate or not to reactivate – Nature and varied behaviour of structural inheritances in the Proterozoic basement of the eastern Colorado Mineral Belt over 1.7 billion years of earth history. *The Geological Society of America Field Guide* **18**.

Catchpole, H., Kouzmanov, K., Fontbote, L., Guillong, M. and Heinrich, C.A. (2011). Fluid evolution in zoned Cordilleran polymetallic veins – Insights from microthermometry and LA-ICP-MS of fluid inclusions. *Chemical Geology* **281**, 293 – 304.

Catchpole, H., Kouzmanov, K. and Fontboté L. (2012). Copper-excess stannoidite and tennantite-tetrahedrite as proxies for hydrothermal fluid evolution in a zoned Cordilleran base metal district, Morococha, central Peru. *The Canadian Mineralogist* **50**, 719 – 743.

Chapin, E.C. (2012). Origin of the Colorado Mineral Belt. *Geosphere* **8**, 28 – 43.

Cooke, D.R. and Bloom, M.S. (1990). Epithermal and subjacent porphyry mineralization, Acupan, Baguio District, Philippines; a fluid inclusion and paragenetic study. *Journal of Geochemical Exploration* **35**, 297 – 340.

Cooke, D.R. and Bloom, M.S. (1990). The evolution of gold-bearing fluids at the Acupan epithermal deposit, Baguio mineral district, Philippines. In *Epithermal Gold Mineralization of the Circum-Pacific: Geology, Geochemistry, Origin and Exploration*, Hedenquist, N.C., White and Siddeley, G. Journal of Geochemical Exploration **35**, 297 – 340.

Cunningham, C.G., Naeser, C.W., Marvin, R.F., Luedke, R.G. and Wallace, A.R. (1994). Ages of selected intrusive rocks and associated ore deposits in the Colorado Mineral Belt. *United States Geologic Survey Bulletin* **2109**.

Czamanske, G.K. (1974). The FeS content of sphalerite along the chalcopyrite-pyrite-bornite sulfur fugacity buffer. *Economic Geology, Special Publication* **69**, 1328-1334.

Drew, L.J. (2005). A tectonic model for spatial occurences of porphyry copper and polymetallic vein deposits – applications to central Europe. *US Geologic Survey Scientific Investigations Report* **2005 – 5272.**

Drummond, S.E. and Ohomoto, H. (1985). Chemical evolution and mineral deposition in boiling hydrothermal systems. *Economic Geology* **80**, 126 – 147.

Duan, Z., Møller, N., Derocher, T. and Weare, J.H. (1996). Prediction of boiling, scaling and formation conditions in geothermal reservoirs using computer programs TEQUIL and GEOFLUIDS. *Geothermics* **25**, 663 – 678.

Einaudi M.,T. (1977). Environment of ore deposition at Cerro de Pasco, Peru. *Economic Geology* **72**, 893 – 924.

English J.M. and Johnston S.T. (2004). The Laramide Orogeny: What were the driving forces? *International Geology Review* **46**, 833 – 838.

Erslev, E.A. (2005). 2D Laramide geometries and kinematics of the Rocky Mountains, Western U.S.A. Rocky Mountain Region: An evolving lithosphere tectonics, geochemistry, and geophysics. In The Rocky Mountain Region: An Evolving Lithosphere Tectonics, Geochemistry, and Geophysics. *Geophysical Monograph Series* **154,** 7 – 20.

Fontboté, L. and Bendezú, R. (2009). Cordilleran or Butte-type veins and replacement bodies as a deposit class in porphyry systems. in *Proceedings of the 10th Biennial Society of Geology Applied to Ore Deposits Meeting*, 521-523.

Fournier, R.O. (1987). Conceptual models of brine evolution. *US Geological Survey Professional Paper* **1350,** 1487 – 1506.

Fournier, R.O. (1991). The influences of depth of burial and the brittle-plastic transition on the evolution of magmatic fluids. *Japan Geological Survey Report* **279**, 57 – 59.

Geraghty, E.P., Carten, R.B. and Walker, B.M. (1988). Tilting of the Urad-Henderson and Climax porphyry molybdenum systems, central Colorado, as related to northern Rio Grande rift tectonics. *Geological Society of America Bulletin* **100**, 1780 – 1786.

Giggenbach, W.F., Garcia, N.P., Londono, A.C., Rodriguez, L.V., Rojas, N.G. and Calvache, L.V. (1990). The chemistry of fumarolic vapor and thermal springs discharges from the Nevado del Ruiz volcanic-magmatic-hydrothermal system. *Journal of Volcanology and Geothermal Research* **42**, 13 – 39.

Giggenbach, W.F. (1997). The origin and evolution of fluids in magmatic-hydrothermal systems. In *Geochemistry of Hydrothermal Ore Deposits*, Barnes, H.L. (ed.), New York, John Wiley, pp. 737 – 796.

Goodell, P.C. and Petersen, U. (1974). Julcani mining district, Peru: A study of metal ratios. E*conomic Geology* **69**, 347 – 361.

Gutscher, M.A., Maury, R., Eissen, J.P. and Bourdon, E. (2000). Can slab melting be caused by flat slab subduction? *Geology*, **28**, 535 – 538.

Hall, W.E., Friedman, I. and Nash, J.T. (1974). Fluid inclusion and light stable isotope study of the Climax molybdenum deposit, Colorado. *Economic Geology* **69**, 884 – 901.

Hedenquist, J.W. (1990). The thermal and geochemical structure of the Broadlands-Ohaaki geothermal system, New Zealand. *Geothermics* **19**, 151 – 185.

Hedge, C.E. (1969). Petrogenetic and geochronologic study of migmatites and pegmatites in the central Front Range (Colorado). Golden, Colorado School of Mines Ph.D thesis.

Heinrich, C.A. (1990). The chemistry of hydrothermal tin(-tungsten) ore deposits. *Economic Geology* **85**, 457 – 481.

Heinrich, C.A. (2005). The physical and chemical evolution of low-salinity magmatic fluids at the porphyry to epithermal transition: a thermodynamic study. *Mineralium Deposita* **39**, 865 – 889.

Hemley, J.J. and Hunt, J.P. (1992). Hydrothermal ore-forming processes in the light of studies in rock-buffered systems; II, Some geological applications. *Economic Geology* **87**, 23 – 43.

Holmes, H.F., Simonson, J.M., Mesmer, R.E. (1997). Additions and corrections. Aqueous solutions of alkaline earth metal chlorides. Corrected constants for ion-interaction model. *Journal of Chemistry and Thermodynamics* **29**, 1363 – 1373.

Ineson, P.R. (1989). *Introduction to Practical Ore Microscopy*, Singapore, Longman Publishers Ltd.

Landtwing, M.R., Furrer, C., Redmond, P.B., Pettke, T., Guillong, M. and Heinrich, C.A. (2010). The Bingham Canyon porphyry Cu-Mo-Au deposit. III. Zoned copper-gold ore deposition by magmatic vapor expansion. *Economic Geology* **105**, 91 – 118.

Lang, J.R. and Eastoe, C.J. (1988). Relationships between a porphyry Cu-Mo deposit, base and precious metal veins and Laramide intrusions, Mineral Park Arizona. *Economic Geology* **83**, 551 – 567.

Lovering, T. (1930). Localization of ore in schists and gneisses of the mineral belt of the Front Range, Colorado. *Colorado Scientific Society Proceedings* **12**, 233 – 268.

Lovering, T.S. (1935). Geology and ore deposits of the Montezuma Quadrangle, Colorado. *US Geologic Survey Professional Paper* **178**.

Lerchbaumer, L. and Audétat, A. (2013). The metal content of silicate melts and aqueous fluids in subeconomically Mo mineralized granites: Implications for porphyry Mo genesis. *Economic Geology* **108**, 987 – 1013.

Lüders, V., Romer, R.L., Gilg, H.A., Bodnar, R.J., Pettke, T. and Misantoni, D. (2009). A geochemical study of the Sweet Home Mine, Colorado Mineral Belt, USA: hydrothermal fluid evolution above a hypothesized granite cupola. *Mineralium Deposita* **44**, 415 – 434.

Ludington, S. and Plumlee, G.S. (2009). Climax-type porphyry molybdenum systems. *US Geological Survey Open-File Report* **2009-1215**.

Matthews,V. and Morgan, M.L. (2012). A GIS test of two models for the distribution of Tertiary epithermal ore deposits in Colorado. *The Mountain Geologist* **49**, 1 – 17.

McDowell, F.W. (1971). K-Ar ages of igneous rocks from the western United States. *Isochron/West* **2**, 1-16.

McGeary, S., Nur, A. and Ben-Avraham, Z. (1985). Spatial gaps in arc volcanism: The effect of collision or subduction of oceanic plateaus. *Tectonophysics* **119**, 195 – 221.

Meyer, C. and Hemley, J.J. (1967). Wall rock alteration. In *Geochemistry of Hydrothermal Ore Deposits*, Barnes, H.L. (ed.), New York, Holt, Rinehart and Winstone, p. 166 – 232.

Meyer, C., Shea, E.P., Goddard, C.C. *et al.* (1969). Ore deposits at Butte, Montana. In *Ore Deposits of the United States 1933 – 1967 (Graton-Sales Volume)*, Ridge, J.D., (ed.), New York , American Institute of Mining, Metallurgy and Petroleum Engineers, 1363 – 1416.

Mikulski, S.Z. (2005). Geological, mineralogical and geochemical characteristics of the Radzimowice Au-As-Cu deposit from the Kaczawa Mountains (Western Sudetes, Poland): an example of the transition of porphyry and epithermal style. *Mineralium Deposita* **39**, 904 – 920.

Miller, B. (2004). Fluid inclusions in the Butte, Montana main stage veins; reconstructing fluid orgin and fate. *Geological Society of America Abstracts with Programs* **36**, 23.

Muntean, J.T. and Einaudi, M.T. (2001). Porphyry-epithermal transition: Maricunga Belt, northern Chile. *Economic Geology* **96**, 743 – 772.

Müller, D., Kaminski, K., Uhlig, S., Graupner, T., Herzig, P.M. and Hunt, S. (2002). The transition from porphyry- to epithermal-style gold mineralization at Ladolam, Lithir Island, Papua New Guinea: a reconnaissance study. *Mineral Deposita* **37**, 61 – 74.

Neuerburg, G.J., Botinelly, T. and Watterson, J.R. (1974). Molybdenite in the Montezuma District of central Colorado. *US Geological Survey Circular* **704**.

Reed, J.C., Jr., Brickford, M.E., Premo, W.R., Aleinikoff, J.N. and Pallister, J.S. (1987). Evolution of the Early Proterozoic Colorado province: constraints from U-Pb geochronology. *Geology* **9**, 861-865.

Reed, M. (1999). The Butte, Montana main stage vein system; structural style, alteration, and mineral zoning, and their relationship to pre-main stage sericite alteration. *Geological Society of America Abstracts with programs* **31**, 382.

Reed, M., Rusk, B. and Palandri, J. (2013). The Butte magmatic-hydrothermal system: one fluid yields all alteration and veins. *Economic Geology* **108**, 1379 – 1396.

Rusk, B.G. and Reed, M.H. (2008). Fluid inclusion evidence for magmatic-hydrothermal fluid evolution in the porphyry copper-molybdenum deposit at Butte, Montana. *Economic Geology* **103**, 307 – 334.

Rice, C.M., Lux, D.R. and Macintyre, R.M. (1982). Timing of mineralization and related intrusive activity near Central City, Colorado. *Economic Geology* **77**, 1655 – 1666.

Rice, C.M., Harmon, R.S. and Shepherd, T.J. (1985). Central City, Colorado: the upper parts of an alkaline porphyry molybdenum system. *Economic Geology* **80**, 1769 – 1796.

Ridley, J. (2013). *Ore Deposit Geology*, New York, NY, Cambridge University Press.

Rimstidt, J.D. (1997). Gangue mineral transport and deposition. In *Geochemistry of Hydrothermal Ore Deposits*, Barnes, H.L. (ed.), New York, John Wiley, pp. 487 – 516.

Robinson, C.S., Warner, L.A. and Wahlstrom, E.E. (1974). General geology of the Harold D. Roberts Tunnel, Colorado. *US Geological Survey Professional Paper* **831-B**.

Rusk, B.G., Miller, B.J. and Reed, M.H. (2008). Fluid inclusion evidence for the formation of main stage polymetallic base-metal veins, Butte, Montana, USA. *Arizona Geological Society Digest* **22**, 573-581.

Rye, R.O. and Sawkins (1974). Fluid inclusion and stable isotope studies on the Casapalca Ag-Pb-Zn-Cu deposit Central Andes, Peru. *Economic Geology* **69**, 181 – 205.

Rye, R.O. (1993). The evolution of magmatic fluids in the epithermal environment: the stable isotope perspective. *Economic Geology* **88**, 733 – 753.

Scott, S.D. and Barnes, H.L. (1971). Sphalerite geothermometry and geobarometry. *Economic Geology* **66**, 653-669.

Seedorf, E. and Einaudi, M.T. (2004). Henderson porphyry molybdenum system, Colorado I. Sequence and abundance of hydrothermal mineral assemblages, flow paths of evolving fluids. *Economic Geology* **99**, 3 – 38.

Seward, T.M. and Barnes, H.L. (1997). Metal transport by hydrothermal ore fluids. In *Geochemistry of Hydrothermal Ore Deposits*, Barnes, H.L. (ed.), New York, John Wiley, pp. 435 – 486.

Simmons, E.C. and Hedge, C.E. (1978). Minor-element and Sr-isotope geochemistry of Tertiary stocks, Colorado Mineral Belt. *Contributions to Mineralology and Petrology* **67**, 379 – 396.

Simmons, S.F. and Christenson, B.W., 1994. Origins of calcite in a boiling geothermal system. *American Journal of Science* **294**, 361 – 400.

Sims, P.K. and Barton Jr., P.B. (1962). Hypogene zoning and ore genesis, Central City district, Colorado. *Petrologic Studies: a volume to honor A.F. Buddington*, 373 – 395.

Sims, P.K. (1983). Geology of the Central City area, Colorado – A Laramide mining district. In *The Genesis of Rocky Mountain Ore Deposits; changes with time and tectonics.* Denver Region Exploration Geologist Symposium, 95 – 100.

Skinner, B.J. (1997). Hydrothermal mineral deposits: what we do and don't know. In *Geochemistry of Hydrothermal Ore Deposits,* Barnes, H.L. (ed.), New York, John Wiley, pp. 1 – 30.

Šoštarić, B., Palinkaš, L.A., Neubauer, F., Hurai, V., Cvetković, V., Roller-Lutz, Z., Mandić, M. and Genser, J. (2013). Silver-base metal epithermal vein and listwanite hosted deposit Crnac, Rogozna Mts., Kosovo; part II, a link between magmatic rocks and epithermal mineralization. *Ore Geology Reviews* **50**, 98 – 117.

Sourirajan, S. and Kennedy, G.C. (1962). The system H_2O-NaCl at elevated temperatures and pressures. *American Journal of Science* **260**, 115 – 141.

Spry, P.G.(1987). A fluid inclusion and sulfur isotope study of the precious and base metal mineralization spatially associated with the Patch and Gold Cup breccia pipes, Central City, Colorado. *Economic Geology* **82**, 1632 – 1639.

Stanton, R.L. (1972). *Ore Petrology,* United States of America, McGraw-Hill, Inc.

Stefanova, E., Driesner, T., Zajacz, Z., Heinrich, C.A., Petrov, P. and Vasilev, Z. (2014). Melt and fluid inclusions in hydrothermal veins: the magmatic to hydrothermal evolution of the Elastsite Porphyry Cu-Au deposit, Bulgaria. *Economic Geology* **109**, 1359 – 1381.

Stein, H.J. (1993). A mantle component for Climax-type granite-molybdenum systems our first glimpse at Re-Os in the lower continental crust? *Earth and Space Sciene News* **74**, 121.

Stein, H.J. and Crook, J.G. (1990). Late Cretaceous-Tertiary magmatism in the Colorado mineral belt; rare earth element and samarium-neodymium isotopic studies *in* Anderson, J.L., ed. The nature and origin of Cordilleran magmatism. *Geological Society of America Memoir* **174**, 195 – 223.

Stein, H.J. and Hannah, J.L. (1985). Movement and origin of ore fluids in Climax-type systems. *Geology* **13**, 469 – 474.

Tikoff, B. and Maxson J. (2001). Lithospheric buckling of the Laramide foreland during Late Cretaceous and Paleogene, western United States. *Rocky Mountain Geology* **36**, 13 – 35.

Tweto, O. and Sims, P.K. (1963). Precambrian ancestry of the Colorado Mineral Belt. *Geological Society of America Bulletin* **74**, 991-1014.

Van Der Pluijm, B.A. and Marshak, S. (2004). *Earth Structure an introduction to structural Geology And tectonics, second edition,* New York ,W.W. Norton and Company Ltd.

Voudouris, P.C., Melfos, V., Spry, P.G., Kartal, T., Schleicher, H., Moritz, R. and Ortelli, M. (2013). The Pagoni Rachi/Kirki Cu-Mo±Re±Au deposit; Northern Greece: Mineralogical and Fluid Inclusion Constraints on the evolution of a telescoped porphyry-epithermal system. *The Canadian Mineralogist* **51**, 253-284.

Wahlstrom, E.E. and Kim, O.J. (1959). Precambrian rocks of the Hall Valley area, Front Range, Colorado. *Geological Society of America Bulletin* **70**, 1217-1244.

Wallace, S.A. (1995). The Climax-type molybdenite deposits: what they are, and why they are. *Economic Geology* **90**, 1359 – 1380.

Wessel, Z. and Ridley, J. (2010). Structural analysis of the Idaho Springs-Ralston shear zone: a new look at an ancient structure. *Abstracts Geological Society of America Annual Meeting* **42**, 654.

Wilkinson, J.J. (2001). Fluid inclusions in hydrothermal ore deposits. *Lithos* **55**, 229 – 272.

Woitsekhowskaya, M.B. and Hemley, J.J. (1995). Modelling metal transport and deposition in Butte-type hydrothermal systems. *Economic Geology* **90**, 1329 – 1337.

Zeng, Q., Liu, J., Zhang, Z., Zhang, W., Chu, S., Zhang, S., Wang, Z. and Duan, X. (2011). Geology, fluid inclusions, and sulfur isotope studies of the Chehugou porphyry molybdenum-copper deposit, Xilamulun Metallogenic Belt, NE China. *Resource Geology* **61**, 241 – 258.

Zukowski, W., Cooke, D.R., Deyell, C.L., McInnes, P. and Simpson, K. (2014). Genesis and exploration implications of epithermal gold mineralization and porphyry-style alteration at the Endeavour 41 prospect, Cowal District, New South Wales, Australia. *Economic Geology* **109,** 1079 – 1115.

Appendix A. The Porphyry Environment and Juvenile Waters

With decreasing economic significance of high-grade low-tonnage deposits, the prospect of bulk-tonnage low-grade porphyries below Cordilleran vein fields is an important consideration of these systems. Several authors (Bartos, 1989; Rice el al., 1985; Reed et al. 2013; and others) have investigated this association, and this research was also inspired by the question. As noted above, not all Cordilleran-type vein fields have proven underlying mineralized porphyry. Conversely polymetallic vein fields at Yauricocha (Peru), Bisbee (Arizona, USA), Butte (Montana, USA) and Morococha (Peru), Victoria (Philippines), Cerro de Pasco (Peru), Casapalca (Peru), Chuquicamata (Chile) and La Escondida (Chile) are all spatially associated with mineralized porphyry deposits (Bartos, 1989; Catchpole et al., 2011). Some of these porphyries are subeconomic while others are economic. Can particular trends or patterns in the Cordilleran veins aid in differentiation of subeconomic vs. economic porphyries? If so, what are these patterns or trends? Perhaps particular fluid evolution histories of underlying porphyries can be detected in the above vein fields. The frequency of proven links invokes a review of the general porphyry model (Sillitoe, 2010; Sillitoe, 1973). The purpose of this section is to overview early influences of a magmatic-hydrothermal fluid, which are present in the porphyry ore environment in order to better understand the variables than may render economic porpyries. This is intended to highlight the connection between a parent fluid exsolved from a felsic pluton to the daughter fluids observed in the Cordilleran-type environment.

Figure 3.0.1 is the current model of potential ore deposits that are spatially related to a mineralized porphyry deposit. The following review will place an emphasis on fluid evolution of porphyry deposits and Cordilleran-type veins. In figure 3.0.1 Sillitoe (2010) has term Cordilleran veins as “subepithermal veins.” This fluid evolution model will assume a connection between mineralized porphyries and Cordilleran-type veins, and accordingly, will address the system beginning with porphyry.

The term "mineralized porphyry" has been favoured to deemphasise the significance of economics, rather to simply suggest stockwork style mineralization of base metals that may or may not be ore in grade or tonnage. The formation of a stockwork fracturing is due to the build-up of fluid pressure in a cupola that exceeds lithostatic pressure of marginal country rock.

Alteration and Veinlets

Stockwork or sheeted veinlets that record several generations of hydrothermal fluids are a distinguishing feature of porphyry deposits (Ridley, 2013). Cross-cutting relationships indicate a three stage sequence of vein fill that is observed at many porphyry deposits from: 1. early, quartz and sulphide free veinlets containing one or more of actinolite, magnetite (M-type), biotite (EB-type) and potassium feldspar; 2. granular quartz veinlets bearing chalcopyrite±bornite (A-type) or molybdenite±chalcopyrite (B-type); 3. late, crystalline quartz-sulphide with prominent potassium feldspar destructive alteration selvages (D-type) (Sillitoe, 2010). For the porphyry-epithermal Pagoni Rachi/Kirki deposit in Greece, Voudouris et al. (2013) added an E-type vein to describe the late stage base and precious metal veins found in the district, which may be equivalent to epithermal or Cordilleran veins.

Porphyry deposits commonly exhibit distinct alteration halos that occur in zones, which occur over several cubic kilometres of rock (Figure A.A.1). Like the veinlets, an overprinting sequence of alteration facies has been identified: 1. sodic-calcic; 2. potassic; 3. chlorite-sericite; 4. phyllic; 5. argillic. Propylitic alteration is an additional alteration facies that can occur at any time during the above sequence. Solution pH is the principal control on alteration type, which generally decreases with time and fluid ascent. Potassic alteration occurs as the fluid cools from 500 to 450°C and the fluid becomes saturated with Na^+ and K^+ and is generally associated with ore deposition. Veinlets groups have been linked to alteration facies. Groups one (M-type and EB-type) and two (A-type and B-type) are emplaced during potassic alteration while mineralization of the third group (D-type) accompanies chlorite-sericite, phyllic, and advanced argillic alterations (Sillitoe, 2010).

Metal Source and Magmatic Fluids

Based on fluid Cs/Na values (Catchpole et al., 2011), district wide spatial ICP-MS analysis of fluid inclusions and isotope data (Beuchat et al., 2004), fluid δD values (Rice et al., 1985), geochemical modelling (Reed et al., 2013), and metal content in fluid inclusions (Bodnar, 1995; Lerchbaumer and Audétat, 2013) it has been concluded that metals in both polymetallic veins and Cu-Mo porphyries are from a magmatic source. Similarly, Stein and Hannah (1985) and Stein (1988) have found that metals and sulfur in Climax-type porphyry Mo systems are derived from source plutons based on lead, sulfur and oxygen isotope ratios.

In the 1970s and 1980s, a debate existed of whether metals in porphyries were soured from leached wall rocks or magmas (Bodnar, 1995). In addition to other data sources of the time, wall rock leaching was supported by the fact that magmatic fluids can travel several kilometres from mineralized porphyries, and that circulating meteoric waters can be equally extensive (Bodnar, 1995). But now through stable isotope and fluid inclusion studies, it is now clear that magmas have sourced both Mo and Cu to economic porphyry metal deposits (Bodnar, 1995; Lerchbaumer and Audétat, 2013). The systematic mapping of metal content in hydrothermal inclusions and melt inclusions are the basis for proving this.

In some instances magmatic fluid inclusions from the barren cores of porphyry deposits contains daughter chalcopyrite as triangular opaque solid phase. These have been proven to be daughters and not accidental proving that chalcopyrite exists in equal proportions to other phases present during the primitive stages of fluid evolution (Bodnar, 1995). In addition, Anderson et al. (1989) assayed (PIXE and PIGE) fluid inclusions from the core of the Bingham Canyon Cu-Mo porphyry where only molybdenite existed in mineralized veins. Despite the fact that only Mo was mineralized in this region of the porphyry, fluid inclusions proved to contain significant amounts of Cu, Pb, Zn and Fe. A mass balance calculation of the amount of these base metals in inclusions was found to be sufficient for adjacent Cu

stockwork mineralization and distal Pb-Zn fissure fill mineralization. This proves base metals can be transported through barren potassic cores with selective precipitation, and that magmatic fluids are indeed the source of metals in both porphyries and adjacent polymetallic veins.

A follow up as to the source of metals in these systems has come from the assay of silicate melt inclusions from expected source magmas of Mo porphyries. Lerchbaumer and Audétat (2013) have confirmed that with increasing degrees of magma evolution, there is an increase in molybdenum concentration as an incompatible element. The study stresses the importance of using fluid inclusions because they represent one fluid at a snapshot in time, while whole rock geochemistry represents integrated products. Cs was plotted against Mo because Cs is a strongly incompatible trace element, and it is easily detected with LA-ICP-MS. Therefore Cs concentrations track increasing degrees of magma evolution. The results were that Mo rates increase uniformly in all magmatic systems with increased degrees of differentiation. When Mo/Cs ratios of economic, subeconomic and barren porphyries were plotted, it was found that that is no systematic difference among the categories. To explain economic porphyries vs. sub-economic porphyries, the study indicated that the size of the intrusive body and degree of fluid focusing are the key variables with regard to forming an initial magmatic fluid with economic potential. With the knowledge that chemistries of felsic melts are uniform with respect to Cs + Mo, it can be inferred that it would require a several hundred km^3 body of magma with efficient fluid focusing to form a Climax-type high grade and high bulk tonnage deposit (Lerchbaumer and Audétat, 2013). At porphyry Cu deposits the enrichment factor is 200 time that of an average igneous rock, which implies that a Cu ore body 1 km^3 in size would require a source magma chamber of at least 200 km^3 in volume (Ridley, 2013). The concentration of a metal rich aqueous magma is believed to be made possible by the formation of a cupola above a magma body. Fluid pressure increase in the cupola is believed to induce subsequent stockwork vein formation in host rocks. Brittle fracture is favoured in environments above the brittle-ductile transition, which will be discussed in the next section.

With regard to overlying Cordilleran type deposits, a magmatic source seems to be the favoured interpretation by most modern researchers (Catchpole et al. 2011; Beuchat et al. 2004; Rice et al. 1985, Rusk et al., 2008), which strengthens the postulated connection between the two deposit types. At Morococha, Peru Catchpole et al. (2011) found high concentrations of caesium in hotter earlier fluid inclusions of this vein field. Caesium is highly incompatible in magmatic systems, and is therefore used to interpret magmatic origins of a fluid (Audétat and Pettke, 2003; Audétat et al., 2008). Beuchat et al. (2004) interpreted δD vs $\delta^{18}O$ data from fluids responsible for base metal mineralization in the San Cristobal vein of Peru to indicate a dominantly magmatic source. This was supported by high salinity fluid inclusions also found in this mineralizing phase. At Central City, USA, Rice et al. (1985) interpreted a similar magmatic fluid using isotope data from molybdenite veins and precious-base metal veins found in the district. This will be the favoured source for metals at Montezuma, but it should be noted that earlier studies of such veins have not come to the same conclusion.

Depth and Pressure Variables

Depth and pressures at which a hydrous hydrothermal fluid is exsolved from a magma and passes through a cupola is a key consideration in the evaluation of a porphyry mineralization system. The porphyry-epithermal system from strato-cone summit to magmatic fluid source can span 10 kilometres vertically, which renders an equally large range of pressures as the fluid rises. Primary fluid inclusions in this system are an ideal tool in evaluating the evolution of a fluid with regard to depth and pressure. They record fluid conditions by preserving a fossil fluid that is representative of the time at which a particular mineral grew under particular pressures, temperatures and compositions of hydrothermal fluid. In order to address the multitude of fluid inclusion character in porphyry systems, the diagram in Figure A.A.2 has been produced. For example the deepest of Cu-Mo porphyries at Butte, Montana is known to have been emplaced at 9 km (Rusk and Reed, 2008), while Red Mountain, Arizona was emplaced at less than 5 km depth (Bodnar, 1995). By inspection of Figure A.A.2, it can be found that at low pressures an exsolved

magmatic fluid will contain a high salinity liquid and low salinity vapour, while at higher pressures only one phase will exist (Bodnar, 1995).

The initial fluid at many deposits is of intermediate density with low salinity and homogenizes at high temperatures. Pressures are dependent on the depth of emplacement of the magmatic fluid: at depth the fluid tends to be lithostatic pressured, while shallower porphyries may be at hydrostatic pressures. These primitive magmatic fluids dominant in the potassic barren cores of porphyries. As the fluid rises from the barren core, depressurization occurs inducing boiling. This is how multiple FIA are produced at porphyry deposits, which are dependant on the degree and rate of boiling at within a deposit. Boiling renders a two phase fluid that is composed of highly saline brine and a low density vapour. At room temperature the former is reflected as an inclusion containing halite and a gas bubble. Inclusions may indicate a variety of temperatures, but pressures will be uniformly lower than the initial fluid.

At the Chehugou porphyry in China (Zeng et al., 2011) there is a gap in salinities from 15 – 30% considering all observed FI at the deposit. Systematic gaps in salinities like these are commonly attributed to boiling, as progressive decrease in salinity would be expected by mixing with meteoric waters. The gap between the two salinities is roughly concurrent with the ore zone. The solubility of metals decreases in hydrous vapors, which can render precipitation on boiling (Heinrich et al., 1999), which explains the location of ore along this boiling interface. Rapid boiling vs. gradual boiling is believed to be the major control on metal zonation at Bingham Canyon (Landtwing et al., 2010). Cu-Au precipitation in the centre of ore body are believed to be rapid boiling while the Cu-rich precipitation in peripheral portions of the ore body.

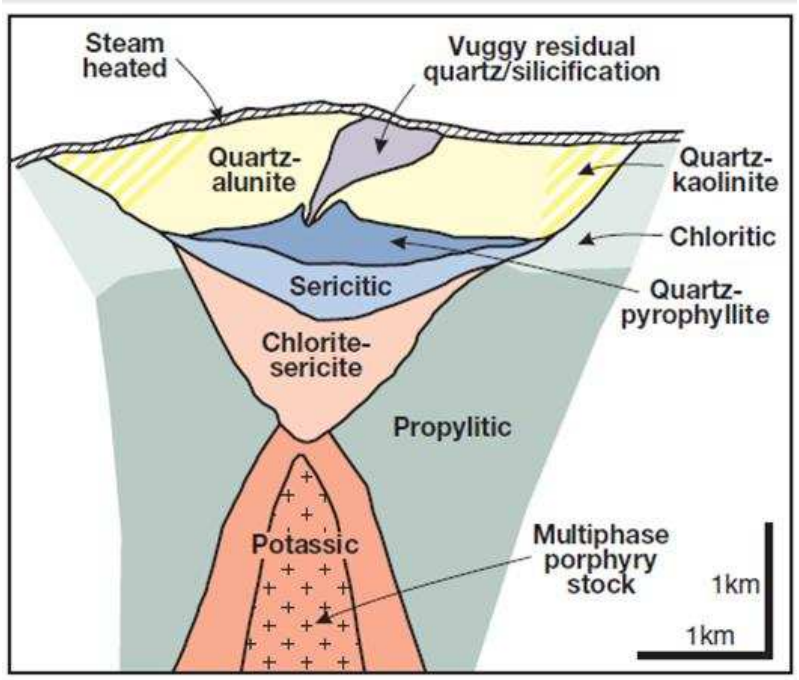

Figure A.A.1 from Sillitoe (2010). Generalized alteration-mineralization for a non-telescoped porphyry Cu system.

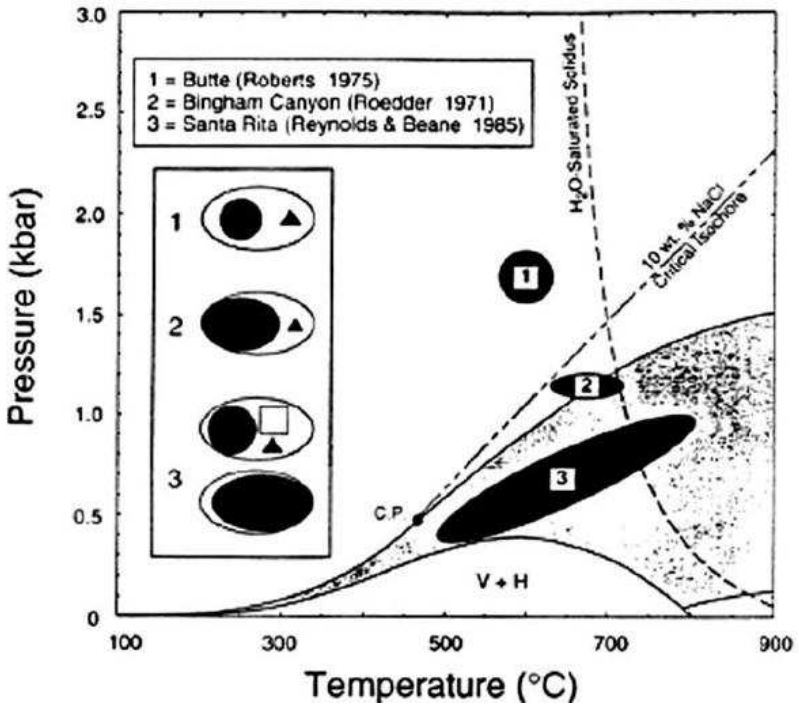

Figure A.A.2 from Bodnar (1995). Pressure-temperature diagram showing the varability in room temperature appearance of magmatic fluid inclusions trapped at different P-T conditions representing the Butte (area 1), Bingham Canyon (area 2) and Santa Rita (area 3) porphyry copper deposits. The shaded aea represents two phase (liquid + vapor) region for aqueous solution with a bulk composition of 10 qt.% NaCl.

Appendix B. Production Data used for Zonation Maps

Longitude	Latitude	Mine Name	Au fine oz	Ag fine oz	Pb assay lb	Cu wet assay lb	Zn lb
-105.874	39.574	Adder	0.100	1992.000	9606.000	0.001	0.001
-105.809	39.581	Baltic	2.890	48016.000	0.001	0.001	0.001
-105.813	39.583	Revenue	116.330	37775.000	5275.000	42709.000	0.001
-105.871	39.565	Bell and California groups	14.130	66910.000	2495179.000	3839.000	617917.000
-105.844	39.560	Blanche	0.001	4040.000	81765.000	0.001	0.001
-105.849	39.572	Bullion	0.700	5473.000	142569.000	3996.000	0.001
-105.857	39.534	Cashier	178.220	180537.000	0.001	75849.000	0.001
-105.871	39.553	Chatauque	114.520	11148.000	338629.000	0.001	0.001
-105.815	39.606	Congress	3.060	3950.000	47821.000	0.001	0.001
-105.872	39.592	Fisherman	6.470	2636.000	65179.000	0.001	19452.000
-105.773	39.692	Hamill Tunnel	0.400	70166.000	57414.000	0.001	70887.000
-105.875	39.576	Harrison	0.001	10134.000	60061.000	8.000	0.001
-105.897	39.587	Hunkidori	0.110	538.000	13289.000	0.001	0.001
-105.920	39.591	Ida Belle	29.280	2755.000	120060.000	174.000	15241.000
-105.871	39.580	Jerry, Equity, Denver, and Celtic	7.610	9323.000	97761.000	295.000	55156.000
-105.803	39.673	Josephine	228.060	27039.000	2250802.000	5118.000	24053.000
-105.806	39.670	Kelso	25.380	1413.000	117100.000	0.001	3543.000
-105.769	39.658	Kitty Owsley	94.570	4574.000	183904.000	160.000	297153.000
-105.854	39.601	Maid of Orleans	3.510	287.000	8810.000	0.001	0.001
-105.876	39.572	Mark Twain and St. Elmo	0.001	431.000	2311.000	0.001	0.001
-105.859	39.517	Missouri	198.670	24152.000	26203.000	28948.000	4927.000
-105.857	39.551	Mohawk	0.600	1130.000	108213.000	0.001	0.001
-105.878	39.571	More Work	0.170	1197.000	11140.000	0.001	21645.000
-105.857	39.583	Morgan	1.350	491.000	25371.000	662.000	47689.000
-105.865	39.580	Alladins Lamp vein from New York Tunnel	0.860	183.000	0.001	9926.000	6839.000
-105.866	39.573	Old Timer	0.001	80.000	5362.000	0.001	0.001
-105.802	39.623	Pay Master	1.950	353.000	14778.000	74.000	0.001
-105.809	39.601	Pennsylvania Group	3474.260	901335.000	7455139.000	74336.000	916069.000
-105.800	39.617	Peruvian	1.120	12630.000	141177.000	451.000	6384.000
-105.847	39.581	Quail	0.600	1841.000	156228.000	239.000	0.001
-105.867	39.543	Radical	0.001	124.000	11681.000	0.001	0.001
-105.821	39.603	Roschild Tunnel	14.800	18109.000	77259.000	7156.000	47000.000

-105.879	39.570	Sts. Johns	10.350	110842.000	3146354.000	1904.000	382810.000
-105.771	39.644	Santiago	12816.210	314214.000	2097719.000	1147048.000	86693.000
-105.866	39.573	Silver King	87.790	9858.000	188446.000	451.000	40122.000
-105.837	39.566	Silver Wave	151.830	58835.000	1006034.000	35604.000	188553.000
-105.784	39.656	Stevens	249.370	119638.000	4860660.000	0.001	0.001
-105.875	39.568	Tiger and Extension	0.001	2443.000	41670.000	0.001	0.001
-105.802	39.623	Paymaster	123.200	63801.000	1456771.000	0.001	0.001
-105.844	39.580	Washington	0.001	150.000	219.000	0.001	0.001
-105.863	39.527	Whale	9.550	77248.000	513561.000	22946.000	0.001
-105.887	39.560	Wild Irishman	0.001	10347.000	171741.000	45.000	0.001

Appendix C. Fluid Inclusion Data

Sample ID	Salinity wt%	Total Homogenization	HM + 25	FI Host	Bubble Moves	HM Double bubble
BS-1 5 A 1	13.28912	167	192	ag	-9.4	
NT-1 2 A 1	6.448448	143	168	ag	-4	
NT-1 2 A 2	7.306944	127	152	ag	-4.6	
NT-1 2 A 3	6.593387	131	156	ag	-4.1	
NT-1 2 A 4	6.593387	131	156	ag	-4.1	
NT-1 2 A 5	6.302759	133	158	ag	-3.9	
NT-1 4 B 1	6.737579	125	150	ag	-4.2	
PERU-1 3 B 1	10.97732	129	154	Ag sph	-7.4	
PERU-1 3 B 2	10.97732	129	154	Ag sph	-7.4	
PERU-1 3 B 3	10.97732	129	154	Ag sph	-7.4	
PERU-1 3 A 1	16.61793	164	189	Ag sph	-12.7	
PERU-1 3 A 2	16.61793	164	189	Ag sph	-12.7	
PERU-1 3 A 3	16.98503	161	186	Ag sph	-13.1	
PERU-1 2 A 1	6.881027	122	147	Ag sph	-4.3	
PERU-1 2 A 2	6.737579	122	147	Ag sph	-4.2	
PERU-1 2 B 1	7.165707	125	150	Ag sph	-4.5	
EQUITY-3 4 A 1	3.06404	340	365	ba	-1.8	
EQUITY-3 4 A 2	2.073314	290	315	ba	-1.2	
EQUITY-3 4 B 1	3.708003	268	293	ba	-2.2	
EQUITY-3 4 B 2	3.708003	275	300	ba	-2.2	
NT-1 3 A 1	4.338998	330	355	ba	-2.6	
RADICAL-1 1 A 1	10.85526	281	306	ba	-7.3	
TIGER-2 A 1	6.593387	182	207	ba	-4.1	
TIGER-2 B 1	6.737579	200	225	ba	-4.2	
TIGER-2 B 2	11.21952	219	244	ba	-7.6	
TIGER-2 C 1	8.813095	207	232	ba	-5.7	
NT-1 3 B 1	4.957239	229	254	ba	-3	
NT-1 3 B 2	3.866959	377	402	ba	-2.3	
TIGER-2 2 A 1	10.23533	210	235	ba	-6.8	
QOW-1 2 A 1	4.338998	307	332	CO2	7.4	30.8
QOW-1 5 B 3			25	CO2	6.5	31
QOW-1 5 A 1		307	332	CO2	8	30.5
SRQ-8 3 A 1	48.125	542	567	Hyper salineqtz	-50	
SRQ-8 1 A 1	39.0996	322	347	Hyper salineqtz	-43	
SRQ-8 1 A 2	42.56895	330	355	Hyper salineqtz	-46	

SRQ-8 2 A 1	36.128	390	415	Hyper salineqtz	-40	
SRQ-8 2 A 2	40.19629	349	374	Hyper salineqtz	-44	
SRQ-8 2 A 3	39.0996	408	433	Hyper salineqtz	-43	
BS-1 3 A 1	12.62073	318	343	qtz	-8.8	
BS-1 3 A 2	12.62073	318	343	qtz	-8.8	
BS-1 3 B 1	11.09873	291	316	qtz	-7.5	
BS-1 3 B 2	11.09873	286	311	qtz	-7.5	
CHAT-1 3 A 1	9.855516	273	298	qtz	-6.5	
MORGAN-1 2 A 1	2.57243	289	314	qtz	-1.5	
MORGAN-1 2 A 2	2.57243	272	297	qtz	-1.5	
MORGAN-1 3 A 4	15.66756	332	357	qtz	-11.7	
MORGAN-1 4 A 1	8.813095	236	261	qtz	-5.7	
MORGAN-1 4 A 2	8.945789	285	310	qtz	-5.8	
MORGAN-1 4 A 4	8.945789	280	305	qtz	-5.8	
MORGAN-1 4 A 5	10.23533	279	304	qtz	-6.8	
MORGAN-1 5 B 1	7.587232	290	315	qtz	-4.8	
QOW-1 2 B 1	8.545621	292	317	qtz	-5.5	
QOW-1 4 A 2	9.598978	298	323	qtz	-6.3	
QOW-1 5 B 1	10.48525	285	310	qtz	-7	
QUAIL-1 1 A 1	8.945789	256	281	qtz	-5.8	
QUAIL-1 1 A 2	9.339746	269	294	qtz	-6.1	
QUAIL-1 1 A 3	5.861155	299	324	qtz	-3.6	
QUAIL-1 3 A 2	6.156316	270	295	qtz	-3.8	
QUAIL-1 3 A 3	5.712431	270	295	qtz	-3.5	
QUAIL-1 5 A 1	11.81405	270	295	qtz	-8.1	
RADICAL-1 4 A 1	14.35788	276	301	qtz	-10.4	
REVEN-4 1 A 1	12.73359	326	351	qtz	-8.9	
REVEN-4 1 A 2	14.14853	352	377	qtz	-10.2	
REVEN-4 2 A 1	11.81405	315	340	qtz	-8.1	
REVEN-4 2 A 2	11.09873	316	341	qtz	-7.5	
REVEN-4 2 A 3	10.85526	315	340	qtz	-7.3	
SILL-2 3 A 2	11.33967	259	284	qtz	-7.7	
SILL-2 3 A 9	10.23533	248	273	qtz	-6.8	
STS JOHNS-1 1 A 2	5.109832	330	355	qtz	-3.1	
STS JOHNS-1 2 A 1	9.982783	266	291	qtz	-6.6	
STS JOHNS-1 2 A 2	6.593387	399	424	qtz	-4.1	
STS JOHNS-1 2 A 3	9.469701	281	306	qtz	-6.2	
STS JOHNS-1 2 A 4	8.002245	392	417	qtz	-5.1	
BS-1 3 A 3	12.27862	331	356	qtz	-8.5	
BS-1 3 B 3	11.09873	286	311	qtz	-7.5	
BS-1 4 A 1	8.813095	259	284	qtz	-5.7	

EQUITY-3 2 A 1	3.226258	360	385	qtz	-1.9	
QOW-1 4 A 1	4.025108	232	257	qtz	-2.4	
QOW-1 5 B 2	11.21952	292	317	qtz	-7.6	
QOW-1 5 B 4	10.73257	300	325	qtz	-7.2	
QUAIL-1 1 A 4	7.447451	292	317	qtz	-4.7	
QUAIL-1 5 B 1	7.165707	316	341	qtz	-4.5	
SILL-2 9 A 2	10.48525	270	295	qtz	-7	
BLANCHE-1 1 A 1	5.412679	192	217	sph	-3.3	
BLANCHE-1 2 A 1	10.73257	222	247	sph	-7.2	
BLANCHE-1 2 A 2	10.73257	222	247	sph	-7.2	
BLANCHE-1 2 A 3	11.9311	222	247	sph	-8.2	
BLANCHE-1 2 A 5	10.48525	222	247	sph	-7	
BLANCHE-1 2 A 6	14.25347	216	241	sph	-10.3	
BLANCHE-1 3 A 1	13.72328	215	240	sph	-9.8	
BLANCHE-1 3 B 1	13.39851	210	235	sph	-9.5	
BLANCHE-1 4 A 1	11.4592	217	242	sph	-7.8	
BLANCHE-1 4 A 2	12.73359	222	247	sph	-8.9	
BLANCHE-1 6 B 1	8.813095	175	200	sph	-5.7	
BLANCHE-1 6 B 2	9.209112	175	200	sph	-6	
EQUITY-3 3 A 1	7.165707	200	225	sph	-4.5	
EQUITY-3 3 A 2	8.002245	183	208	sph	-5.1	
MORGAN-1 1 A 1	7.165707	255	280	sph	-4.5	
MORGAN-1 1 A 2	7.165707	255	280	sph	-4.5	
MORGAN-1 1 A 3	6.737579	255	280	sph	-4.2	
MORGAN-1 5 A 1	11.69638	275	300	sph	-8	
MORGAN-1 5 A 2	11.69638	267	292	sph	-8	
MW-1 1 A 1	5.712431	190	215	sph	-3.5	
NT-1 2 B 1	6.881027	222	247	sph	-4.3	
NT-1 2 B 2	6.881027	222	247	sph	-4.3	
NT-1 2 B 3	6.881027	222	247	sph	-4.3	
NT-1 2 B 4	6.448448	195	220	sph	-4	
NT-1 2 B 5	6.881027	222	247	sph	-4.3	
NT-1 A 1	4.649699	233	258	sph	-2.8	
NT-1 A 4	5.412679	233.4	258.4	sph	-3.3	
NT-1 A 5	5.712431	233.4	258.4	sph	-3.5	
NT-1 A 6	5.712431	233.4	258.4	sph	-3.5	